

Master thesis

**Simulation, design, fabrication of novel AFM
cantilevers for cell measurements**

Host Structures: Advanced NEMS lab - EPFL

Written by Renato Gaudio

Supervised by PhD. Carlo Ricciardi

Under the guidance of PhD. Guillermo Villanueva

MSc in Nanotechnologies for ICTs - International program

Politecnico di Torino - Grenoble INP-Phelma - EPFL



Politecnico
di Torino



EPFL

Abstract

The change in oscillation frequency of a cantilever is proportional to the mass on top of the cantilever and to the amplitude of vibration. This causes a cross-sensitive between both effects and makes it difficult to have proper detection with a single cantilever beam. The goal of this project is to decouple both effects by engineering a mode shape to maintain as constant as possible the vibrational amplitude at the region of interest (typically the free edge of the cantilever). I perform this mode shape engineering by fabricating cantilever structures with a region where the stiffness is discontinuous in the cross section, over a portion of the length. The rest of the length is much stiffer and corresponds to the flat part within the engineered mode-shape. This project simplifies the use of cantilevers for mass measurements since it enables their use without the need of deconvoluting the effect of mass and position. The project has been patented under EPFL rights.

Contents

1 Acknowledgements	3
List of Figures	4
2 State of the art	7
2.1 Applications	8
3 Simulations	9
3.1 Geometry	9
3.2 2D Simulations	9
3.3 Improved geometry	17
3.4 2D simulation with improved geometry	18
3.5 3D Simulations	21
3.6 Stress simulations and applied load	27
3.7 Temperature actuation	31
3.8 Power actuation	38
4 Design	43
4.1 Process flow	43
4.2 Cantilever design	48
4.3 Chip design	51
5 Fabrication	54
5.1 First fabrication batch	58
5.2 Second batch	73
6 Characterization	81
6.1 LDV measurements	81
6.2 DHM measurements	81
6.3 Power actuation with AFM laser	83
7 Conclusion	85
References	86
A Clean room machines	1
A.1 ACS200 - Coater and developer system for positive resist	1
A.2 Photolithography wet bench	1
A.3 Zeiss LEO 1550 SEM	1
A.4 Alcatel AMS 200 SE	2
A.5 Tepla GiGAbatch	2
A.6 UFT remover	3
A.7 EVG 150	3
A.8 ATMssse OPTIspin SB20	3
A.9 Raith EBPG5000 – Ebeam tool	3
A.10 Alliance-Concept EVA 760	4
A.11 Heidelberg Instruments MLA150	4

1 Acknowledgements

First of all, I would like to acknowledge my main supervisor, Prof. Guillermo Villanueva, for giving me the opportunity to realize my master thesis in his lab Advanced NEMS. He has been incredibly helpful in all tasks from the start to the finish of my master thesis semester. I learned a lot both regarding the design and fabrication of devices thanks to his advices.

A special thanks goes to Damien Millard for sharing with me his deep knowledge on the fabrication processes of the CMi clean room. Without him I would have needed more tries on the various steps of the fabrication before having the complete device working.

I kindly acknowledge Daniel Moreno Garcia for the help on the measurements with LDV (Laser Doppler Velocimetry) and DHM (Digital Holographic Microscopy). The results coming from these measurements have been very useful.

I also want to thank Florian Hartmann for helping me with the e-beam exposure, his advices have been very helpful for a correct exposure of the wafers. Moreover, this work would have not been possible without the help of all the clean room staff.

In addition, I would like to acknowledge all the people from the lab Advanced NEMS, they have been always available for every question I had regarding my project.

I kindly acknowledge Gotthold Fläschner for the important measurements that we did together at Nanosurf on this project. Thanks to these results the actuation of gold can be observed clearly.

I would like to deeply acknowledge my parents and my sister for all their support through the years but mostly during these past 6 months.

Finally, I would like to thank Anastasia, for all her love and support.

List of Figures

1	Mode shape of the standard cantilever with cell on it	7
2	First geometry of the modified cantilever	9
3	Mode shape of the cantilever shown in figure 2	10
4	Dimensions of the 4 parameters for this simulation	10
5	Values for the parametric sweep	11
6	Optimized combination of the parametric sweep	11
7	Mode shape for the optimized combination	12
8	Relative bending as a function of T1	12
9	Relative bending as a function of T2	13
10	Relative bending as a function of L1	14
11	Relative bending as a function of L2	14
12	Fundamental mode for the cantilever made of Si_3N_4	15
13	Fundamental mode for the cantilever with low density internal material	15
14	Fundamental mode for the cantilever with 3 plates	16
15	Mode shape for low density internal material and optimized parameters	16
16	Resonance frequency and calculated figure of merit for simulation in figure 15	17
17	Mode shape in the case the internal material is 200 kg/m^3 dense	17
18	Resonance frequency and figure of merit from figure 17	17
19	Cantilever with 6 equally spaced pillars along L1	18
20	Mode shape for cantilever with 6 equally spaced pillars	18
21	Figure of merit for cantilever with 6 equally spaced pillars	19
22	Mode shape for cantilever with 3 equally spaced pillars	19
23	Figure of merit for cantilever with 3 equally spaced pillars	19
24	Mode shape for 3-plate cantilever with 6 equally spaced pillars	20
25	Figure of merit for 3-plate cantilever with 6 equally spaced pillars	20
26	Mode shape for 3-plate cantilever with 3 equally spaced pillars	20
27	Figure of merit for 3-plate cantilever with 3 equally spaced pillars	21
28	Geometry of the cantilever for the 3D simulations	21
29	Geometry of the cantilever for the 3D simulations from another angle	21
30	Mode shape of the 3D cantilever	22
31	Mode shape of the 3D cantilever from another angle	22
32	Figure of merit for the 3D cantilever	22
33	Geometry of the cantilever with square base pillars	23
34	Mode shape of the square base pillar cantilever in the xz plane	23
35	Mode shape of the square base pillar cantilever in the yz plane	24
36	Figure of merit for the 3D cantilever with square base pillars	24
37	Relative bending of the different models with respect to the simple cantilever	24
38	Figure of merit and resonance frequency for cantilevers with different number of pillars	25
	(a) Factor for the cantilever with 3 square base pillars, improvement=96	25
	(b) Factor for the cantilever with 2 square base pillars, improvement=118	25
	(c) Factor for the cantilever with 1 square base pillars, improvement=185	25
39	Resonance frequency and figure of merit for different depths pillars	26
	(a) 6 pillars with double depth, improvement=41	26
	(b) 6 pillars with triple depth, improvement=37	26
	(c) 3 pillars with double depth, improvement=87	26
	(d) 3 pillars with triple depth, improvement=81	26

(e)	2 pillars with double depth, improvement=110	26
(f)	2 pillars with triple depth, improvement=103	26
(g)	1 pillar with double depth, improvement=176	26
(h)	1 pillar with triple depth, improvement=170	26
40	Mode shape in the xz plane for the cantilever with $L_2=75 \mu m$	27
41	Figure of merit for the cantilever with $L_2=75 \mu m$	27
42	Stress in cantilever due to the applied power on the gold layer	28
43	Mode shape of the cantilever considering quality factor of 50 with $2 \mu N$ on the right edge	28
44	Frequency sweep of the displacement of the cantilever with a load applied	29
45	Second eigenfrequency for the cantilever with gold on top	29
46	Second eigenfrequency for the cantilever with gold on top	29
47	Resonance plot with $Q=10$ and applied load	30
48	Simulated eigenfrequency for the cantilever with $Q=10$	30
49	Fundamental mode for $Q=10$ and load applied	31
50	Resonance plot with $Q=10$, applied load and adaptive frequency sweep	31
51	Fundamental mode of the cantilever with temperature actuation	32
52	Frequency response of the cantilever for 30 K perturbation	32
53	Frequency response of the cantilever for 60 K perturbation	33
54	Frequency response of the cantilever for 15 K perturbation	33
55	Fundamental mode of the cantilever with gold on L_1+L_2	34
56	Frequency response for 30 K perturbation and gold on L_1+L_2	34
57	Frequency response with gold on $L_1/2$	35
58	Frequency response with gold on $L_1/4$	36
59	Frequency response with gold on $L_1'/2$	36
60	Frequency response with gold on $L_1'/4$	37
61	Frequency response with 50 nm gold on L_1	37
62	Frequency response with 4 equally spaced gold layers	38
63	Fundamental mode in case of power actuation on all L_1	38
64	Frequency response in case of power actuation on all L_1	39
65	Frequency response in case of power actuation and gold on L_1	39
66	Frequency response in case of power actuation and gold on $L_1/2$	40
67	Frequency response in case of power actuation and gold on L_1'	40
68	Frequency response in case of power actuation and gold on $L_1'/2$	41
69	Frequency response in case of power actuation and gold on each $L_1'/2$	41
70	Power actuation for the different cantilever's designs	42
71	Page 1 process flow	44
72	Page 2 process flow	45
73	Page 3 process flow	46
74	Page 4 process flow	47
75	Page 5 process flow	48
76	Cantilever design for chip 1	49
77	Cantilever design for chip 2	49
78	Pillars design in chip 2	49
79	Cantilever design for chip 7	50
80	Cantilever design for chip 11, standard cantilever	50
81	Cantilever shape lithography step	51
82	Design chip	52
83	Complete chip design	52

84	complete wafer design	53
85	Test for the different widths of the backside bridges	54
86	Complete etching of test wafer with design of multiple bridges	55
87	Back side of the wafer after KOH	56
88	Test wafer after cleaving of chips	57
	(a) 50 μm bridge	57
	(b) 50 μm bridge for another chip	57
	(c) 75 μm bridge	57
	(d) 100 μm bridge	57
	(e) 125 μm bridge	57
	(f) 150 μm bridge	57
89	Trenches and walls for the cantilever with 5 trenches and 9 walls	58
90	Details of the 9 walls of the cantilever	59
91	Details of the pillars	59
92	Wafers after second lithography step	60
93	Detail wafers after second lithography	61
94	Correct alignment marks exposure	61
95	Detail wafers after second lithography	62
96	Detail of the wafer after 50 nm gold evaporation	63
97	Another detail of the wafer after 50 nm gold evaporation	63
98	Wafer after gold lift-off	64
99	Third lithographic step, for chip with gold on each L1'/2	65
100	Third lithographic step, for chip with gold on L1	65
101	Wafer after cantilever shape definition and resist strip	66
102	Back side etching of SiN_x	67
103	Cantilever released from the back side	68
104	Different cantilever released from the back side	68
105	Detail of the walls after the releasing of the cantilever	69
106	Cantilever survived to KOH	70
107	Another cantilever survived to KOH	71
108	Detached cantilever from the chip after KOH	71
109	Cross section of the complete cantilever	72
110	Cross section of the walls of the complete cantilever	73
111	Top side bridge for the chip's stability	74
112	Walls and trenches without tail's defects	74
113	Cantilever after second lithographic step	75
114	Cantilever defined	76
115	Back side releasing of the cantilever	77
116	KOH test for Poly-Si etch rate	77
117	Complete Poly-Si etching	78
118	Complete Poly-Si etching for another chip	79
119	Complete cantilever with Au + Cr on top	80
120	Oscillation amplitude and phase of the cantilevers	81
121	2D profile of the oscillation at 1 V applied	82
122	2D profile of the oscillation at 500 mV applied	83
123	2D profile of the oscillation at 200 mV applied	83
124	Power actuation of the cantilever in air	84
125	Power actuation of the cantilever in water	85
126	SEM holders [19]	2

2 State of the art

The topography of a sample surface is photographed using the original atomic force microscope (AFM) [1] by scanning a sharp sensor tip, fixed to a soft cantilever, over the surface and measuring the cantilever deflection. Dynamic techniques like force modulation microscopy [2], tapping [3], or atomic force acoustic microscopy [4, 5, 6] have been developed in response to the need to assess surface attributes like adhesive energy or sample stiffness with the same high local resolution as the topography. In these methods, the sensor tip is in touch with the sample surface at least for a portion of the vibration cycle. The cantilever vibrates as it scans across the surface.

The AFM can be operated in a number of modes, depending on the application. In general, possible imaging modes are divided into static (also called contact) modes and a variety of dynamic (non-contact or "tapping") modes where the cantilever is vibrated or oscillated at a given frequency. [8]

The change in oscillation frequency of a cantilever is proportional to the mass on top of the cantilever and to the amplitude of vibration, the function that regulates this relationship is the following:

$$\Delta f = \Delta m * \Phi(x)^2 \quad (1)$$

Therefore we can say that the measurement of the cell's mass is dependant both by the frequency of the cantilever and by the position of the mass on the beam. With this project I am going to make the mass measurement of the cell independent from the position of it on the free edge. The goal is to make the measurement independent from the position of the mass, in this way it is possible to have a better sensitivity of the measurement.

As we can see in figure 1, the oscillation at the right edge varies significantly with respect to x, therefore the change in frequency of the cantilever greatly depend on the position in which the cell is located.

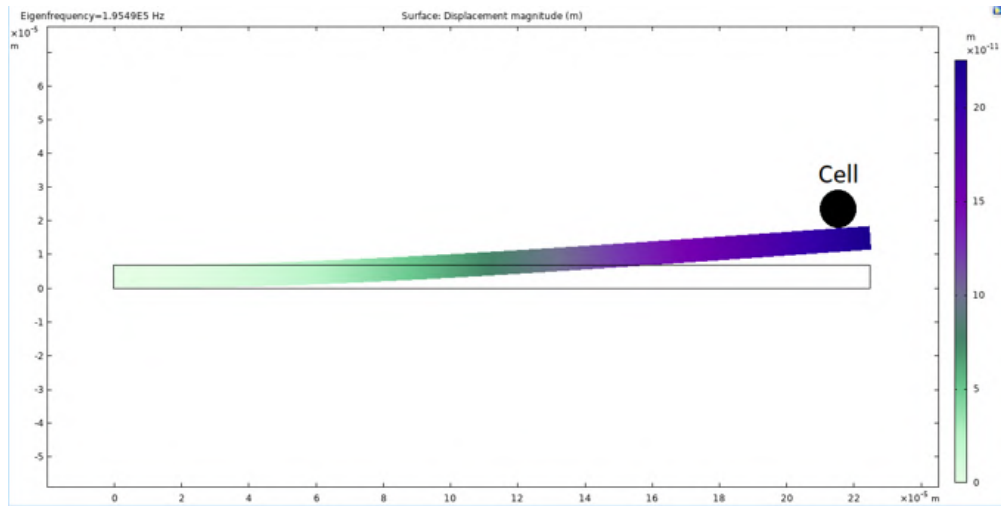


Figure 1: Mode shape of the standard cantilever with cell on it

Figure 1 shows the fundamental mode of oscillation of a standard cantilever which is formed by only 1 beam of the same material, in this case I can see a noticeable bending of the cantilever

where the cell is positioned, this will affect the resonance frequency of the cell and therefore the mass measured. The goal of this project is to maintain as constant as possible the fundamental mode at the free moving edge of the cantilever (right edge), this increases the sensitivity for mass measurements.

2.1 Applications

A wide range of natural scientific disciplines, including solid-state physics, semiconductor science, molecular engineering and cell biology have used the AFM to solve challenges.

The study of changes in physical properties resulting from atomic manipulation is one application of solid state physics. Other applications include: the identification of atoms at a surface, the assessment of interactions between a particular atom and its neighboring atoms, and the evaluation of changes in physical properties resulting from atomic manipulation.

AFM can be used in molecular biology to examine the composition and mechanical characteristics of protein complexes and assemblies. AFM has been used, for instance, to visualize and assess the stiffness of microtubules.

In cellular biology, AFM can be used to analyze interactions between a particular cell and its nearby cells in a competitive culture system and to try and distinguish cancer cells from normal cells depending on how hard the cells are. AFM can also be used to indent cells and examine how they control the rigidity or shape of the cell wall or membrane.

In some versions, conducting cantilevers can also be used to scan electric potentials. In more sophisticated models, currents can be fed through the tip to examine the electrical conductivity or transport of the underlying surface, but this is a difficult process and only a small number of research organizations have consistently reported results on it. [7]

Recent initiatives to combine biological and nanotechnology research have been successful and hold a lot of promise for the future, especially in areas like nanobiomechanics [9]. Since nanoparticles are a possible drug delivery method, the biological reactions of cells to them are constantly being researched in order to increase their efficacy and discover new design possibilities [10]. By affixing the designed nanoparticles to the AFM tip, Pyrgiotakis et al. were able to analyze the interaction between CeO_2 and Fe_2O_3 manufactured nanoparticles and cells [11]. AFM has been used in studies to learn more about the behavior of live cells in biological medium. Studies of live cells and membrane proteins' dynamic behavior at the nanoscale have been conducted using real-time atomic force spectroscopy (also known as nanoscopy) and dynamic atomic force spectroscopy. Insight into chemical processes and mechanisms that arise from interactions between cells and with other signaling molecules has also been gained through imaging and learning about the topography and characteristics of the cells (ex. ligands). To investigate cell adhesion forces, bond kinetics/dynamic bond strength, and its function in chemical processes such cell signaling, Evans and Calderwood used single cell force microscopy. [12]

Studies using AFM to investigate the crystal structure of membrane proteins of photosynthetic bacteria were reviewed by Scheuring, Lévy, and Rigaud [13]. As an illustration of the more thorough analysis of pathogen-drug interactions that can be done through AFM. The analysis of the interaction between live mycobacteria and antimycobacterial drugs (specifically, isoniazid, ethionamide, ethambutol, and streptomycin) [14] was carried out using AFM-based nanoscopy.

3 Simulations

Simulation is one of the first steps in the development of a new device, this is why I want to start with my simulation results. The simulations that I am going to show in the future are done using COMSOL Multiphysics®. I will start with 2D simulations and then later get to 3D simulations.

3.1 Geometry

The first geometry of the cantilever that I am going to simulate is shown in figure 2. The cantilever is made of 2 parallel plate, one on top of the other, separated by a layer of material at the free moving edge of the cantilever. For explanation purposes I will always consider the left edge the one edge that is fixed and the right edge the free moving edge.

In this geometry I consider 4 parameters of interest, which are shown in figure 2. L1 is the distance between the left edge and the start of the internal material, L2 is the length of the internal material, T1 is the thickness of the 2 plates and T2 is the height of the internal material.

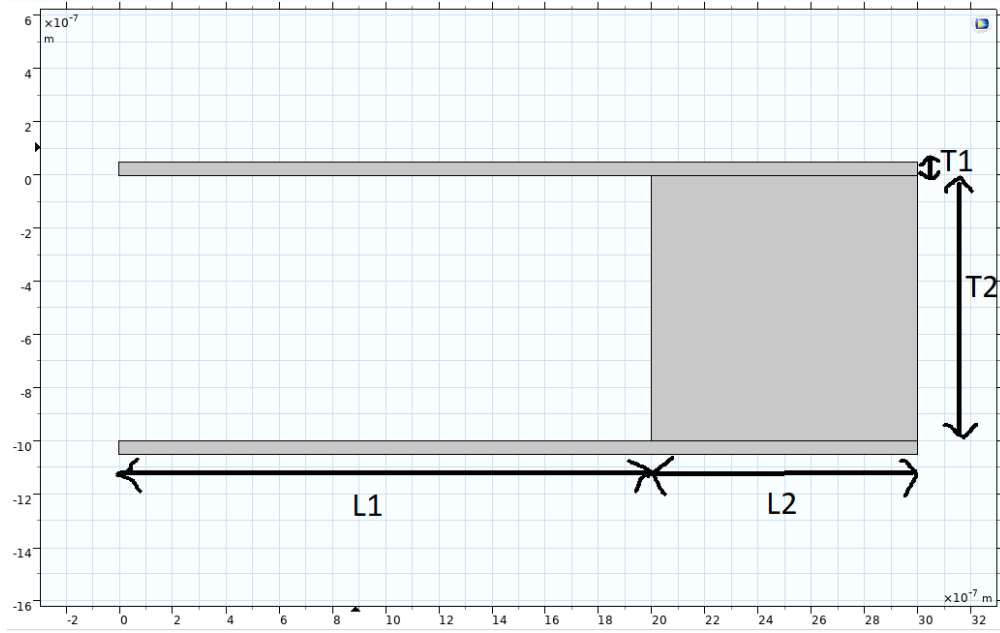


Figure 2: First geometry of the modified cantilever

The goal is to measure the mass on the cantilever by measuring its oscillation frequency. However, the frequency of oscillation depends on the mode shape from the formula: $\Delta f = \Delta m * \phi(x)^2$, where $\phi(x)$ is the mode shape. This means I want the mode shape as horizontal as possible, in this way it is possible to decouple both effects of mass and vibration. The effective mass does not change with respect to the position in the cantilever.

3.2 2D Simulations

The first simulation was done considering the whole cantilever made of Poly-Si and choosing the 4 parameters as shown in figure 4, the mode shape was calculated using the eigenfrequency

simulation in COMSOL, the result is shown in figure 3. We can see that the expected result is met, because the mode shape is constant on the free moving edge of the cantilever.

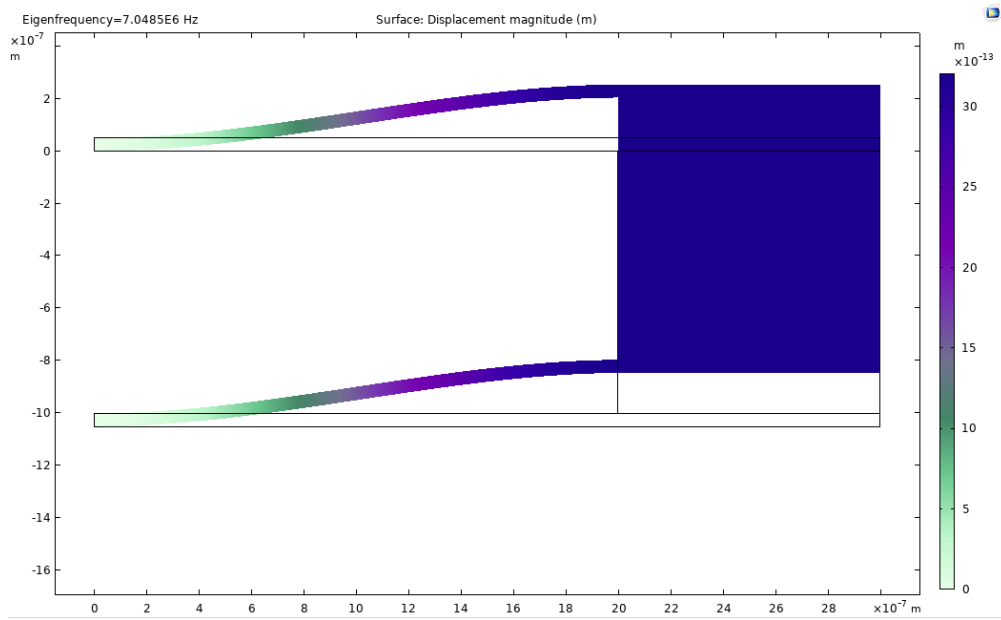


Figure 3: Mode shape of the cantilever shown in figure 2

Parameters			
Name	Expression	Value	Description
T1	50[nm]	5E-8 m	
T2	1[um]	1E-6 m	
L1	2 [um]	2E-6 m	
L2	1 [um]	1E-6 m	

Figure 4: Dimensions of the 4 parameters for this simulation

I then did a parametric sweep over all 4 parameters L1, L2, T1 and T2, the goal of this simulation is to check all the possible combinations and find the quartet of parameters for which the mode shape is as constant as possible. I want to search for the combination that minimizes the figure of merit

$$\frac{W_{max} - W(L1)}{L2 * W_{max}} \quad (2)$$

in which W_{max} is the maximum vertical displacement of the mode shape (that is found at $x = L1 + L2$) and $W(L1)$ is the vertical displacement of the mode shape when $x=L1$. The parameter value list for the 4 parameters is shown in figure 5.

The minimum of the expression is achieved for $T_1=50$ nm, $T_2=5$ μm , $L_1=50$ μm , $L_2=10$ μm and the associated eigenfrequency of the cantilever is $f=8514.1$ Hz, the figure of merit is 4.3806 and can be seen in figure 6 under the column Factor. The mode shape for this optimized combination of parameters can be seen in figure 7.

Study Settings		
Sweep type: All combinations		
Parameter name	Parameter value list	Parameter unit
T1	50 100 200 300 400 500	nm
T2	1 2 3 4 5	um
L1	10 20 30 40 50	um
L2	10 20 30 40 50	um

Figure 5: Values for the parametric sweep

T1 (nm)	T2 (um)	L1 (um)	L2 (um)	Eigenfrequency (Hz)	Factor (1/m)
50.000	5.0000	50.000	10.000	8514.1	4.3806

Figure 6: Optimized combination of the parametric sweep

We can therefore deduce that in order to have a small relative bending we need to increase T_2 and L_1 and to decrease L_2 and T_1 .

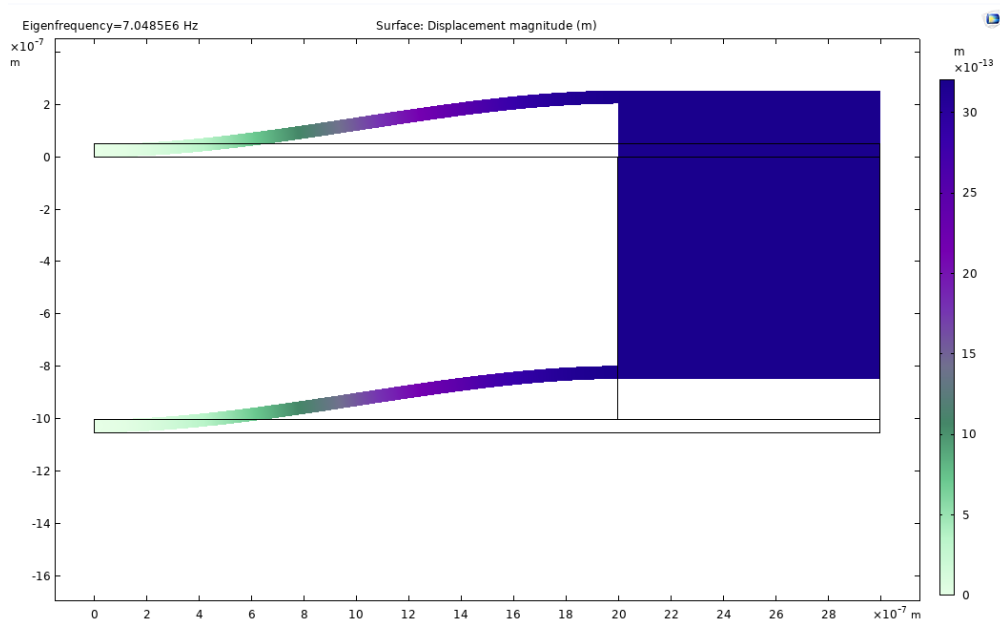
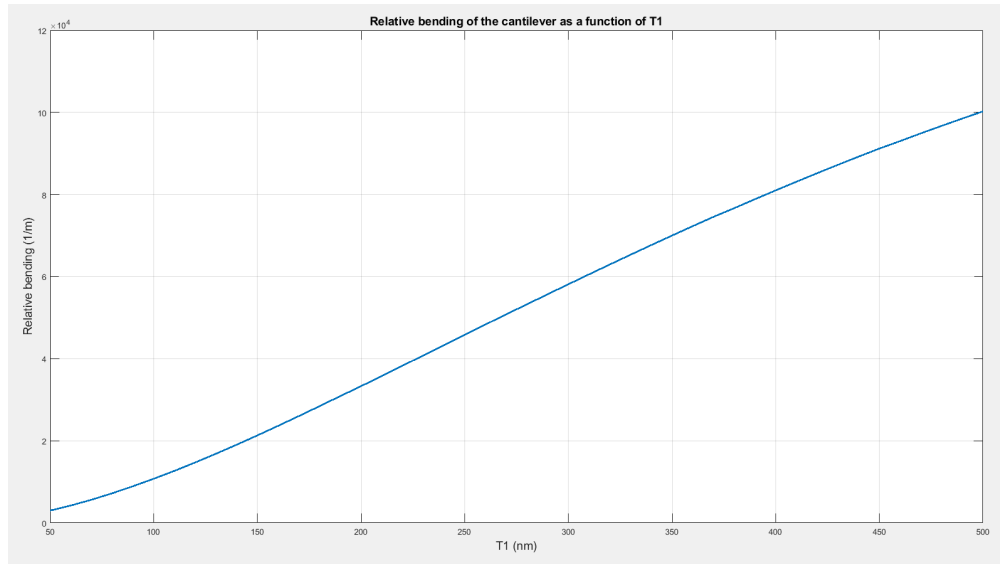


Figure 7: Mode shape for the optimized combination

I inspected the behavior of the relative bending as function of T_1 , T_2 , L_1 , L_2 respectively and one at a time. I start with T_1 , I will fix all the parameters and make T_1 change. I then plotted in MATLAB the figure of merit shown in equation 2 as a function of T_1 , the result is displayed in figure 8.

Figure 8: Relative bending as a function of T_1

Concerning the figure of merit with respect to T_2 I get a trend that is shown in figure 9,

it is possible to state that as thicker is the internal material as lower is the relative bending of the cantilever, moreover the behaviour is parabolic, not linear, therefore there is no benefit in increasing too much the thickness of the internal material because there will be one thickness for which the relative bending saturates and can not decrease, this trend is totally opposite to what I have found with respect to T1. All these results are coherent with the most optimized quartet of parameters that I found during my parametric sweep simulation.

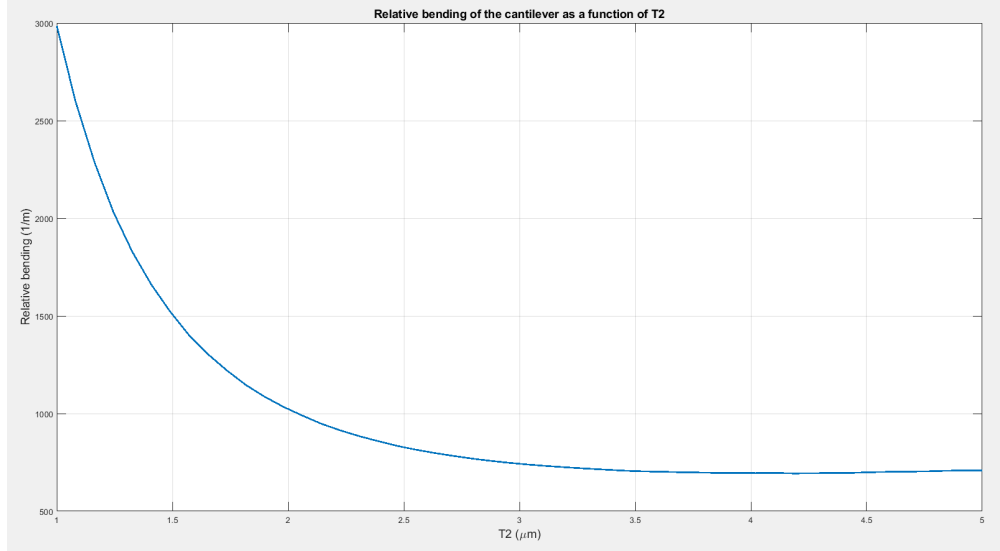


Figure 9: Relative bending as a function of T2

The relative bending of the right part of the cantilever with respect to L1 has a very similar trend to figure 9, so also in this case, the relative bending will not lower much if we increase L1, because of the parabolic behaviour of the curve.

Concerning the behaviour of the relative bending with respect to L2 I found that there is a maximum of bending and then it decreases as it happens for T2 and L1, the maximum could be explained by the fact that the relative bending is a function of all parameters, so, depending on the values of 3 of the 4 parameters I will view a different part of the curve and I will shift the maximum more to the right or more to the left. I will use $L2=75 \mu\text{m}$ in my simulation and fabrication, therefore we can see that it would be better to use very big or very small values for L2, in order to decrease the relative bending of the cantilever.

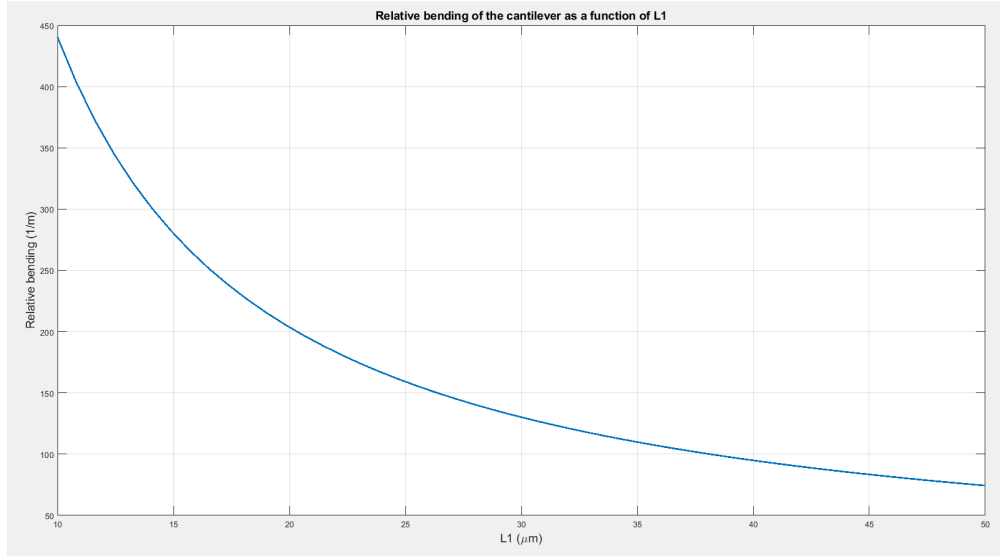


Figure 10: Relative bending as a function of L1

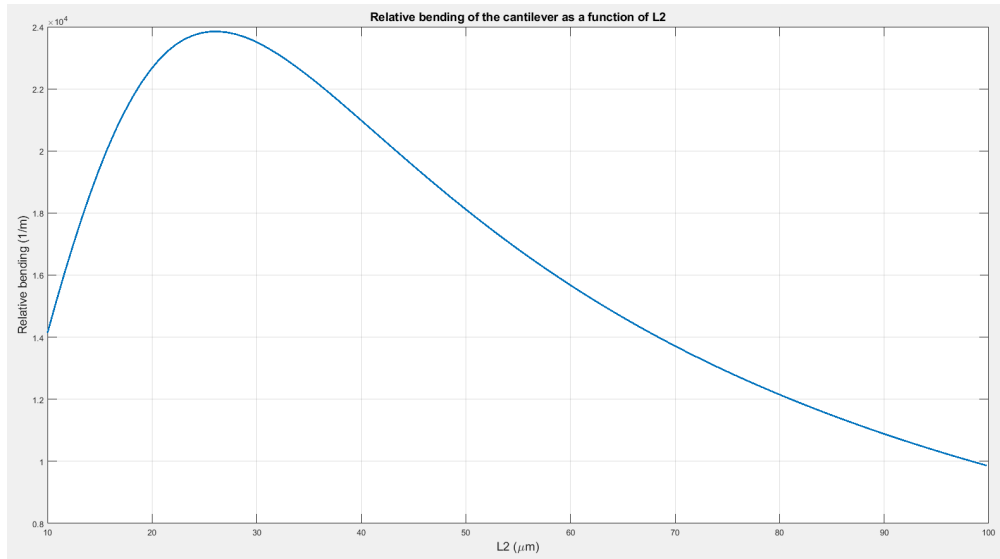
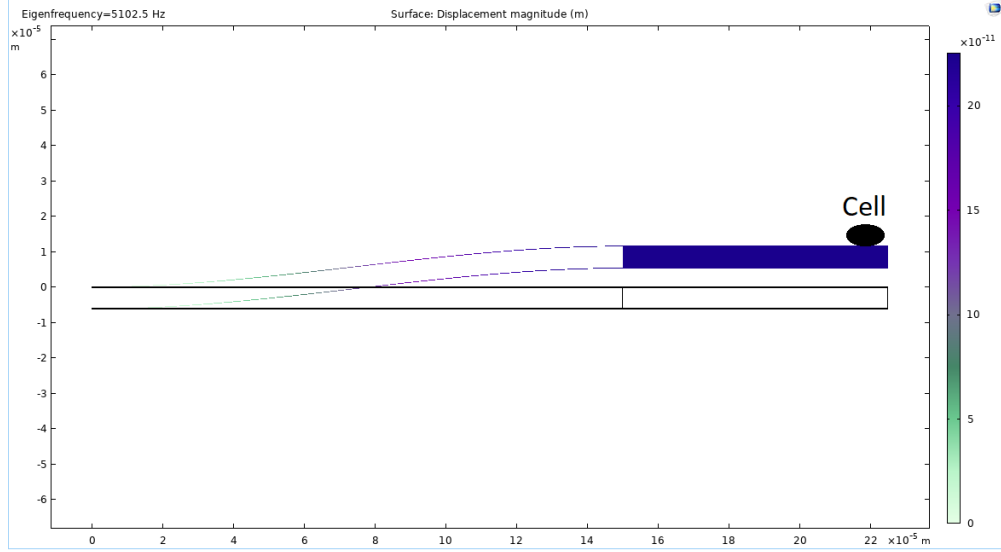


Figure 11: Relative bending as a function of L2

Now that I have information on the behaviour of the mode shape with respect to the four parameters, I will carry out a simulation fixing the four parameters to $L1=150\mu\text{m}$, $L2=75\mu\text{m}$, $T1=200\text{ nm}$ and $T2=6\mu\text{m}$. I also consider the top and bottom beam made of Si_3N_4 , whereas the internal material remains polysilicon. I focus on the resonance frequency for this simulation, in fact I want to achieve a resonance frequency of 15kHz or above. From this simulation I get the figure 12, where I also highlight the position in which I can place the cell for mass measurement. As we can see the oscillation frequency is still low, of just 5.1 kHz.

Figure 12: Fundamental mode for the cantilever made of Si_3N_4

I now decrease the density of the internal material from 2300 kg/m^3 of the polysilicon to 700 kg/m^3 , this decrease in density helps with increasing the oscillation frequency, in fact now I have an eigenfrequency of 8.1 kHz, as it is possible to appreciate in figure 13

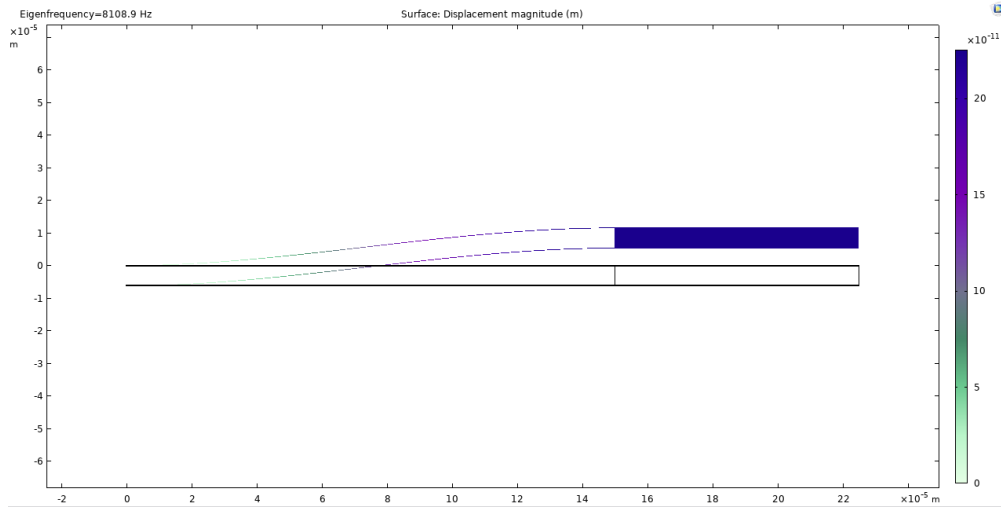


Figure 13: Fundamental mode for the cantilever with low density internal material

To increase even more the frequency oscillation I changed the geometry of the cantilever in order to have a three-plate cantilever, the frequency in this case increases by 1 kHz, so in total I have an oscillation frequency of 9.1 kHz, considering a low density internal material too, the result for this simulation is shown in figure 14.

Now I am going to simulate the modified cantilever fixing 2 parameters: $T_2=6 \text{ }\mu\text{m}$ and $L_1+L_2=225 \text{ }\mu\text{m}$ and I am doing a parametric sweep on T_1 and L_1 , but always considering that L_1+L_2 must be constant, so if I increase L_1 I must decrease of the same value L_2 .

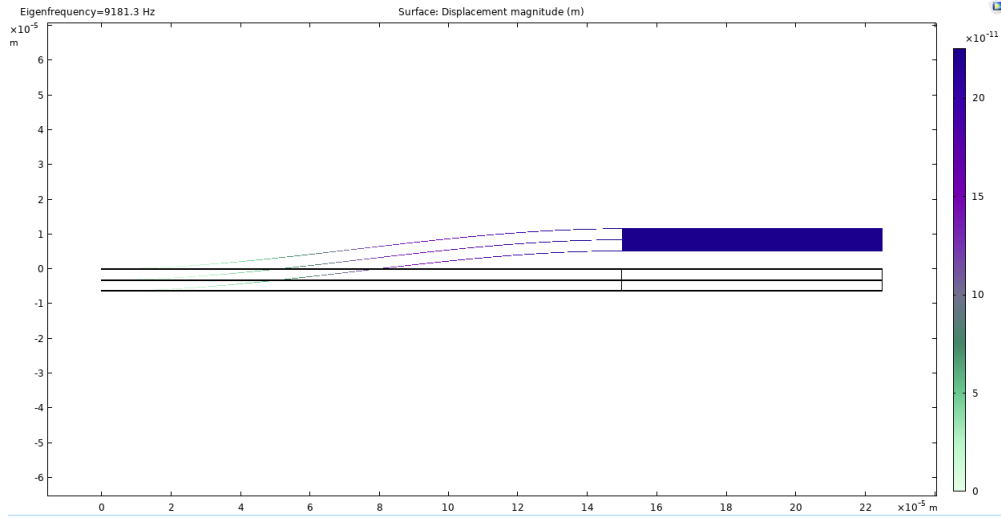


Figure 14: Fundamental mode for the cantilever with 3 plates

In this case I consider the internal material with a density of 500 kg/m^3 , T1 ranging from 200 nm to 500 nm and L1 going from $50 \text{ }\mu\text{m}$ to $175 \text{ }\mu\text{m}$. In this case the figure of merit of our interest is

$$\frac{(W_{max} - W(L1)) * L_{cell}}{L_2 * W_{max}} \quad (3)$$

where we have multiplied by the cell size which can be assumed to be $40 \text{ }\mu\text{m}$.

As expected, the lowest value for the figure of merit (most optimized solution) is when T1 is the smallest and L1 is the biggest, the figure of merit in the best case is equal to $5.26 * 10^{-4}$ with a resonance frequency of 8.212 kHz. The results are shown in figure 15 and figure 16.

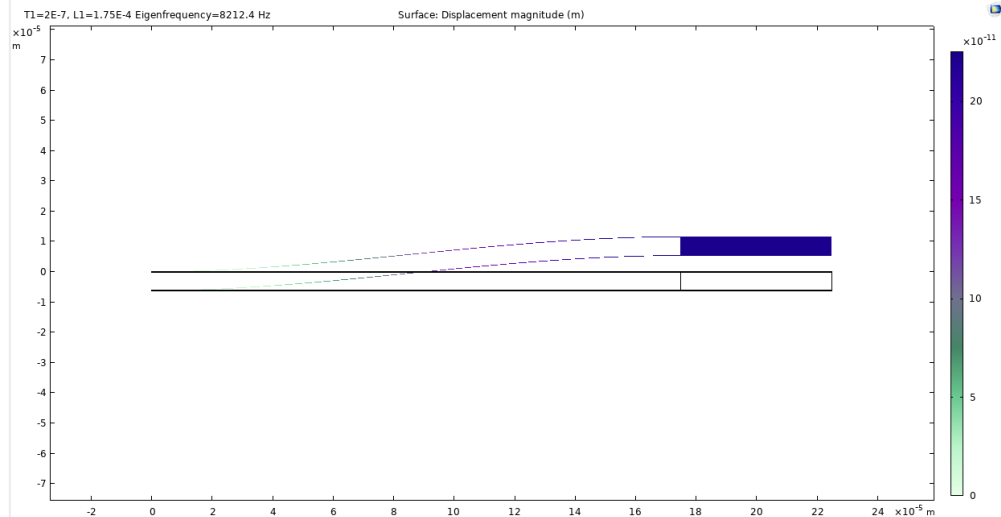
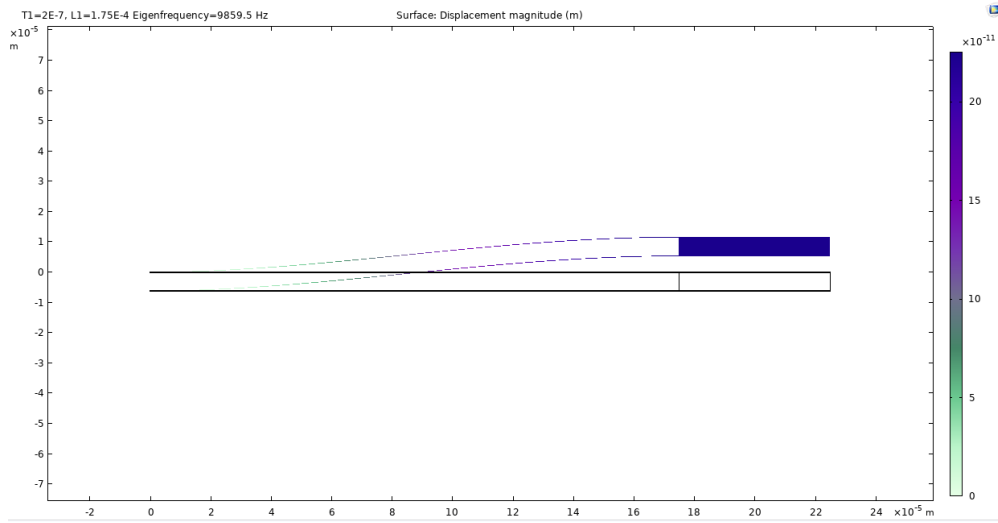


Figure 15: Mode shape for low density internal material and optimized parameters

T1 (m)	L1 (m)	Frequency (Hz)	Factor (1)
2.0000E-7	1.7500E-4	8212.4	5.2584E-4

Figure 16: Resonance frequency and calculated figure of merit for simulation in figure 15

In the case of a lower density of 200 kg/m^3 for the internal material, I get a slightly higher frequency of 9.8 kHz and a better figure of merit too, which now has decreased to 4.93×10^{-4} , that is a very good result. The new simulation can be seen in figure 17.

Figure 17: Mode shape in the case the internal material is 200 kg/m^3 dense

T1 (m)	L1 (m)	lambda (Hz)	Factor (1)
0.00000020000	0.00017500	9859.5	0.00049269

Figure 18: Resonance frequency and figure of merit from figure 17

3.3 Improved geometry

The cantilever of figure 17 is very long and very thin, these features can be a problem for the fabrication of it. In the following simulations I am going to change the structure of the cantilever in order to make it more durable and easy to fabricate, reducing the probability of failures during fabrication steps.

In order to increase the stability of the system we can use some pillars which sustain the long cantilever in the hollow part (through L1), in this way it will be easier to fabricate it. The pillars should not be thinner than 600 nm, which is the smaller dimension for which we can fabricate these high aspect ratio pillars. In the following I will consider pillars 600 nm wide and equally spaced apart, we want them as thin as possible so to not influence the resonance frequency and the fundamental mode.

I considered 6 pillars equally spaced, the geometry of this new system can be seen in figure 19.

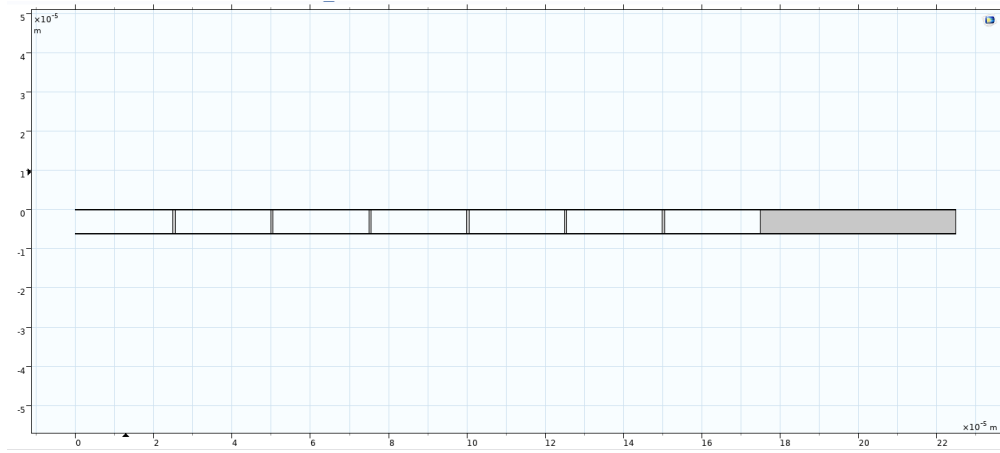


Figure 19: Cantilever with 6 equally spaced pillars along L1

3.4 2D simulation with improved geometry

The mode shape for this geometry is shown in figure 20. The resonance frequency is now 4 times higher and the figure of merit is 0.026, which is 50 times higher than the figure of merit calculated for the same cantilever without any pillar.

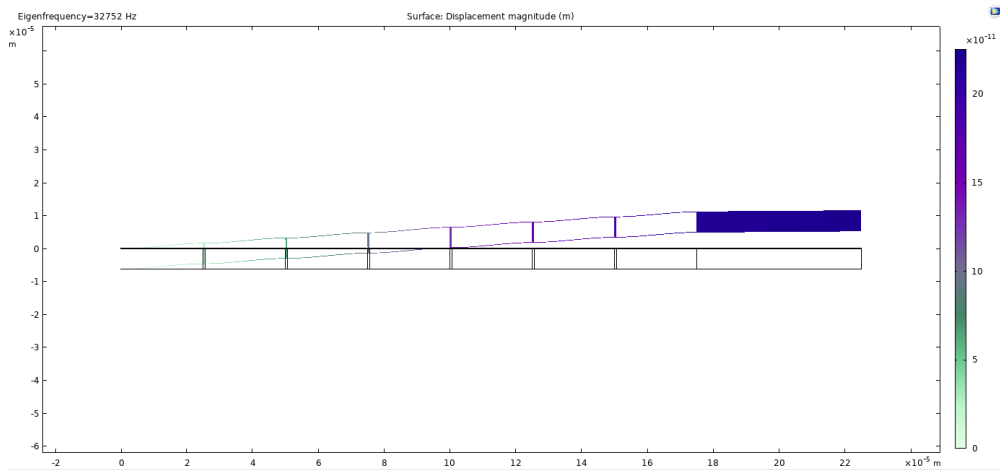


Figure 20: Mode shape for cantilever with 6 equally spaced pillars

Taken into considerations these results, we can say that the pillars increase the manufacturability of the device but the relative bending of the cantilever decreases. Another important aspect to take into consideration is that the resonance frequency increases. Finally now I have an higher resonance frequency that could be used for AFM applications and mass measurements.

I will now do the same simulation with 3 equally spaced pillars because I want to decrease the figure of merit in order to have a lower relative bending. The results are shown in figure 22.

Eigenfrequency (Hz)	Factor (1)
32752	0.026128

Figure 21: Figure of merit for cantilever with 6 equally spaced pillars

We can see that the frequency is now very close to 15 kHz and the relative bending has decreased too, in fact this figure of merit is just 15 times higher than the one for the cantilever without pillars.

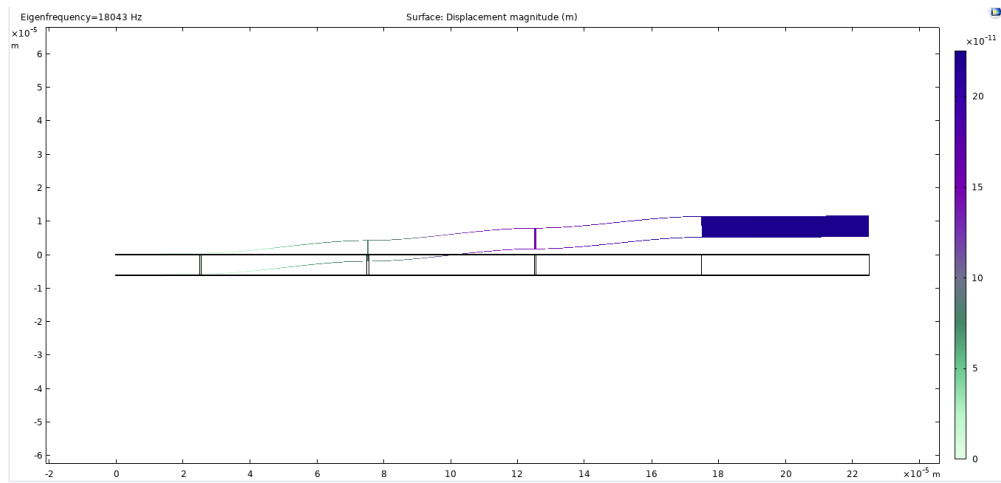


Figure 22: Mode shape for cantilever with 3 equally spaced pillars

Eigenfrequency (Hz)	Factor (1)
18043	0.0079542

Figure 23: Figure of merit for cantilever with 3 equally spaced pillars

I now do the same simulations in the case of a 3-plate cantilever with 6 equally spaced pillars. I can see that I still have a steps-like behavior of the mode, therefore when I add the pillars the mode shape changes. The result for this simulation can be seen in figure 24.

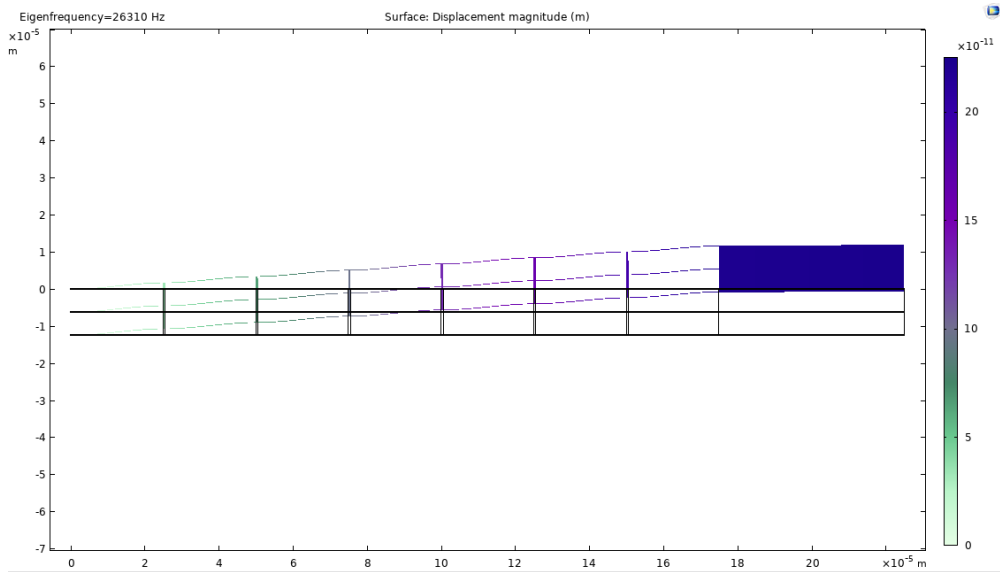


Figure 24: Mode shape for 3-plate cantilever with 6 equally spaced pillars

Eigenfrequency (Hz)	Factor (1)
26310	0.010702

Figure 25: Figure of merit for 3-plate cantilever with 6 equally spaced pillars

I do the same simulation in the case of a 3-plate cantilever with 3 equally spaced pillars, the result is shown in figure 26, it is possible to see that the figure of merit and the frequency of oscillation vary accordingly.

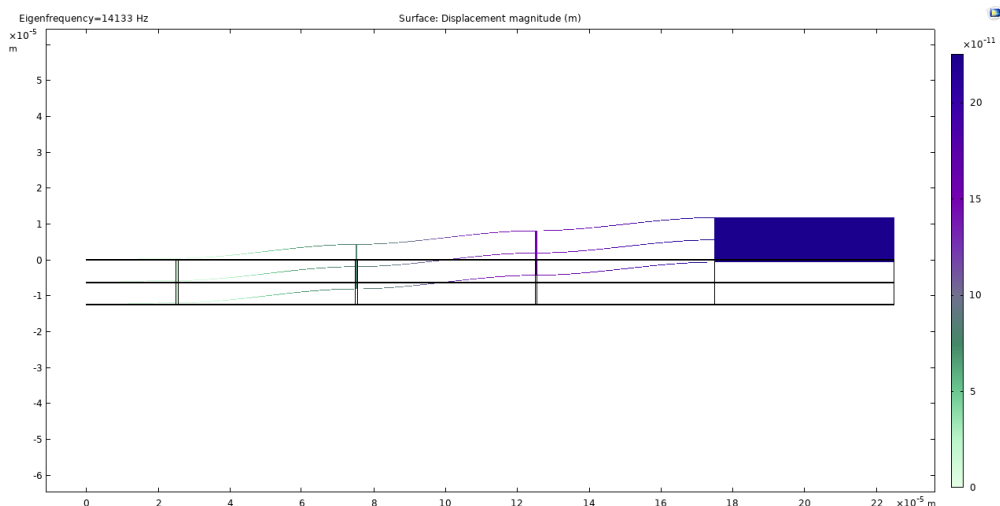


Figure 26: Mode shape for 3-plate cantilever with 3 equally spaced pillars

Eigenfrequency (Hz)	Factor (1)
14133	0.0030881

Figure 27: Figure of merit for 3-plate cantilever with 3 equally spaced pillars

3.5 3D Simulations

Now I am going to simulate the system of the cantilever in 3D, in this case I considered the depth of the cantilever to be $50\text{ }\mu\text{m}$. All the system is made with Si_3N_4 . Again, all along L1 I have 6 equally spaced trenches that help the cantilever to resist stress and failure. These trenches are 600 nm wide and $50\text{ }\mu\text{m}$ in depth, which is the depth of the hole beam. So the trenches are standing all along the cantilever in the depth dimension

In the L2 part in order to decrease the density of the material I built parallel walls of Si_3N_4 spaced by equally long hollow parts. The walls are 12 and each one of them is 600 nm thick, in this simulation the total space occupied by the material is $12 \times 600\text{ nm} = 7.2\text{ }\mu\text{m}$, considering the density of Si_3N_4 to be 3100 kg/m^3 I managed to have inside the cantilever an effective density that is $50\text{ }\mu\text{m} / 7.2\text{ }\mu\text{m} = 6.94$ times lower than the one of Si_3N_4 so the effective density is 446 kg/m^3 .

If I fix the depth of the cantilever I need to consider that the effective density is not a continuous function but more step-like, because we can only add or subtracts new parallel walls without discretize them, and the walls have a minimum thickness of 600 nm , constraint derived from fabrication.

The entire geometry of the system is shown in figure 28 and figure 29.

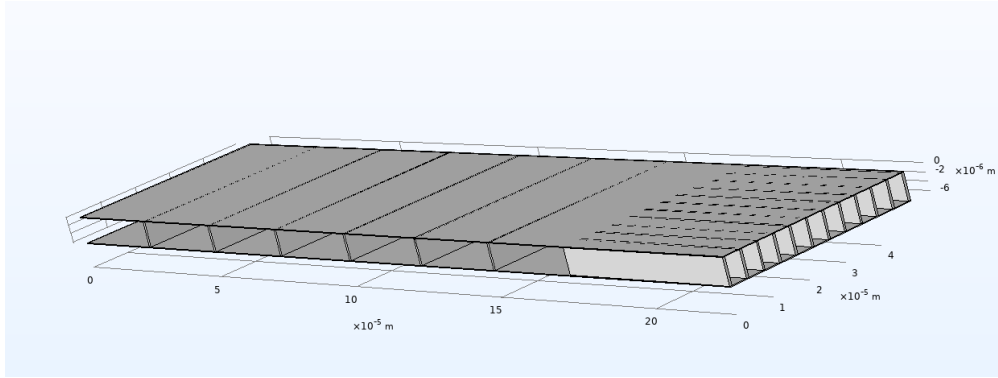


Figure 28: Geometry of the cantilever for the 3D simulations

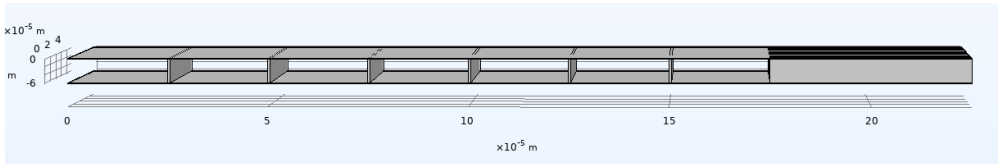


Figure 29: Geometry of the cantilever for the 3D simulations from another angle

The fundamental mode shape is shown in figure 30 and figure 31. The eigenfrequency is quite high, equal to 56.8 kHz.

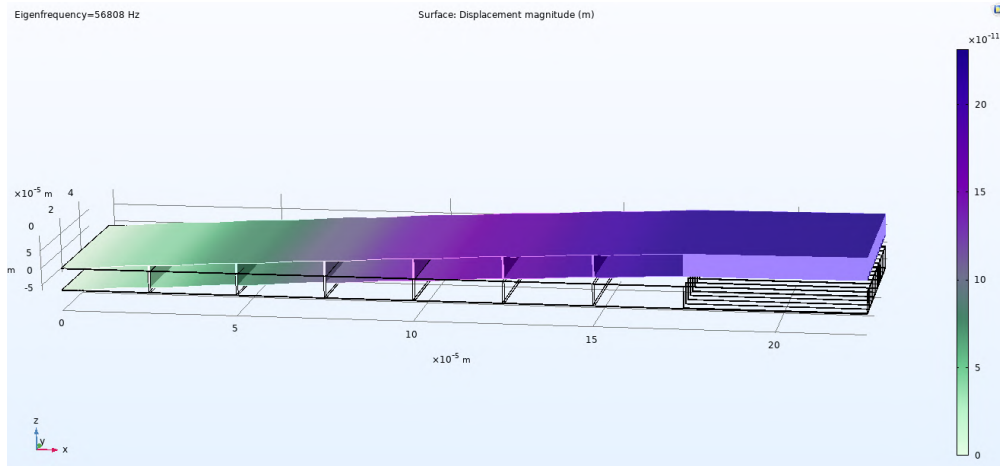


Figure 30: Mode shape of the 3D cantilever

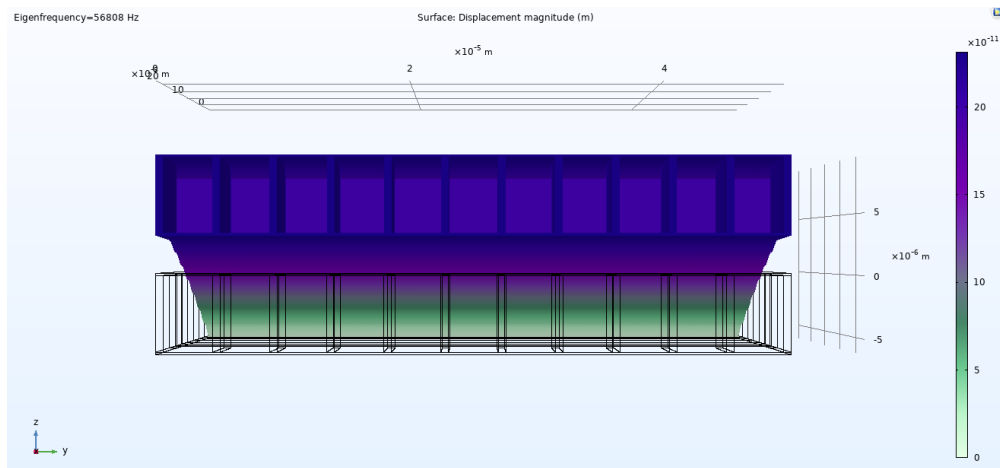


Figure 31: Mode shape of the 3D cantilever from another angle

The figure of merit is 0.025547, which is in line with the figure of merit calculated with the same structure but 2D.

Eigenfrequency (Hz)	Factor (1)
56808	0.025547

Figure 32: Figure of merit for the 3D cantilever

Now I am going to perform an eigenfrequency simulation on a bit different structure. In this case in L1 I do not have trenches but single pillars, positioned in the middle point of the

cantilever, the pillars are always 6 and equally spaced. The base of these new pillars is 600 nm X 600 nm. I chose to simulate this new structure because in this case we still have a robust model and we also decrease the influence of the pillars on the mode shape, in this way I will get a lower figure of merit (better optimization, less relative bending of the cantilever) and a lower resonance frequency because the cantilever is almost free to move in L1.

The new geometry is shown in figure 33.

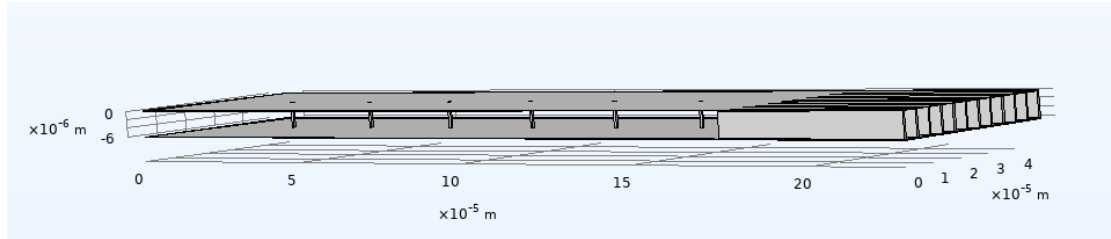


Figure 33: Geometry of the cantilever with square base pillars

The mode shape for this new geometry is shown in figure 34 and figure 35.

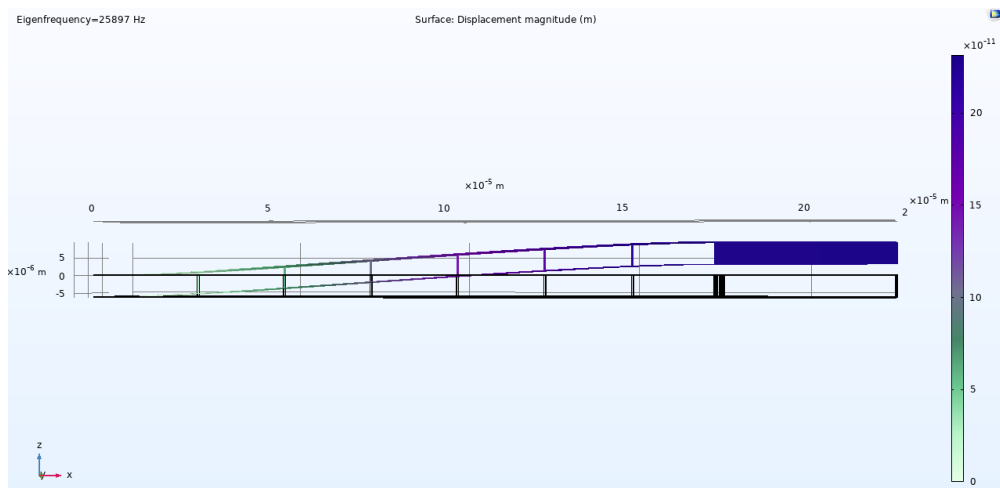


Figure 34: Mode shape of the square base pillar cantilever in the xz plane

As we were expecting, the figure of merit and the resonance frequency are smaller. Because the square base pillars are of less impact in the stiffness of the cantilever motion, this is a middle ground between having no supports in L1 and having trenches all the way deep in the cantilever. In this way with square base pillars I still have some mechanical support but at the same time I reduce the relative bending of the cantilever, because now the cantilever has less mechanical constraints. The figure of merit and the resonance frequency are shown in figure 36.

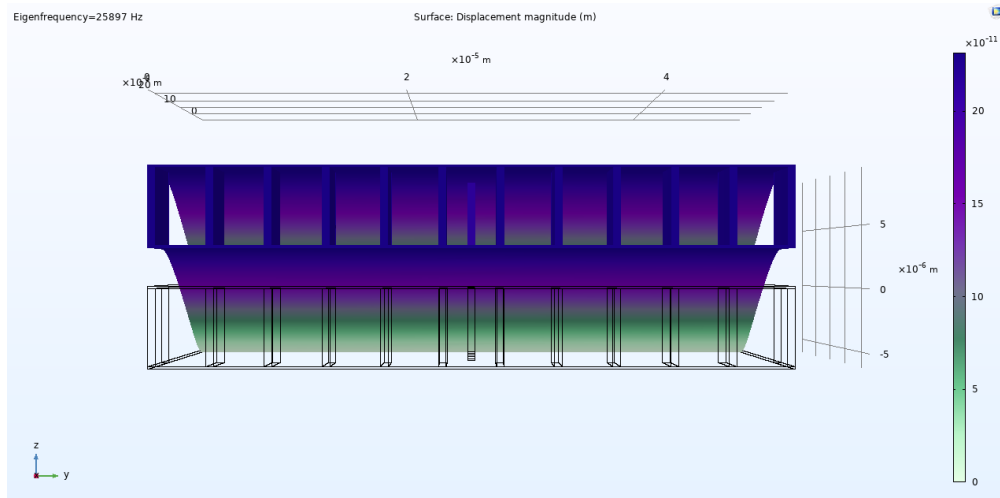


Figure 35: Mode shape of the square base pillar cantilever in the yz plane

Eigenfrequency (Hz)	Factor (1)
25897	0.0051764

Figure 36: Figure of merit for the 3D cantilever with square base pillars

In the following I prepared a table in which I summarized how the figure of merit is dependent on the model and geometry I simulate. We want the ratio between the 2 figures of merit as high as possible, this shows how much we can optimize from the simple cantilever model. ΔW is defined as $W(L1 + L2) - W(L1)$

$FoM = \Delta W * L_{cell} / (L2 * W_{max})$	
$FoM_{simple_cantilever} = W_{max} - W(\text{right edge} - 40 \mu m) / W_{max}$	
MODEL	$FoM_{simple_cantilever} / FoM$
Best parametric combination with density=500 kg/m ³	459
Best parametric combination with density=200 kg/m ³	490
Cantilever with 6 equally spaced pillars	9
Cantilever with 3 equally spaced pillars	30
3 beam cantilever with 6 equally spaced pillars	23
3 beam cantilever with 3 equally spaced pillars	78
3D cantilever with 6 equally spaced pillars	9
3D cantilever with 6 equally spaced square base pillars	47

Figure 37: Relative bending of the different models with respect to the simple cantilever

Now I do the simulation of figure 33 changing the number of pillars. I can see that if I reduce the number of pillars the figure of merit decreases and so does the frequency, therefore

we get better results with a lower number of pillars but we lose in stability and durability of the cantilever. In figure 38 I show the results:

Eigenfrequency (Hz)	Factor (1)	Eigenfrequency (Hz)	Factor (1)
18120	0.0025242	16259	0.0020397

(a) Factor for the cantilever with 3 square base pillars, improvement=96

(b) Factor for the cantilever with 2 square base pillars, improvement=118

Eigenfrequency (Hz)	Factor (1)
13065	0.0013064

(c) Factor for the cantilever with 1 square base pillars, improvement=185

Figure 38: Figure of merit and resonance frequency for cantilevers with different number of pillars

I consider now a change in the depth of the pillars, I simulate the model with 2 times and 3 times deeper pillars ($1.2 \mu m$ and $1.8 \mu m$ respectively) and compare the results with the ones obtained in figure 38.

Eigenfrequency (Hz)	Factor (1)	Eigenfrequency (Hz)	Factor (1)
27661	0.0058697	19020	0.0027649

(a) 6 pillars with double depth, improvement=41 (b) 6 pillars with triple depth, improvement=37

Eigenfrequency (Hz)	Factor (1)
19020	0.0027649

(c) 3 pillars with double depth, improvement=87

Eigenfrequency (Hz)	Factor (1)	Eigenfrequency (Hz)	Factor (1)
19796	0.0029782	16949	0.0022030

(d) 3 pillars with triple depth, improvement=81 (e) 2 pillars with double depth, improvement=110

Eigenfrequency (Hz)	Factor (1)
17486	0.0023344

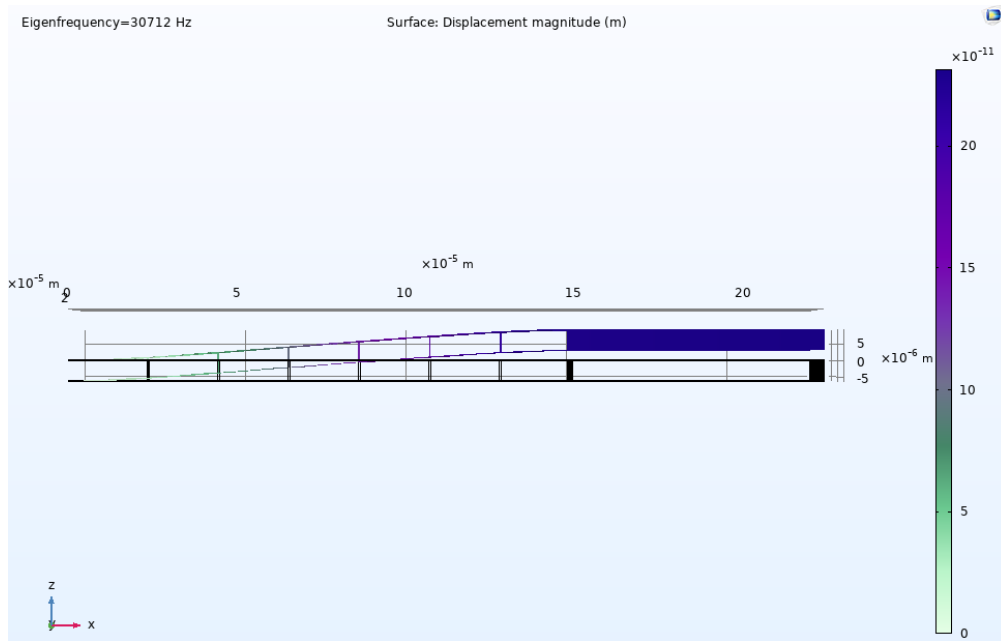
(f) 2 pillars with triple depth, improvement=103

Eigenfrequency (Hz)	Factor (1)	Eigenfrequency (Hz)	Factor (1)
13413	0.0013722	13691	0.0014232

(g) 1 pillar with double depth, improvement=176 (h) 1 pillar with triple depth, improvement=170

Figure 39: Resonance frequency and figure of merit for different depths pillars

The cantilever used in the previous simulations is fine but being $L_2=50 \mu m$ we have to pay attention to measure the cell size in the correct point, we do not have a big error margin because the cell size is already $40 \mu m$, which is almost equals to L_2 . In order to increase this margin I increased L_2 up to $75 \mu m$, in this way we have a slightly worse optimization regarding the relative bending but it is easier to place the cell on the cantilever. The mode shape is shown in figure 40 and the improvement in this case is equal to 28.

Figure 40: Mode shape in the xz plane for the cantilever with $L_2=75 \mu m$

Eigenfrequency (Hz)	Factor (1)
30712	0.0085015

Figure 41: Figure of merit for the cantilever with $L_2=75 \mu m$

3.6 Stress simulations and applied load

Then I placed on top of L_1 a gold layer of the same size of the top and bottom beams, I applied a power of $100 \mu W$ to the top surface of gold and studied the stress and bending of the entire structure. The results of the bending which influence the cantilever mode shape are shown in figure 42. This that I am doing now is a stationary simulation. I want to simulate how the cantilever is affected by a power supply applied on the gold layer.

I will do now a frequency sweep on the cantilever and see the resonance curve, I expect to have the maximum of amplitude corresponding to the resonance frequency.

I started to do simulation of the resonance plot without applying power to the gold layer.

I considered a quality factor of $Q=50$, therefore the damping ratio is $\xi = 1/(2 * Q) = 0.01$. Keeping this in mind, I made the cantilever move under a frequency sweep which went from 1 kHz to 151 kHz, with a step of 5 kHz. From now on I considered L_1 to be $150 \mu m$ and T_1 300 nm. These choices are considered for fabrication purposes.

The fundamental mode is shown in figure 43, whereas in figure 44 I have the oscillation amplitude of the cantilever in function of the frequency. I can see that the resonance frequency of the first mode is a complex number, this is coherent because I simulated a damping in the system. Moreover, the real part of the eigenfrequency (99436 Hz) is very close to the frequency

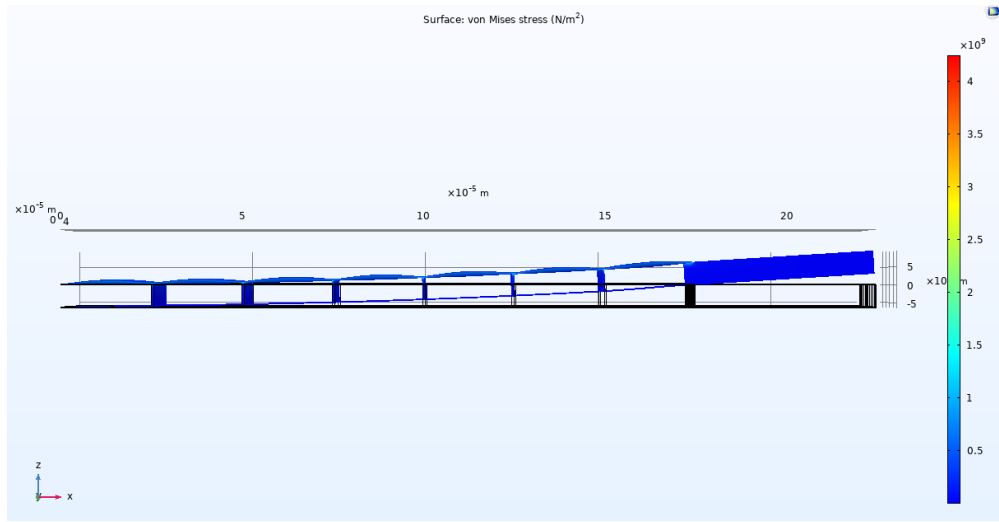


Figure 42: Stress in cantilever due to the applied power on the gold layer

in which there is the peak of amplitude of the cantilever (101 kHz). This is a coherent result. The maximum oscillation is $5 \mu\text{m}$. The force applied is $2 \mu\text{N}$ to the right edge of the cantilever.

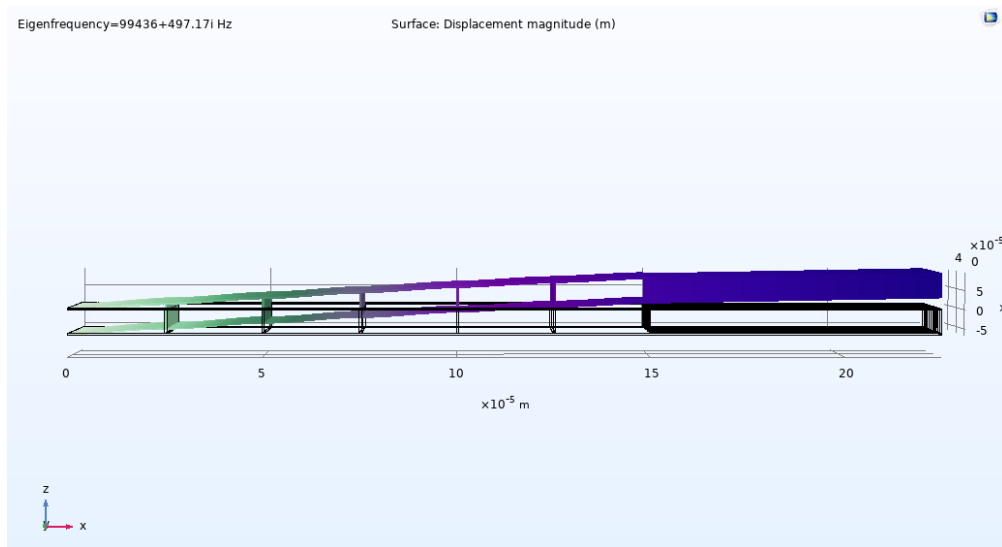


Figure 43: Mode shape of the cantilever considering quality factor of 50 with $2 \mu\text{N}$ on the right edge

The second resonance frequency is seen at 305 kHz (figure 45), also in this case I get a very similar result between the eigenfrequency simulation (figure 46) and the maximum peak of amplitude. Moreover in this case the peak for the oscillation is way smaller (just $1.1 \mu\text{m}$), this is due to the damping of the system.

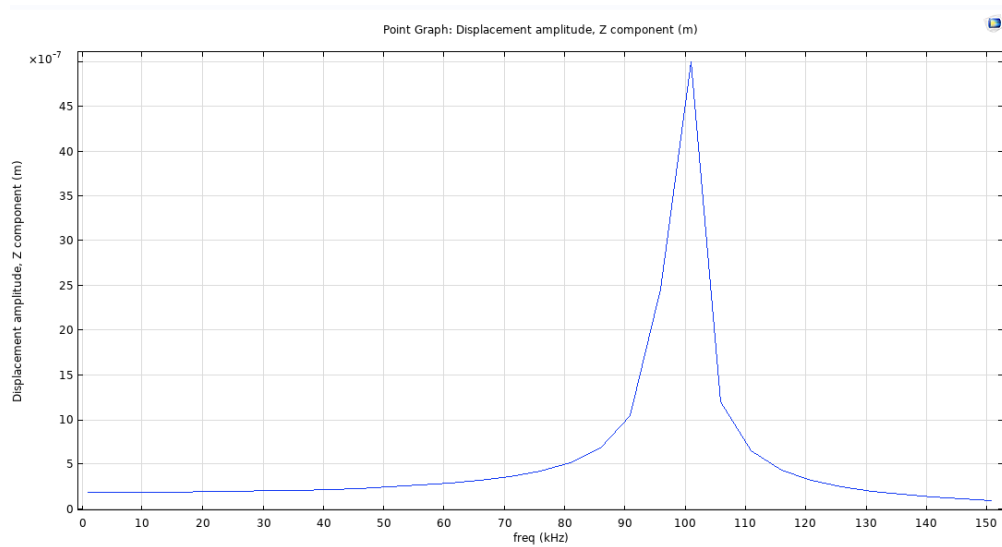


Figure 44: Frequency sweep of the displacement of the cantilever with a load applied

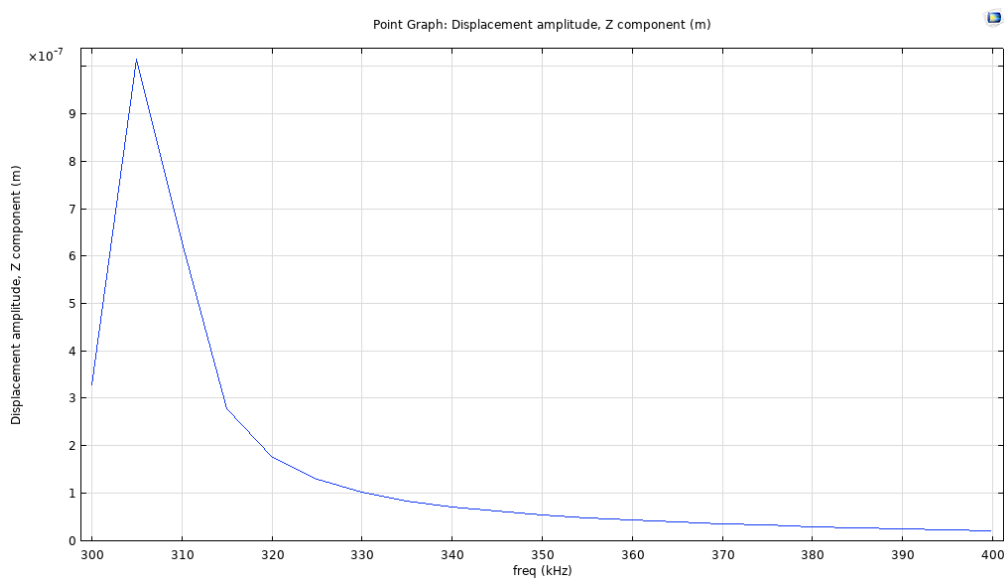


Figure 45: Second eigenfrequency for the cantilever with gold on top

Eigenfrequency (Hz): 3.0667E5+1533.3i

Figure 46: Second eigenfrequency for the cantilever with gold on top

I continue to simulate the cantilever's frequency response with an actuation of only force. This simulation with an external excitation is useful because I aim at simulate the system with a power actuation on gold, so this applied load is important to have an intermediate result on

how the cantilever responds to external excitations. I considered a force acting on the right edge of the cantilever and I fixed the quality factor to 10 ($Q=10$), in this way the peak width has increased. The system simulated was with square base pillars and gold on top of L1. The step for each point in figure 47 is 200 Hz. Considering that the simulated eigenfrequency is shown in figure 48, we can see that the resonance plot shows a coherent result, because the peak is found at the same frequency of the simulated eigenfrequency calculated with the eigenfrequency simulation.

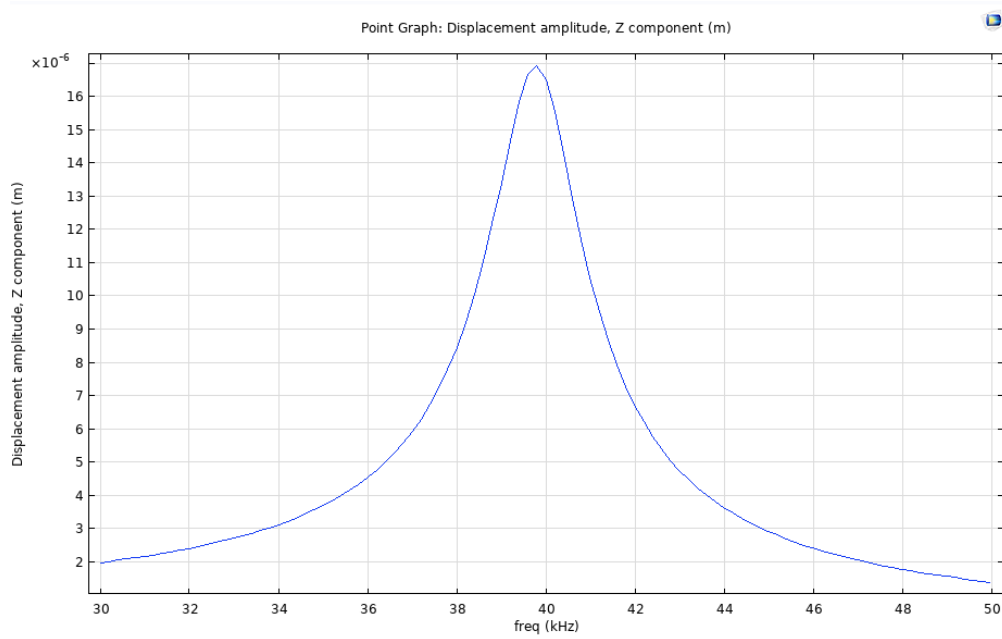
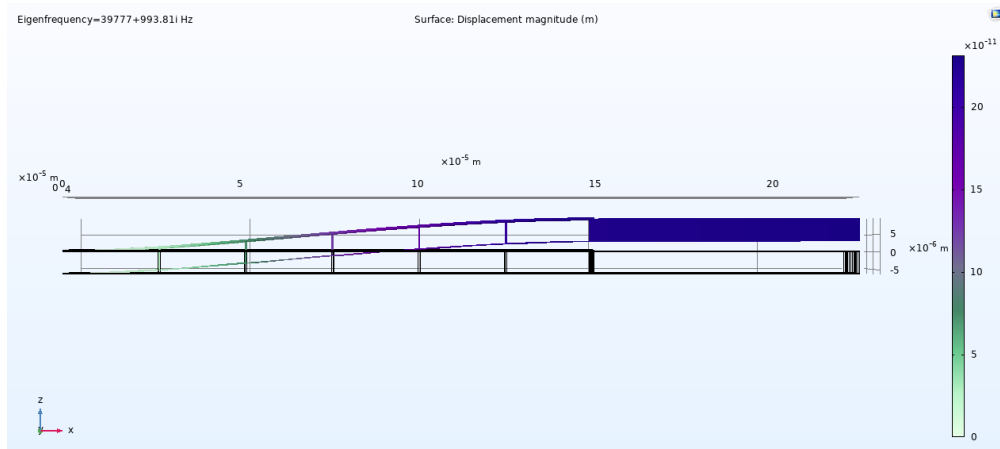


Figure 47: Resonance plot with $Q=10$ and applied load

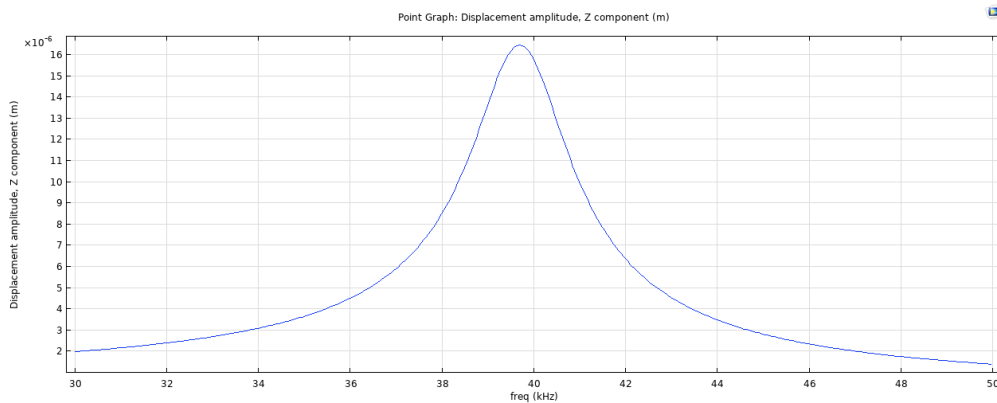
Eigenfrequency=39777+993.81i Hz

Figure 48: Simulated eigenfrequency for the cantilever with $Q=10$

The fundamental mode for this system is shown in figure 49

Figure 49: Fundamental mode for $Q=10$ and load applied

These simulations are conducted on 3D geometries, this results in a slow down of the results, because each simulation takes many hours to finish, in order to solve this problem I used the adaptive frequency sweep setting for the resonance plot construction. In this way the program will sample a lot of points of the curve around the maximum slope of the curve, and sample less point where the curve is horizontal, using this approach I can speed up the simulation that now take just some minutes and I have also quite continuous curves, because now I have an high sampling rate around the points of interest of the curve, where the displacement changes a lot. I considered a step in frequencies of 50 Hz from 30 kHz to 50 kHz, which is our spectral region of interest. The resonance plot for this simulation is shown in figure 50.

Figure 50: Resonance plot with $Q=10$, applied load and adaptive frequency sweep

3.7 Temperature actuation

Now I am going to carry out simulations regarding the frequency response of the cantilever with a temperature actuation, I do multiphysics simulations in this case because I will consider both mechanics and heat conduction in materials.

I did the 2D simulation of the frequency response of the cantilever with temperature actuation. I considered a gold layer along L1 and I heated it with an harmonic perturbation of 30 K, so the temperature was ranging from 293.15 K of plus-minus 30 K. I considered an isotropic dumping of 0.05 and a quality factor of 10, in this way the resonance frequency is $(36713+917i)$ Hz, as shown in figure 51. In this case the gold layer is 300 nm thick.

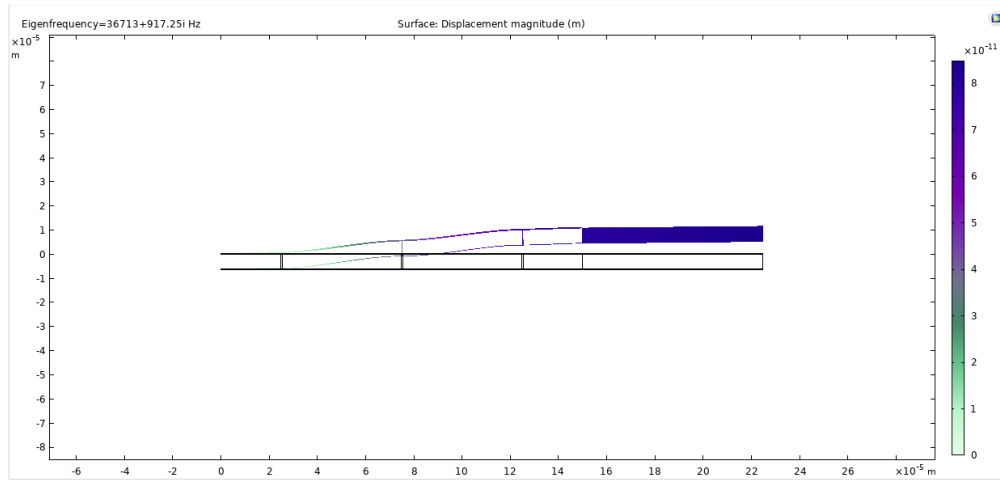


Figure 51: Fundamental mode of the cantilever with temperature actuation

I then plotted the oscillation amplitude of the cantilever with respect to frequency, the result is shown in figure 52, the peak is seen at a slightly lower frequency than the expected resonance frequency, however the results are quite close to each other, the peak is around 35.5 kHz. The step is 50 Hz from 20 kHz to 50 kHz.

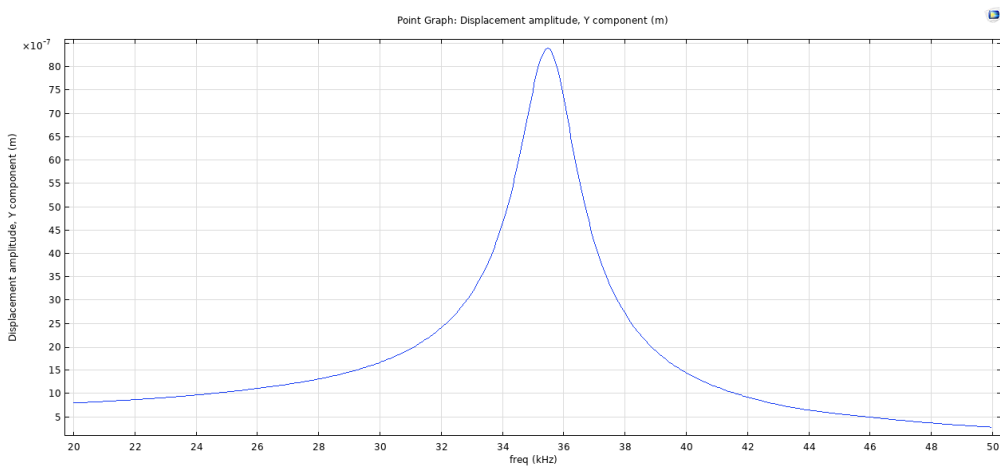


Figure 52: Frequency response of the cantilever for 30 K perturbation

I then plotted the same oscillation amplitude but in the case of an harmonic perturbation of 60 K, which is double the perturbation of before. In this case the oscillation amplitude of the cantilever doubles too.

I also used 15 K temperature perturbation and I saw that the oscillation is directly proportional to the harmonic perturbation in temperature, therefore if we double the perturbation the oscillation will double too.

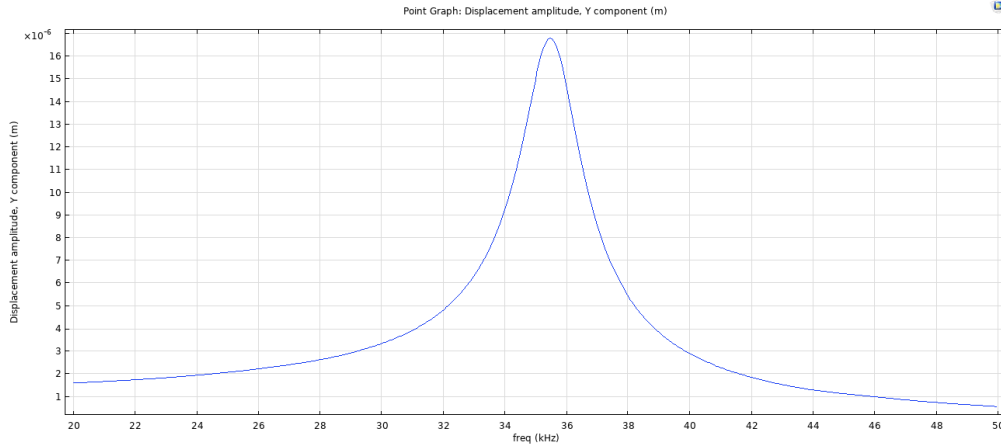


Figure 53: Frequency response of the cantilever for 60 K perturbation

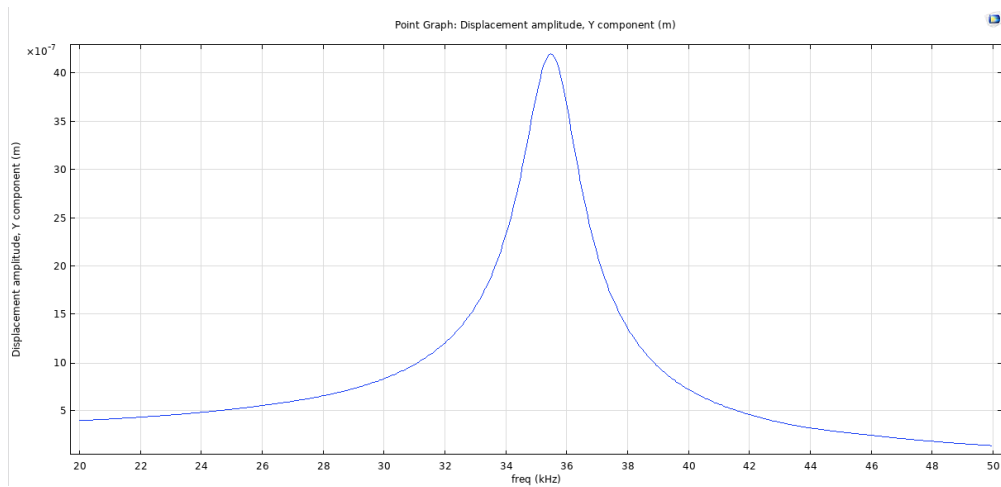


Figure 54: Frequency response of the cantilever for 15 K perturbation

At this point I changed the position of gold and I simulated the device, now the gold layer is on top of L1+L2 and not only L1 the fundamental mode is shown in figure 55. The resonance frequency has slightly decreased, going from $(36713+917i)$ Hz to $(33222+830i)$ Hz.

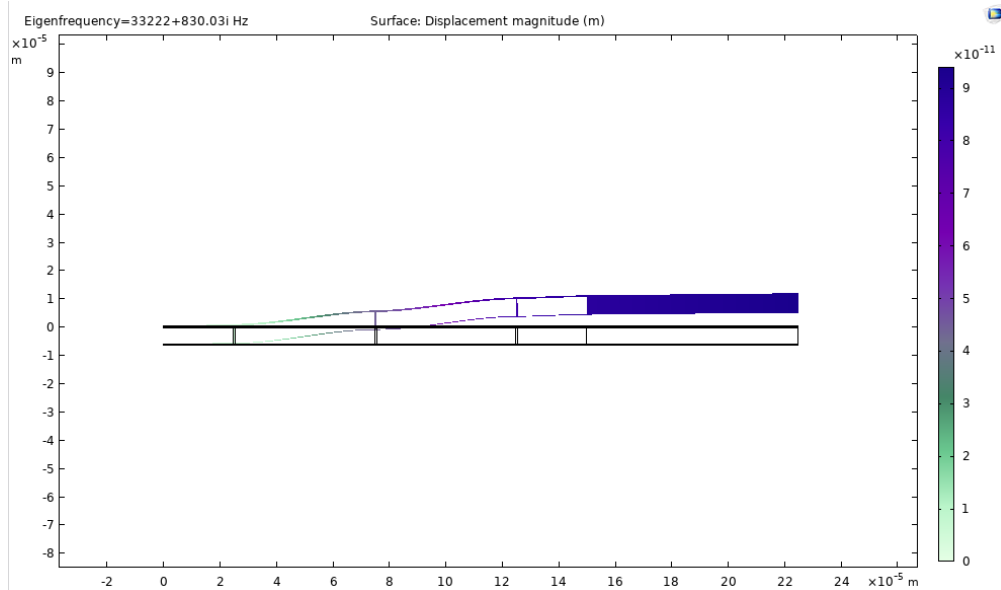


Figure 55: Fundamental mode of the cantilever with gold on L1+L2

I did a frequency analysis measuring the displacement amplitude of the cantilever with temperature actuation and I discovered that the oscillation is very similar to the case in which gold is deposited only on L1. I can then conclude that if I deposit gold on L1+L2 I still have a good actuation and good results. The curve of displacement amplitude with a temperature perturbation of 30 K is shown in figure 56, the peak is at 32.2 kHz, which is quite near the 33.2 kHz that I found during the eigenfrequency study. The step in the graph is 50 Hz.

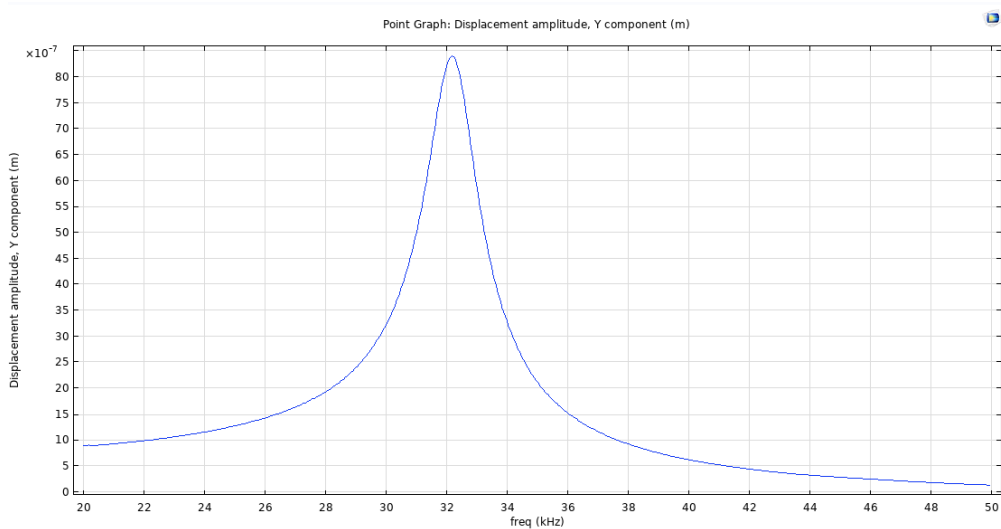


Figure 56: Frequency response for 30 K perturbation and gold on L1+L2

The peak of displacement for the case of gold layer on L1 is $8.4 \mu\text{m}$ as we saw in figure 52. The next simulations are done in order to choose which is the best position for the gold in order

to have the highest actuation possible. We want high actuation so that the signal will be high and we can measure a wider range of oscillations. I will consider in the following a thickness of gold equal to 50 nm, which will be the effective thickness of this layer during the fabrication.

In the case of gold layer on $L1/2$ I get the frequency response shown in figure 57. The pillars are equally spaced and the temperature perturbation will be the standard 30 K. We want the maximum displacement to be as high as possible, in this way we have a better actuation of the cantilever.

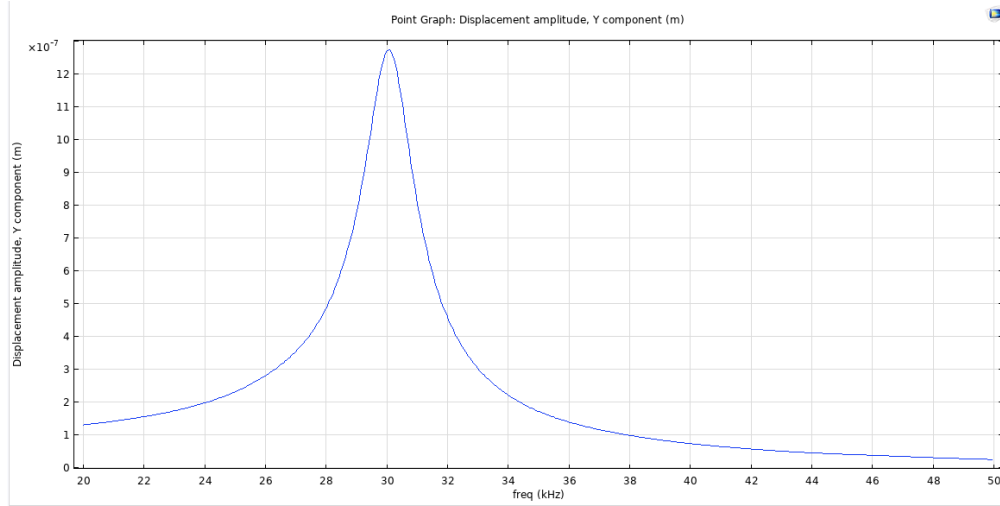


Figure 57: Frequency response with gold on $L1/2$

I am going to simulate now the device in the case of gold layer only on $L1/4$. I define $L1'$ the distance between the fixed edge on the left and the first pillar, in these simulations I am considering a cantilever with exactly 3 pillars, so $L1$ is being divided in 4 equally long parts by the pillars, therefore in this case $L1/4=L1'$ because a quarter of $L1$ is exactly the distance of the first pillar from the mechanical constraint. The frequency response for gold on $L1/4$ is shown in figure 58.

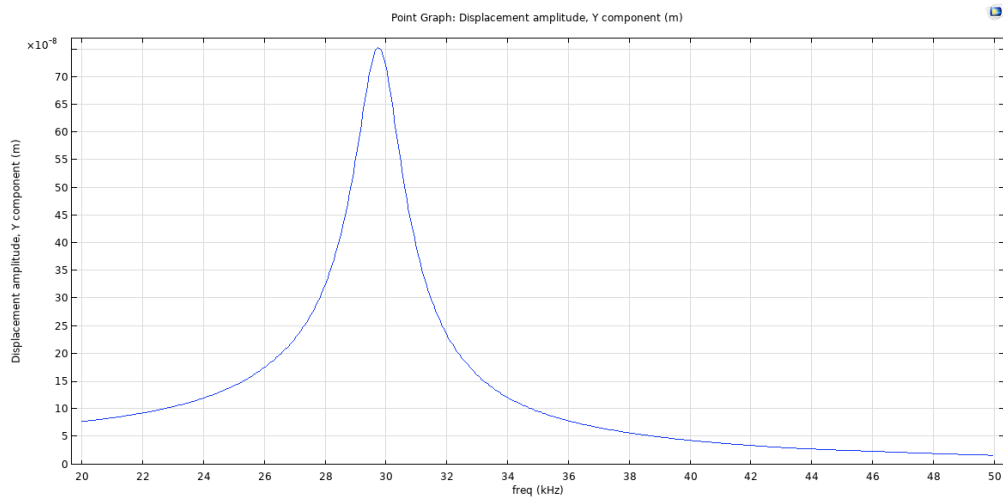


Figure 58: Frequency response with gold on L1/4

In the case of gold layer only on L1'/2 or L1'/4 I get the frequency response shown respectively in figure 59 and 60.

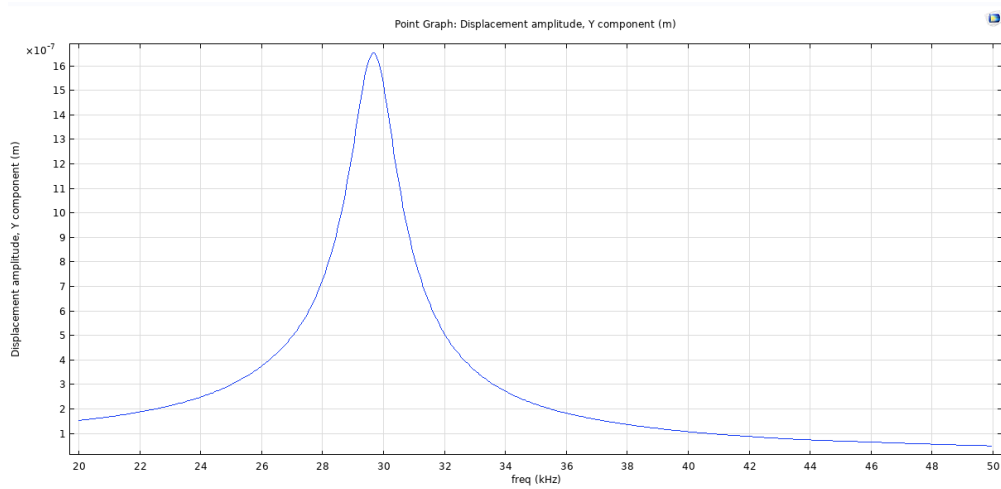
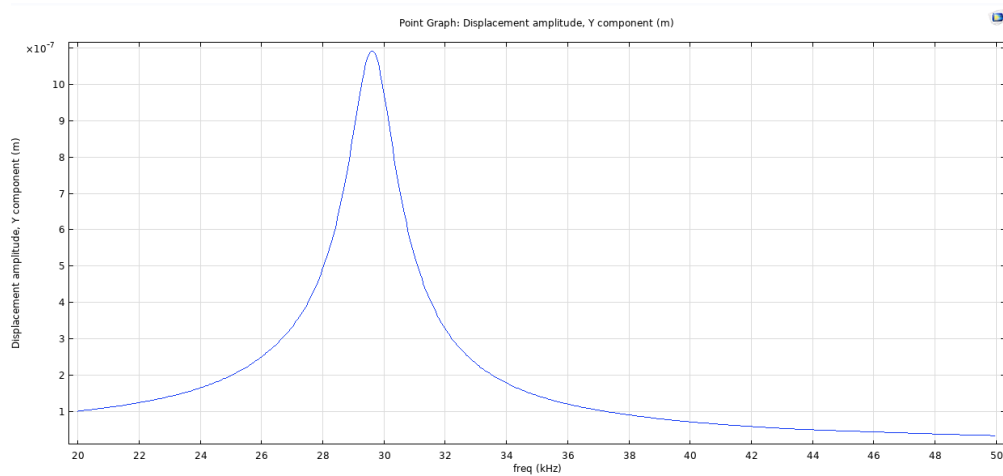
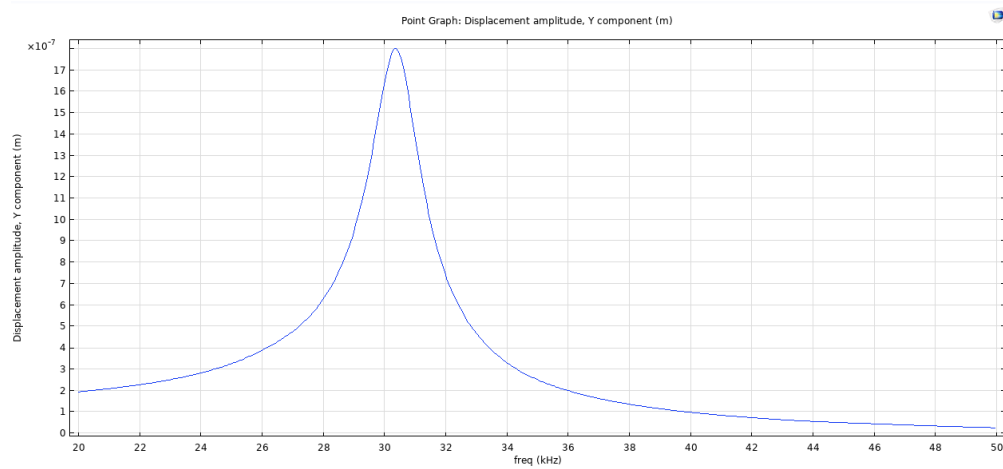


Figure 59: Frequency response with gold on L1'/2

Figure 60: Frequency response with gold on $L1'/4$

Now I need to simulate the frequency response of the cantilever in the case I have gold on all $L1$ and the gold thickness is 50 nm, so that I can compare these results (which were done with 50 nm gold layer) with the case of gold on $L1$. The result is shown in figure 61.

Figure 61: Frequency response with 50 nm gold on $L1$

Now I deposit 4 gold layers, each one starting from one of the pillars and having the length of $L1'/2$ (half the distance between each pillar), in this way it is possible to increase the actuation by quite a while (3 times higher actuation), I show in figure 62 the maximum displacement corresponding to the peak. Each layer is 50 nm thick, and I have applied the temperature perturbation to each one of them. This increase in actuation is due to the fact that now the gold layers sum up their effect because I deposited gold layers always on the first half of each $L1'/2$, in this way the gold is bending in the same way in all the four stripes of gold and so the total bending and oscillation of the cantilever is maximized.

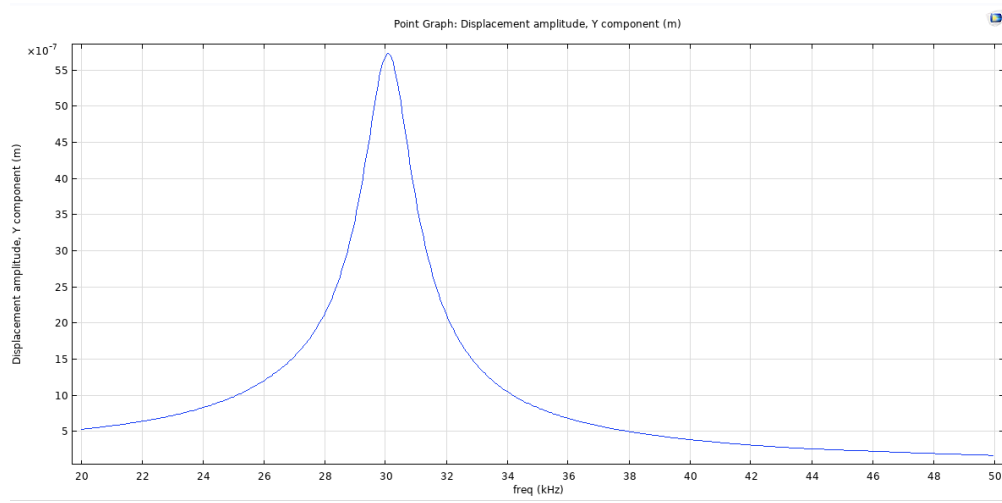


Figure 62: Frequency response with 4 equally spaced gold layers

3.8 Power actuation

In these simulations I managed to apply an harmonic boundary heat source on the top layer of gold. The perturbation is 100 W/m^2 . I simulated the amplitude of the cantilever's oscillation with the frequency domain perturbation step. The simulation was carried out from 20 kHz to 50 kHz with a step of 50 Hz. The peak of the amplitude is very near the resonance frequency, which in this case is $(31805 + 795.13i) \text{ Hz}$. This is very good because it means that the multiphysics simulation works. The gold layer is deposited all along L1. The fundamental mode is shown in figure 63 and the associated frequency response is shown in figure 64.

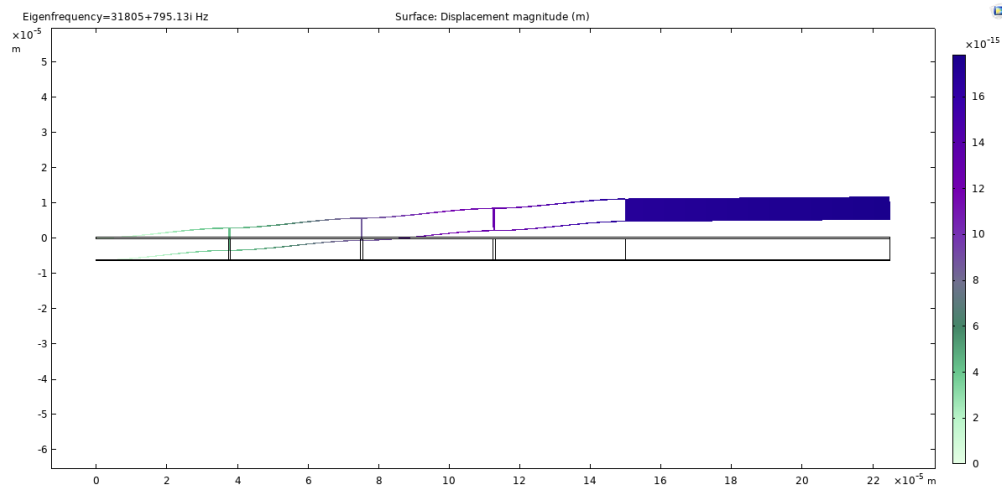


Figure 63: Fundamental mode in case of power actuation on all L1

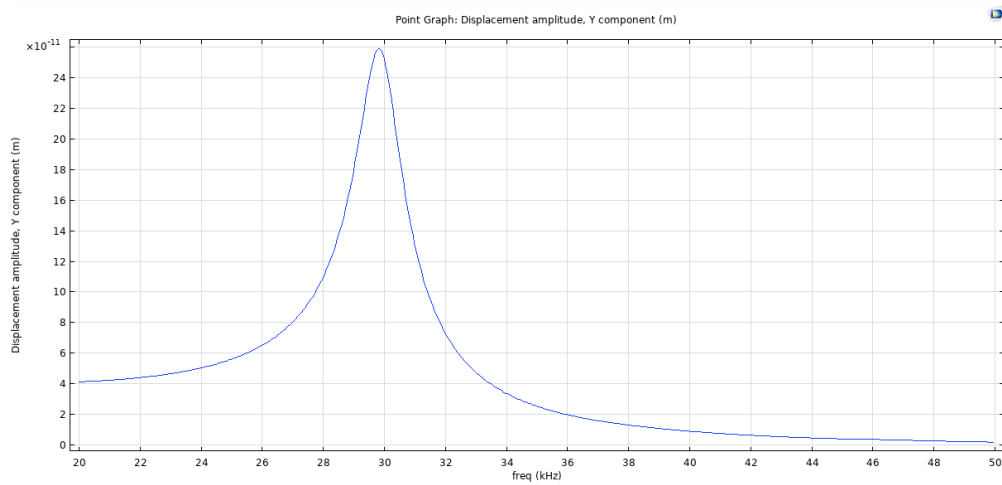


Figure 64: Frequency response in case of power actuation on all L1

In the previous simulation I applied the power perturbation all along the gold layer on L1. In the following simulations I will apply the power perturbation only on the first $L1'/2$ top of the gold layer.

The first simulation I am doing is the one in which the gold layer is all along L1, but still the power actuation is applied only on the first $L1'/2$. The frequency response is shown in figure 65.

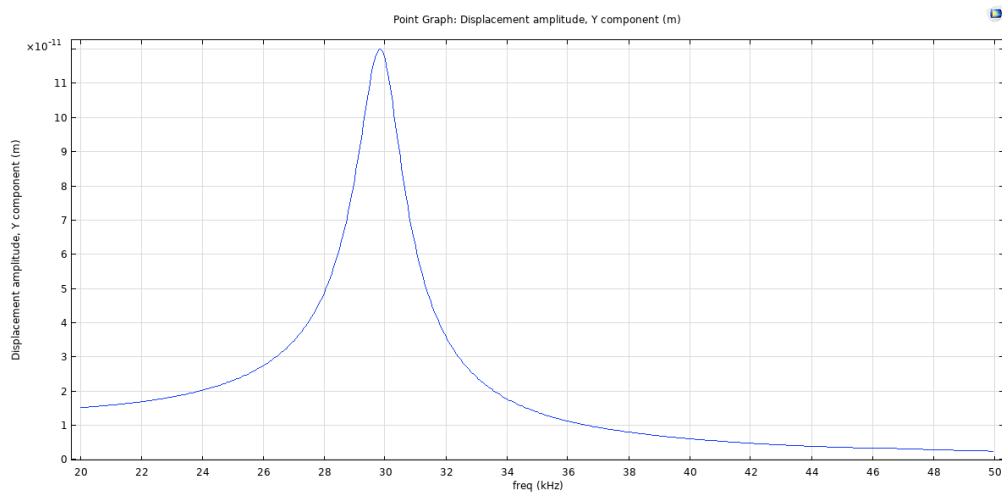


Figure 65: Frequency response in case of power actuation and gold on L1

Now I do the simulation in the case of gold layer deposited only on $L1/2$ and as usual the power actuation is applied only on the first $L1'/2$ of the gold layer.

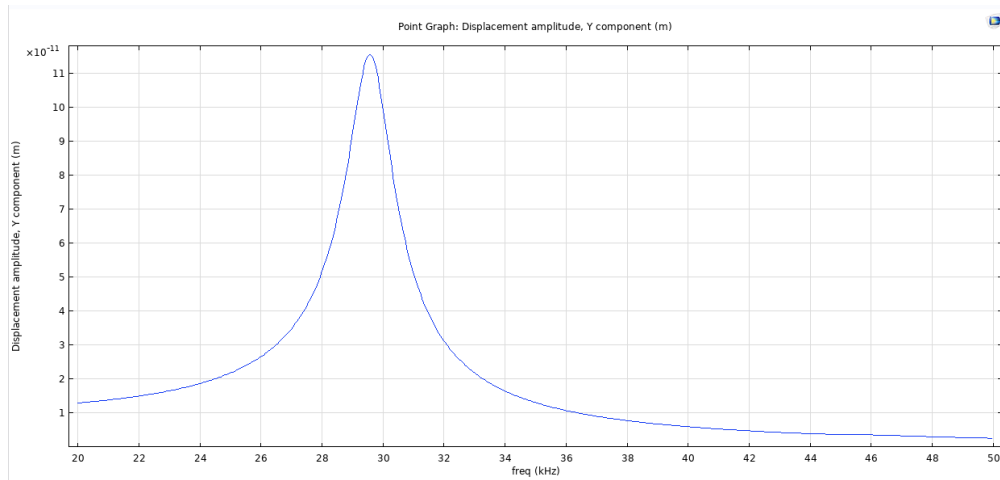


Figure 66: Frequency response in case of power actuation and gold on L1/2

I then simulate 3 other configurations for power actuation:

- The case in which the gold layer is on L1' (figure 67)
- The case with gold on L1'/2 (figure 68)
- The case with gold on each L1'/2 (figure 69), where the actuation has been done always only on the first gold strip in L1'/2

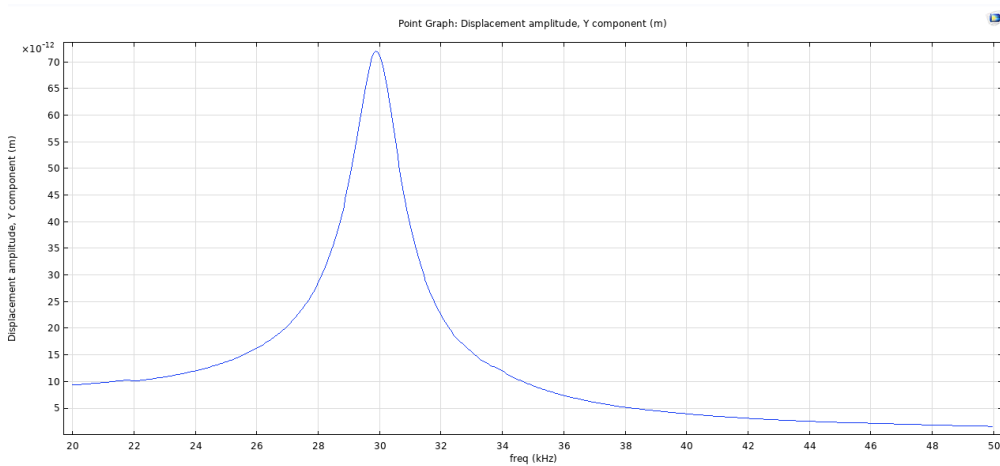
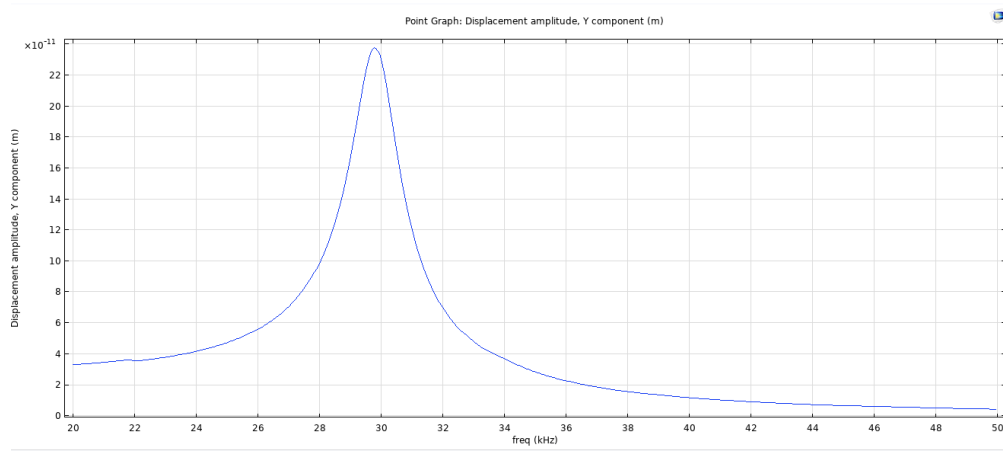
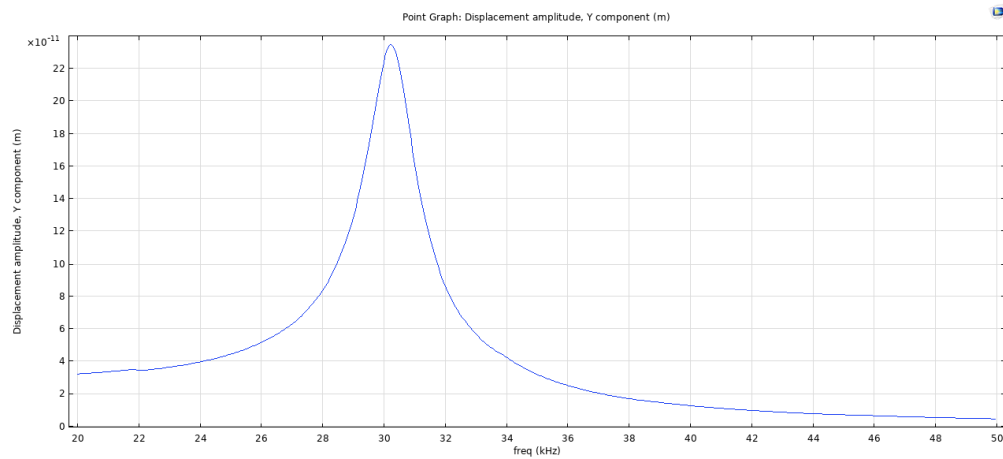


Figure 67: Frequency response in case of power actuation and gold on L1'

Figure 68: Frequency response in case of power actuation and gold on $L1'/2$ Figure 69: Frequency response in case of power actuation and gold on each $L1'/2$

In conclusion the best actuation is attainable in the case I deposit a gold layer on only the first $L1'/2$ or if I deposit it on every $L1'/2$, they have basically the same actuation. In the following I built a table in which I summarize all the peak actuations for all the different configurations.

	Maximum actuation [m]
Gold on L1	$12 \cdot 10^{-11}$
Gold on L1/2	$11.5 \cdot 10^{-11}$
Gold on L1'	$7.3 \cdot 10^{-11}$
Gold on L1'/2	$24 \cdot 10^{-11}$
Gold on each L1'/2	$24 \cdot 10^{-11}$

Figure 70: Power actuation for the different cantilever's designs

4 Design

The design of the cantilever and of the whole chip is an important task that I need to address. I started to plan a process flow that I will follow during the fabrication steps, I use CleWin 5 to create all my designs. In the following subsection I will show my process flow.

4.1 Process flow

The steps that I will carry out during the fabrication are the ones depicted in the process flow below





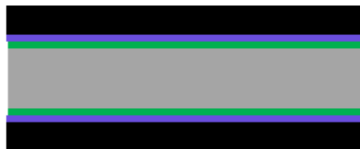

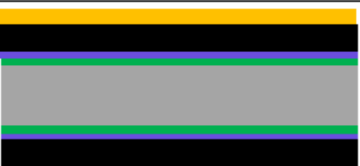
Step	Process description	Cross-section after process* (not in scale)
0	Substrate: test (DSP) silicon wafer	
0a	Wet thermal oxidation – Done by CMi staff <ul style="list-style-type: none"> Material: SiO₂ Thickness: 200 nm Machine: Centrotherm 	
0b	LPCVD – Done by CMi staff Silicon nitride deposition <ul style="list-style-type: none"> Material: 1s-SiN_x Thickness: 300 nm Machine: Centrotherm 	
0c	LPCVD – Done by CMi staff Sacrificial material deposition <ul style="list-style-type: none"> Material: PolySi Thickness: 6 um Machine: Centrotherm 	
1	OXYGEN PLASMA <ul style="list-style-type: none"> Machine: Tepla Z02 5' Strip high 	
2a	COATING (Lithography 1) <ul style="list-style-type: none"> Machine: ATMsse OPTIspin SB200 Z07 CSAR62 13 coating 1500 rpm 	
2b	E-BEAM LITHOGRAPHY (Lithography 1) Patterning of pillars, trenches and walls <ul style="list-style-type: none"> Machine: Raith EBPG5000+ Z07 Critical Dimension: 300 nm 	

Figure 71: Page 1 process flow

2c	<p><i>DEVELOPMENT (Lithography 1)</i></p> <ul style="list-style-type: none"> Manual development Z07 	
3	<p><i>DRY ETCHING</i></p> <p><i>High-aspect ratio trenches definition</i></p> <ul style="list-style-type: none"> Etched Material: PolySi Machine: AMS200 Z2 Etching Depth: 6 um 	
4	<p><i>RESIST STRIP</i></p> <ul style="list-style-type: none"> Machines: UFT + Tepla Gigabatch Z02 	
5	<p><i>LPCVD – Done by CMi staff</i></p> <p><i>Trench filling via silicon nitride deposition</i></p> <ul style="list-style-type: none"> Material: 1s-SiN_x Thickness: 500 nm Machine: Centrotherm 	
6a	<p><i>COATING (Lithography 2)</i></p> <ul style="list-style-type: none"> Machine: EVG150 Z6 Photoresist : AZ1512 1.1 um on LOR 5A 400nm 	
6b	<p><i>PHOTOLITHOGRAPHY (Lithography 2)</i></p> <p><i>Gold layer definition</i></p> <ul style="list-style-type: none"> Machine: MLA150 Z16 Critical Dimension: 2 um Critical alignment: 2 um 	

Figure 72: Page 2 process flow

6c	<p><i>DEVELOPMENT (Lithography 2)</i></p> <ul style="list-style-type: none"> Machine: EVG150 Z6 	
6d	<p><i>PHOTORESIST RESIDUES REMOVAL</i></p> <ul style="list-style-type: none"> Machine: Tepla Gigabatch Z2 Recipe: Strip_Low, 10" 	
7	<p><i>GOLD EVAPORATION</i></p> <ul style="list-style-type: none"> Material: Au Thickness: 50 nm Machine: EVA760 Deposition: RT 	
8	<p><i>LIFT-OFF</i></p> <ul style="list-style-type: none"> Machine: Photolithography bench Z1 Material: Au Solvents: Remover 1165 + IPA 	
9a	<p><i>COATING (Lithography 3)</i></p> <ul style="list-style-type: none"> Machine: ACS200 Photoresist: AZ ECI 3 um Au is fully covered by PR with at least 5-10um overlap 	
9b	<p><i>PHOTOLITHOGRAPHY (Lithography 3)</i> <i>Cantilever shape definition</i></p> <ul style="list-style-type: none"> Machine: MLA150 Z16 Critical Dimension: 2 um Critical alignment: 2 um 	
9c	<p><i>DEVELOPMENT (Lithography 3)</i></p> <ul style="list-style-type: none"> Machine: ACS 200 	

Figure 73: Page 3 process flow

10	<p><i>DRY ETCHING</i> <i>Cantilever shape definition</i></p> <ul style="list-style-type: none"> Etched Material: 1s-SiN_x/PolySi/ 1s-SiN_x Machine: AMS200 Z2 Etching Depth: 0.5/6/0.3 um 	
11	<p><i>RESIST STRIP</i> Machines: UFT remover</p>	
12	<p><i>Aluminum DEPOSITION</i></p> <ul style="list-style-type: none"> Material: Aluminum 1.5 microns Machine: EVA760 	
13	<p><i>DRY ETCHING</i> <i>Back-side</i></p> <ul style="list-style-type: none"> Material: 1s-SiN_x / Poly-Si Thickness: 0.5 um + 6 um Machine: AMS200 Z2 	
14a	<p><i>COATING (Lithography 4)</i></p> <ul style="list-style-type: none"> Machine: EVG150 Z6 Photoresist: AZ 10XT, 8 um 	
14b	<p><i>PHOTOLITHOGRAPHY (Lithography 4)</i> <i>Back-side openings</i></p> <ul style="list-style-type: none"> Machine: MLA150 Z16 Critical Dimension: 50 um Critical alignment: 10 um 	
14c	<p><i>DEVELOPMENT (Lithography 4)</i></p> <ul style="list-style-type: none"> Machine: EVG150 Z6 	

Figure 74: Page 4 process flow

14d	PHOTORESIST HARDENING <ul style="list-style-type: none"> Machine: Oven Z14 Parameters: 85°C, overnight 	
15	DRY ETCHING <i>Back-side openings</i> <ul style="list-style-type: none"> Etched Material: 1s-SiN_x/SiO₂/Si Machine: AMS200 Z2 Etching Depth: 300 nm / 200 nm / 380 um 	
16	RESIST STRIP <ul style="list-style-type: none"> Machines: UFT + Tepla Gigabatch Z2 	
17	WET ETCHING <i>KOH wet etching</i> <ul style="list-style-type: none"> Etched Material: Al and polySi Machine: Wet Bench Base Z14 	
18	WET ETCHING <i>BHF wet etching</i> <ul style="list-style-type: none"> Etched Material: SiO₂ Machine: Wet Bench Acid Z14 	

Figure 75: Page 5 process flow

4.2 Cantilever design

I start with the design of the cantilever. In the design file I create 15 different configurations of cantilevers, and I duplicate these 15 different cantilevers all around the wafer. The different configurations differ from the number of trenches, walls, pillars and also from the positions of gold on top. I will show in the following some of the cantilevers' configurations.

The figure 76 shows the cantilever design for chip 1. In the design I drew in red the walls and the trenches and in blue the gold layer, the trenches and walls are drawn in the same color because they are done using the same lithography step, in fact I will use e-beam lithography for both of these features, whereas I will use a laser writer with wavelength of 405 nm for the gold patterning. The trenches, walls and pillars are all done using e-beam because their critical dimensions is of 300 nm, which is a resolution that can not be achieved with standard laser writing machines, this exposure is depicted in step 2 of the process flow. The gold patterning is done using lift-off of the photoresists on which I deposited gold, the patterning of gold is shown in step 6 of the process flow. The cantilever is 225 μm long, with 3 trenches along L1 that are 37.55 μm distant to each other, the height of the cantilever is of 45 μm . Along L2 I have 9 parallel walls, distant 5 μm from each other.

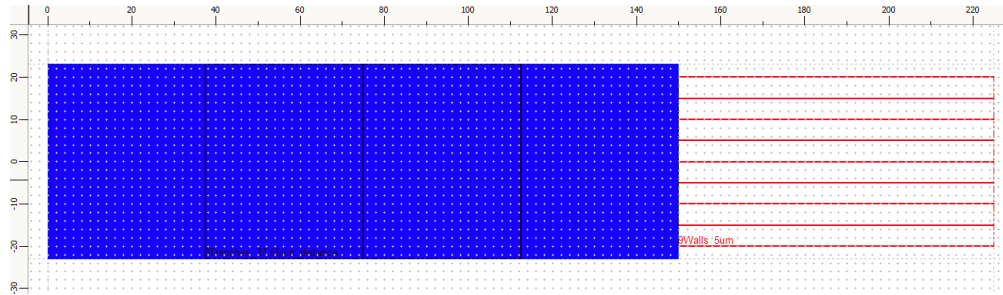


Figure 76: Cantilever design for chip 1

The cantilever from chip 2, shown in figure 77, has another configuration that I want to talk about. In this case I do not have trenches all along the cantilever but square base pillars, more particularly I designed 3 pillars along each horizontal spot where I want to sustain the cantilever, the pillars can be seen in figure 78. The pillars are equally spaced of the same distance as it was for the trenches in chip 1.

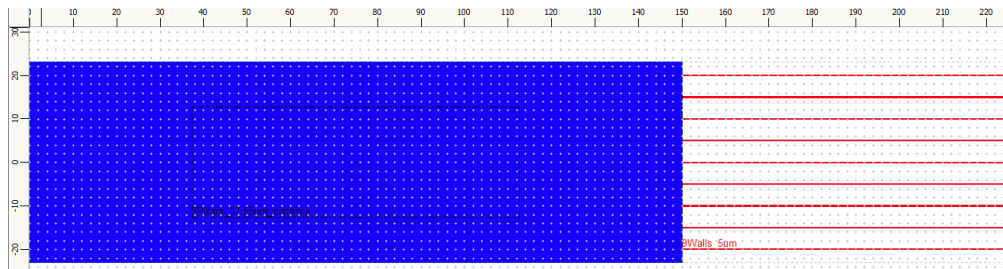


Figure 77: Cantilever design for chip 2

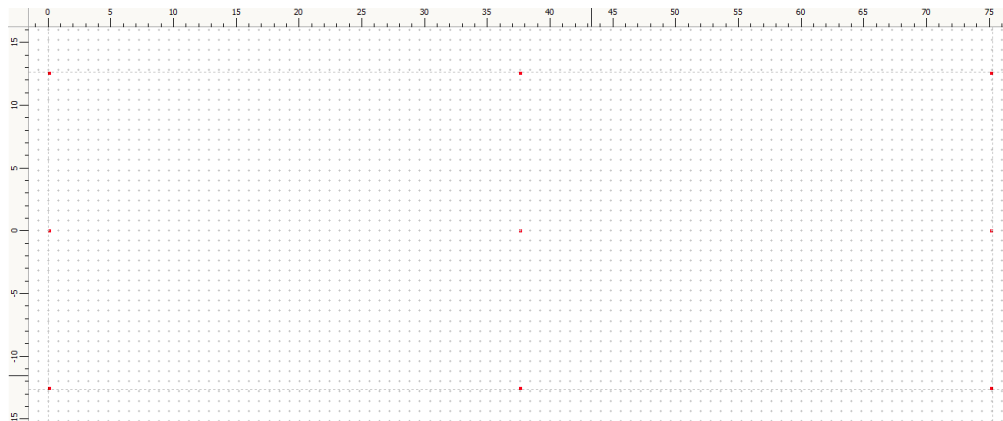


Figure 78: Pillars design in chip 2

Another configuration that I want to show is the one in figure 79, this is chip 7. In this case I have 12 parallel walls along L2 which are $4 \mu m$ distant between each other, then I have 5 trenches distant $25 \mu m$ between each other and more importantly in this case the gold layer is

not all along L1 but it is deposited on each $L1'/2$, in this way the actuation is maximized.

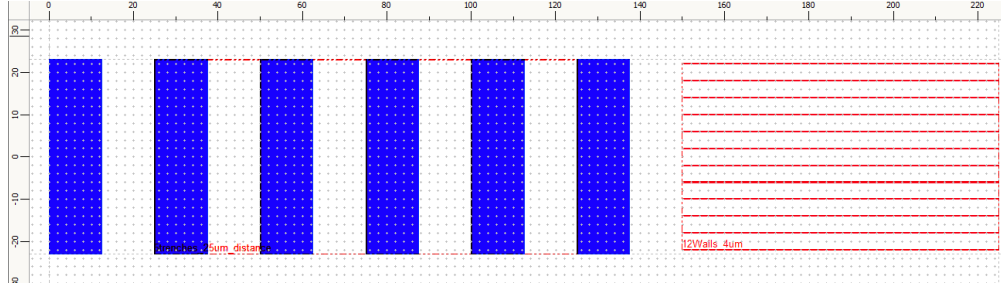


Figure 79: Cantilever design for chip 7

I also designed a standard cantilever, that could be useful to compare at the end with the modified designs, the standard cantilever design can be found in figure 80, this is chip 11.

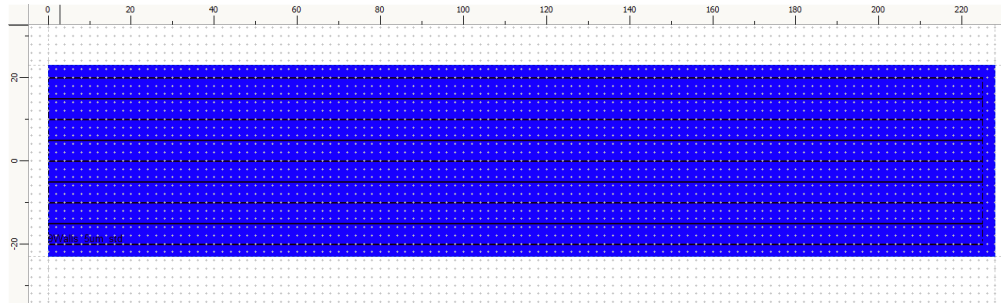


Figure 80: Cantilever design for chip 11, standard cantilever

All the other chips are made of different combinations of these chips above. I will write down in the following the features for the 15 different chips.

- Chip 1: cantilever with 3 trenches, 9 walls and gold on L1
- Chip 2: cantilever with 3 pillars, 9 walls and gold on L1
- Chip 3: cantilever with 5 pillars, 9 walls and gold on L1
- Chip 4: cantilever with 5 pillars, 9 walls and gold on each $L1'/2$
- Chip 5: cantilever with 5 trenches, 6 walls and gold on each $L1'/2$
- Chip 6: cantilever with 5 trenches, 9 walls and gold on L1
- Chip 7: cantilever with 5 trenches, 12 walls and gold on each $L1'/2$
- Chip 8: cantilever with 7 pillars, 9 walls and gold on each $L1'/2$
- Chip 9: cantilever with 7 trenches, 9 walls and gold on each $L1'/2$
- Chip 10: cantilever with 3 trenches, 6 walls and gold on L1
- Chip 11: standard cantilever

- Chip 12: cantilever with 5 trenches, 9 walls and gold on each $L1'/2$
- Chip 13: cantilever with 3 pillars, 9 walls and gold on each $L1'/2$
- Chip 14: cantilever with 3 trenches, 9 walls and gold on each $L1'/2$
- Chip 15: cantilever with 3 trenches, 6 walls and gold on each $L1'/2$

4.3 Chip design

Now that I finished with the design of the cantilever I need to design the chip that will hold the cantilever, from technology I need a chip compatible with AFM machines in Nanosurf, discussing with the experts we considered to design the chips in order to be 1.55 mm of height and 3.6 mm of width.

I need to define the cantilever shape from the rest of the wafer, this is the third lithography that I will do. This step of defining the cantilever shape can be seen in figure 81, in this way I define from the front side the chip that will have these dimensions and this shape, I will etch through the green-ish area until I reach the SiO_2 , so I will etch $ls - SiN_x/Poly - Si/ls - SiN_x$ for a total depth of $6.8 \mu m$, I can do this operation because the resist is a positive resist, so the exposed part will be the only one that will be eliminated during the development step.

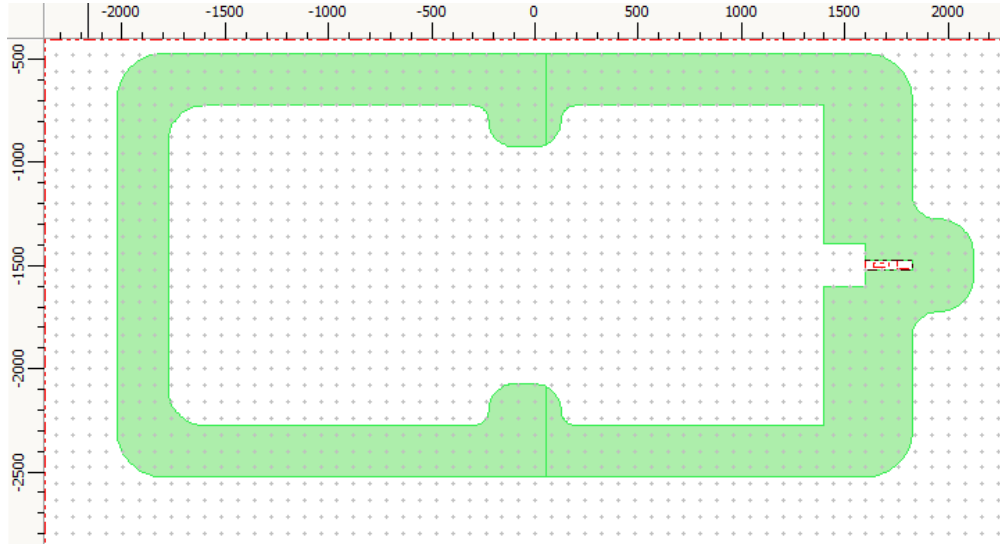


Figure 81: Cantilever shape lithography step

I also need to release the cantilever from the back, therefore I need to etch through the back side, this etching must be done in alignment to the front side of figure 81, the lithography step that will allow me to make apertures on the back side is shown in figure 82, the backside pattern is shown in light blue and it is aligned with the front side cantilever shape definition layer. I considered two $50 \mu m$ wide bridges that connect the chip to the wafer, in this way the chip will still be attached to the wafer even after complete etching of the wafer's thickness.

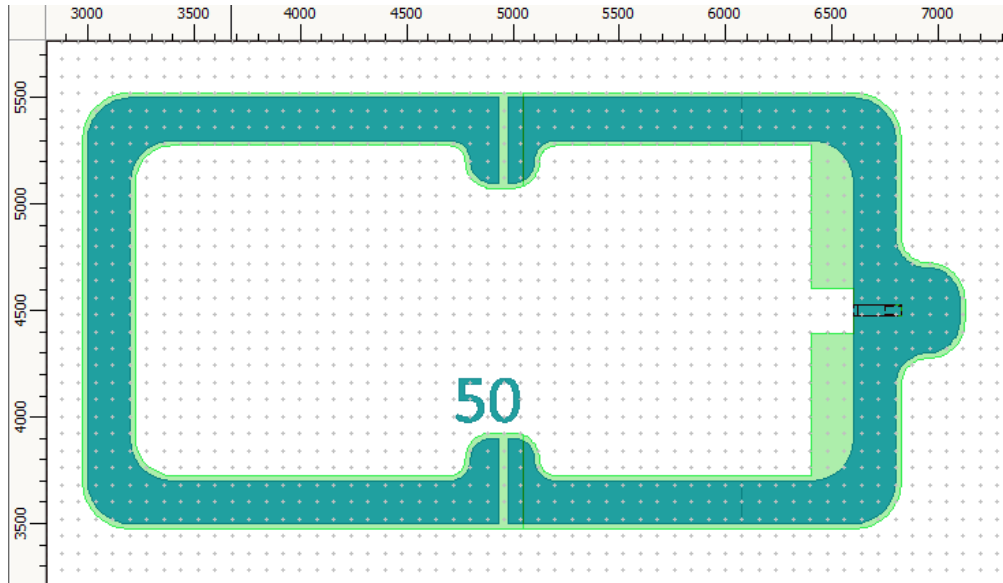


Figure 82: Design chip

Therefore, if we put together the design of the cantilever with the design of the chip we achieve the complete chip design for this project, I can see the complete design of one of the chips in figure 83, where I drew with the gold layer the type of cantilever inside the chip, in this case the cantilever is made of 5 trenches and 9 walls.

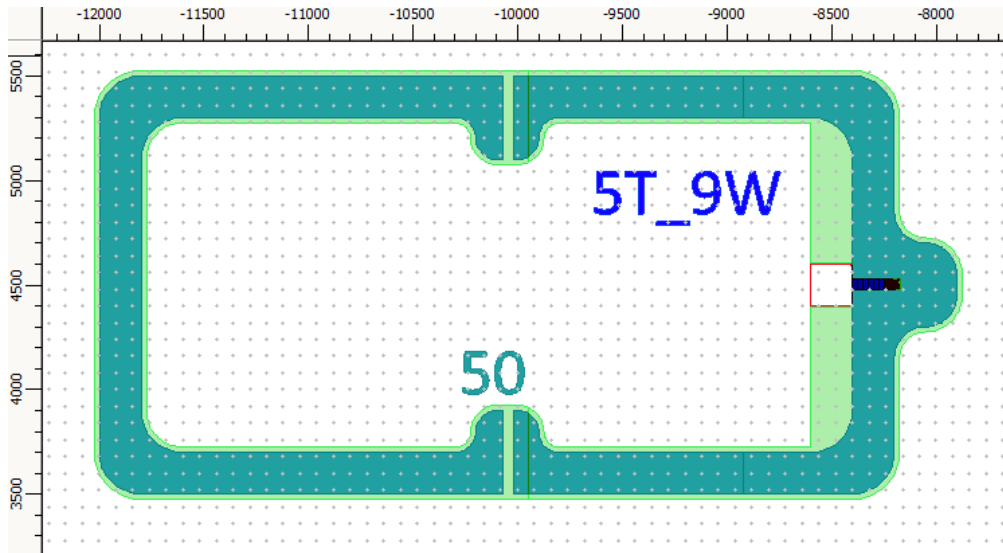


Figure 83: Complete chip design

In conclusion the complete design for the whole wafer is shown in figure 84, in which I duplicated all the chips multiple times in order to have an higher number of working chips at the end. At the four edges of the wafer I also placed alignment marks that are of fundamental

importance for a correct alignment between the various lithography steps.

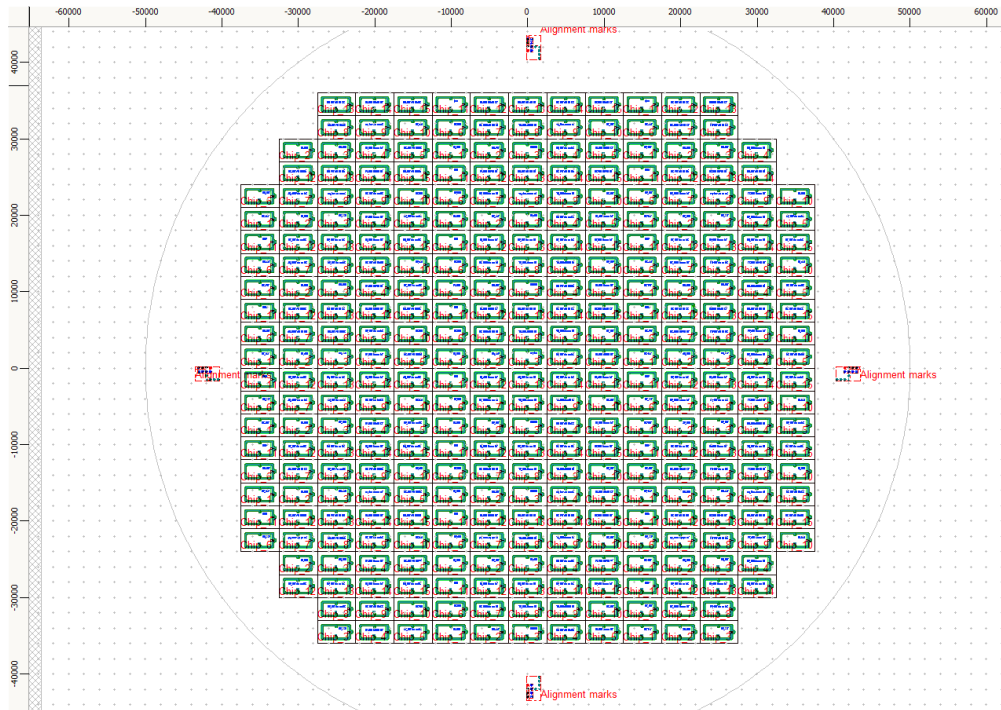


Figure 84: complete wafer design

5 Fabrication

All the fabrication steps are done inside the CMi (Center of MicroNanoTechnology) which is a complex of clean rooms and processing equipment for the training and scientific experimentation. I detail the machines used in the appendix A.

I started my fabrication process testing which should be the correct width of the bridges from the backside. I call the bridge the aperture seen in figure 82, in that pictures I considered bridges of $50\text{ }\mu\text{m}$ width, that will be the slice of Si which will sustain the chip once I etched all the way through and released the cantilevers. This is an important step in my project so I need to accurately chose which is the best width of the bridge for which I have acceptable sustainability of the chip weight.

I drew a new design made of chips with different bridge's widths, in this design I just have one layer, because I just want to check the stability of the bridges. I considered 5 different widths for the bridges: $50\text{ }\mu\text{m}$, $75\text{ }\mu\text{m}$, $100\text{ }\mu\text{m}$, $125\text{ }\mu\text{m}$ and $150\text{ }\mu\text{m}$. The 5 different chips from the design can be seen in figure 85. I will chose the width for which the chips will be enough resistant and easy to cleave too.

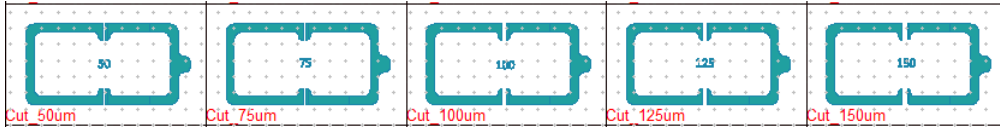


Figure 85: Test for the different widths of the backside bridges

I coated the wafer with $8\text{ }\mu\text{m}$ thick positive resist, then exposed using MLA 150, which is a mask-less aligner which can quickly expose a wafer with a UV light. Then I developed the wafer and I etched all the way through. The wafer that I ordered in CMi is a double side polished Si wafer with thickness $380\text{ }\mu\text{m}$, I etched in AMS200 for 1 hour and 15 minutes and the results are shown in figure 86, this picture was done inside the clean room with the optical microscope, I managed to set the focus on the top surface and then focused on the etched surface, in this way I can manage to find the etching depth of my wafer with sensitivity of $1\text{ }\mu\text{m}$, the etching depth can be seen in the ΔZ data in the bottom right of figure 86. On the front side of the wafer I have $1.5\text{ }\mu\text{m}$ Al to recreate the chip of the main project, which has Al on top in order to protect the front side when I do backside etching.

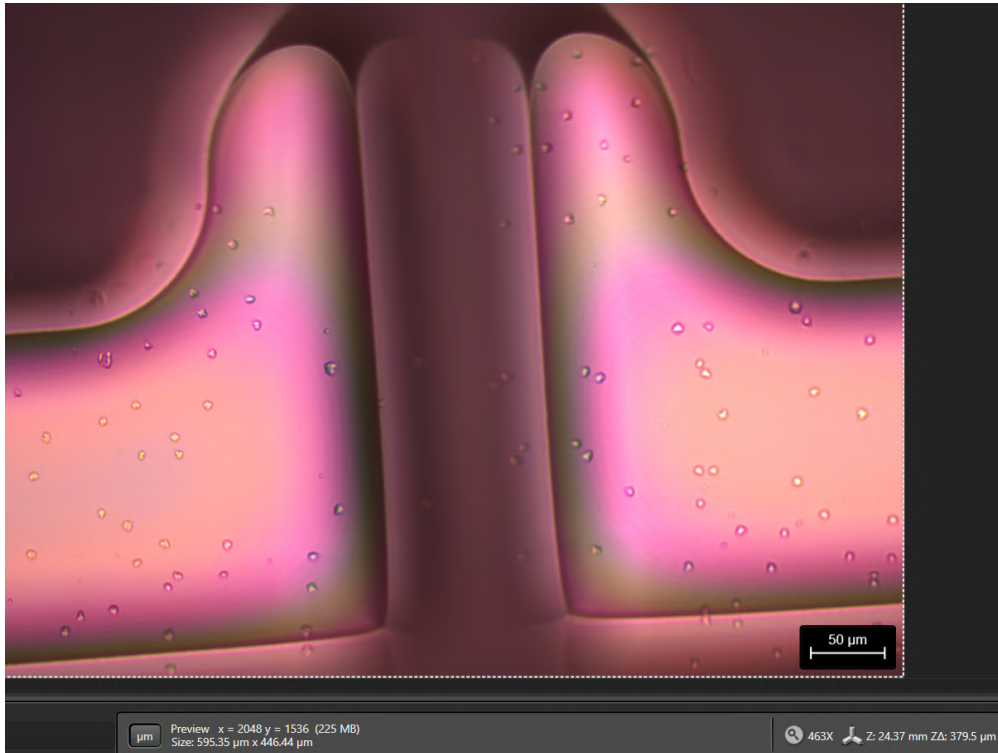


Figure 86: Complete etching of test wafer with design of multiple bridges

I then needed to etch the $1.5\ \mu\text{m}$ of Al with 40 % KOH, the result is quite good, now there is no more Al and also the resist on the other side is completely etched, this is not a problem because with this wafer I want to test the various chips and see which width is the best for cleaving. The Al was on the front side. Figure 87 is from the backside, so from the side in which I etched. I immersed the wafer for 5 minutes in KOH.

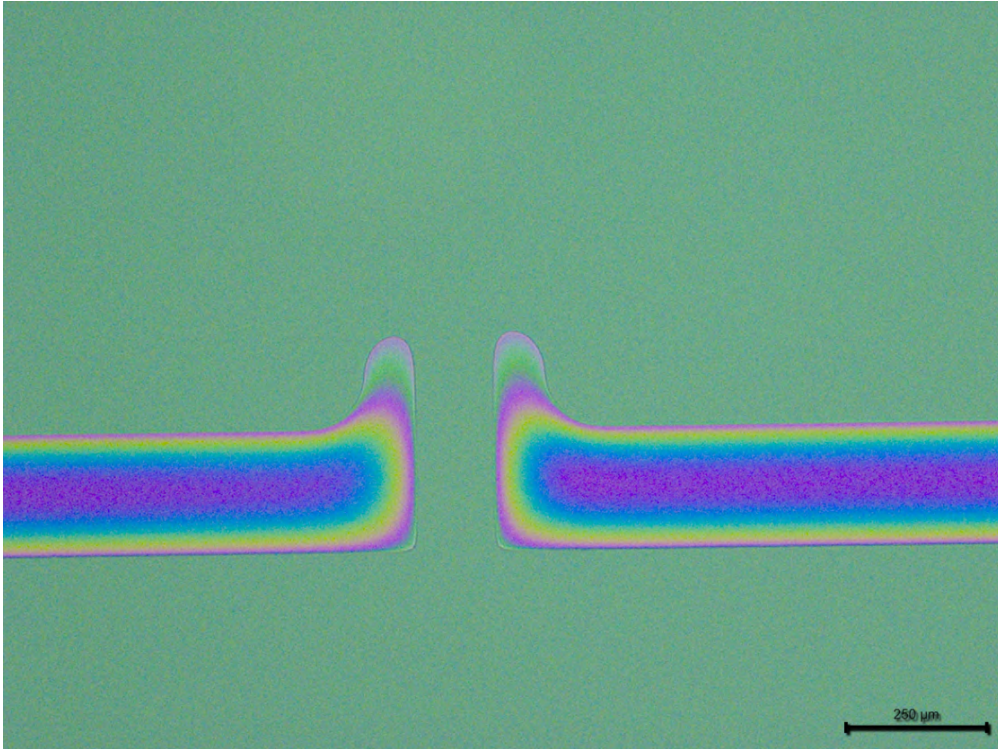


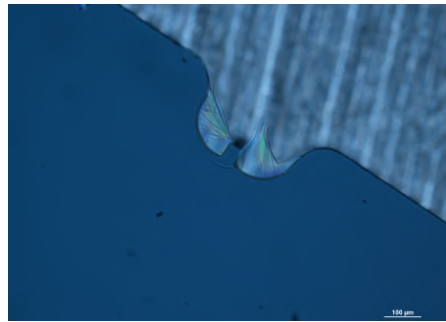
Figure 87: Back side of the wafer after KOH

I then took out this wafer from the clean room to the lab and sliced it in little chips using the etched lines, this is the way I test which is the best width for the bridge. I cleaved multiple chips from all the 5 different widths and the result is that the best width for cleaving the chip is the $50\ \mu\text{m}$ one, in this case I see that the bridges break in a controlled way so that the broken bridge is not outside the body of the chip, this means that the chip can be then used for AFM measurements.

I need to consider carefully to have the broken bridges inside the shape of the chip, because I will later use the chip inside an AFM with standardized space for cantilever and chip, so I should not exceed the dimensions. It is possible to cleave the chips applying a small pressure with the tweezers on the top of the chip, this pressure should be done, in principle, far from the position of the cantilever, so that the chance of breaking the cantilever during this operation is very low.



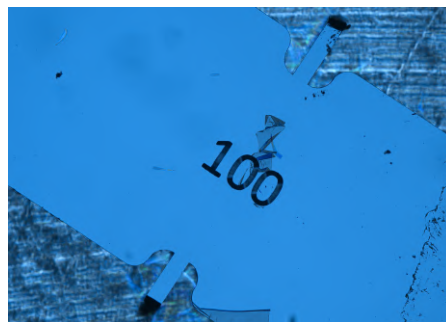
(a) 50 μm bridge



(b) 50 μm bridge for another chip



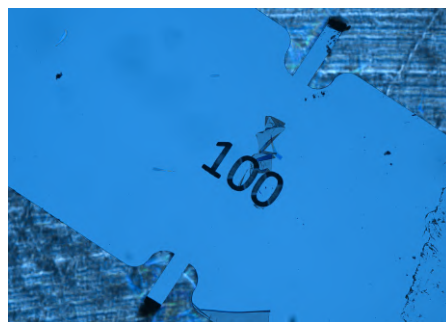
(c) 75 μm bridge



(d) 100 μm bridge



(e) 125 μm bridge



(f) 150 μm bridge

Figure 88: Test wafer after cleaving of chips

5.1 First fabrication batch

Now that I tested the right dimension of the bridge I am going to start with the fabrication of my main project.

I ordered multiple wafers with a 200 nm SiO_2 layer done with wet thermal oxidation, and 300 nm $\text{ls} - \text{SiN}_x$ layer done using LPCVD (low pressure chemical vapor deposition), then I booked a deposition of 6 μm of Poly-Si using again LPCVD.

After these deposition steps I coated 2 wafers with CSAR62 13, which is an electron sensitive film used for electron-beam exposure. I used a quite thick film of 680 nm, this was used because I will after use this resist as a mask for the etching of Poly-Si in a Deep Reactive Ion Etching (DRIE) system. In order to have 680 nm of thickness I need to set the speed of the wafer to 1500 rpm. I then exposed the wafers to the electron beam in order to pattern the features of the pillars, trenches and walls. I then developed the wafers using developer Amyl-Acetate on the wet bench for 2 minutes, finally I rinsed them and dried, the results are shown in figure 89, 90 and 91, I can clearly see the walls, trenches (figure 89 and 90) and pillars (figure 91), even though the critical dimension is of 300 nm, which is quite small for the optical microscope resolution.

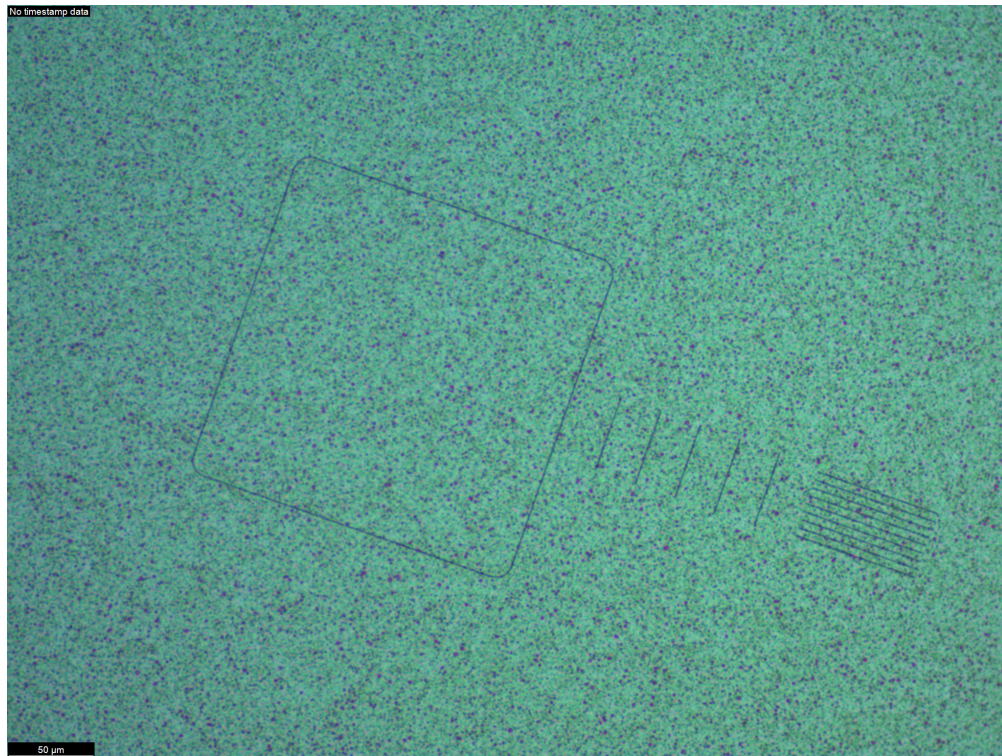


Figure 89: Trenches and walls for the cantilever with 5 trenches and 9 walls

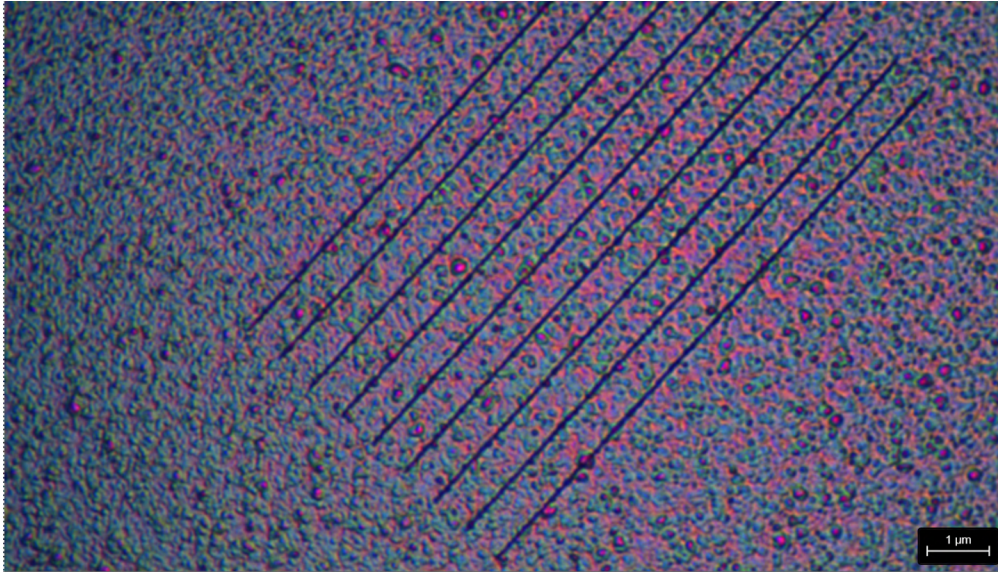


Figure 90: Details of the 9 walls of the cantilever

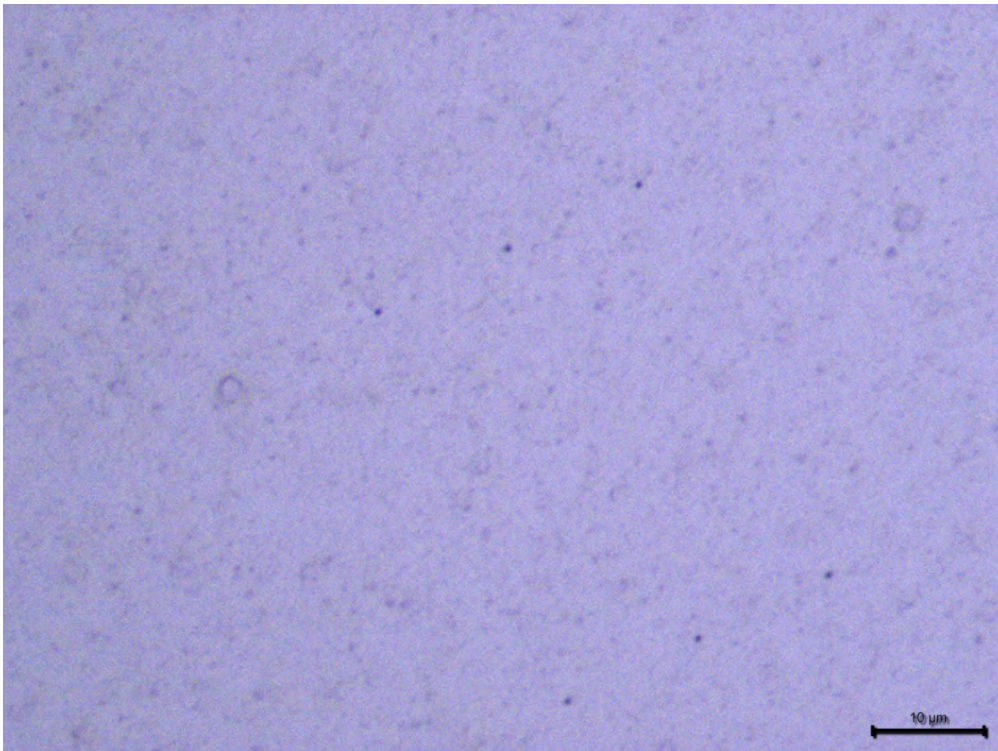


Figure 91: Details of the pillars

After the development of the e-beam resist I need to etch through these apertures, I will use

the Alcatel AMS 200 which is a Deep Reactive Ion Etching (DRIE) system for Silicon (Si) and Silicon on Insulator (SOI) wafers, it is especially good for high aspect ratio etching, because I will use the Bosch process, for which I will have 5 seconds of isotropic plasma etching via SF_6 and 2 seconds of deposition of a chemically inert passivation layer C_4F_8 .

I then need to remove the resist on top of the 2 wafers, in order to do so I use the Tepla GiGAbatch which is a machine that uses high frequency plasma. After the Tepla I use the UFT resist remover, which is a bath of remover 1165 at $70^\circ C$, I immersed the wafers in there for 10 minutes, in this way I manage to eliminate all the resist, even the parts that could be burnt during the plasma etching. I then booked a deposition of 500 nm $ls - SiN_x$ done by LPCVD by the CMi staff, this layer is very important because it consists of the top beam of the cantilever.

I coated these 2 wafers with LOR 5A (400 nm) and AZ1512 ($1.1 \mu m$), then I exposed with the mask-less aligner these 2 wafers and then I developed the wafers. For the development I need to use 2 times the same recipe because with the first development I will develop AZ1512 (which is photosensitive), with the second development I will create big undercut in LOR 5A, I want this because I will later do a lift off of these resists, so I do not want gold to be evaporated on the side walls of the resist. At the end I rinsed and dried the wafers. I also checked with the optical microscope that the alignment between the e-beam lithography and the mask-less aligner lithography is good. The results of this lithography step is seen in figure 92 and 93, as we can see, the alignment was very good, I can see it in figure 94 in fact the crosses in the alignment marks are superimposed.

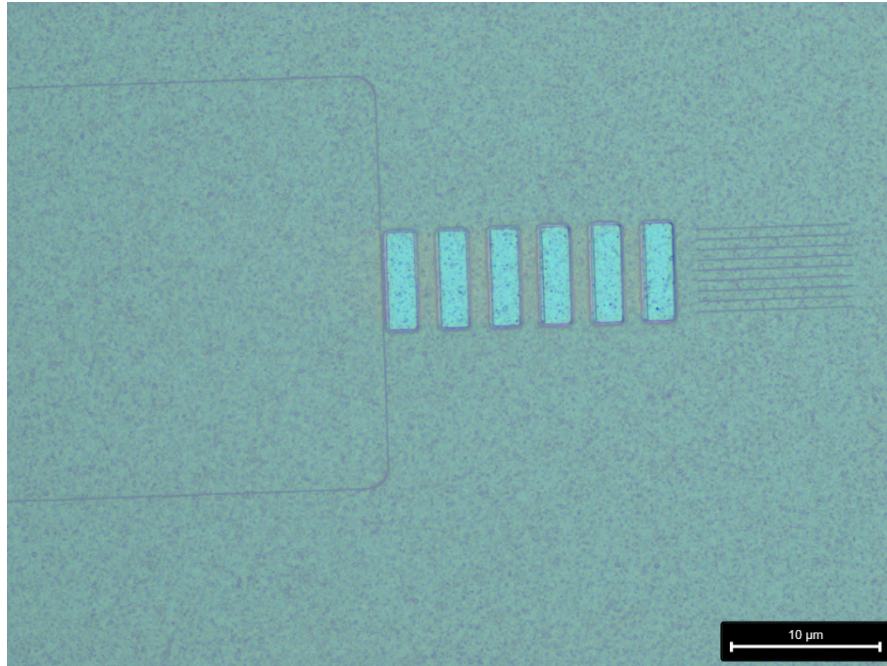


Figure 92: Wafers after second lithography step

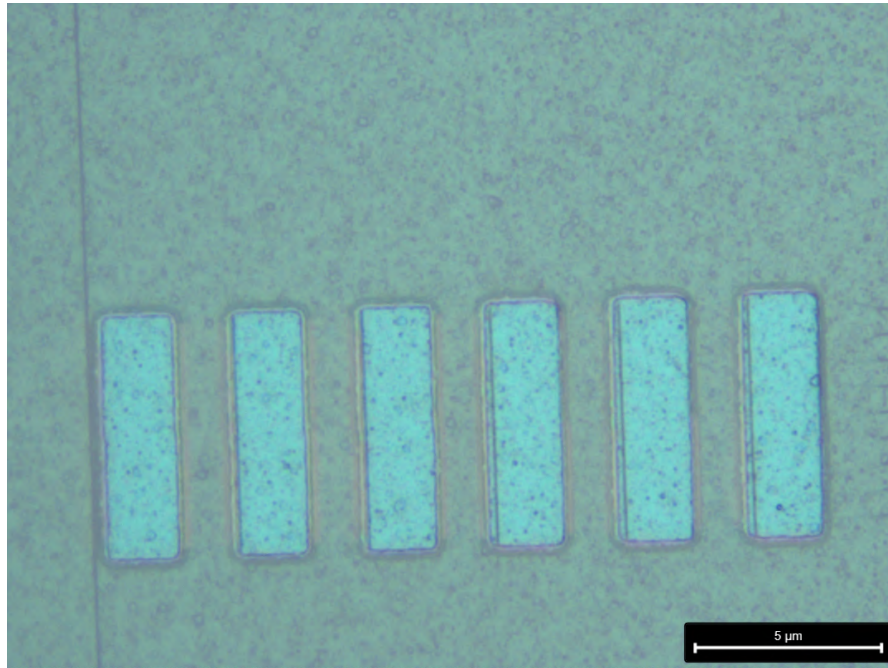


Figure 93: Detail wafers after second lithography

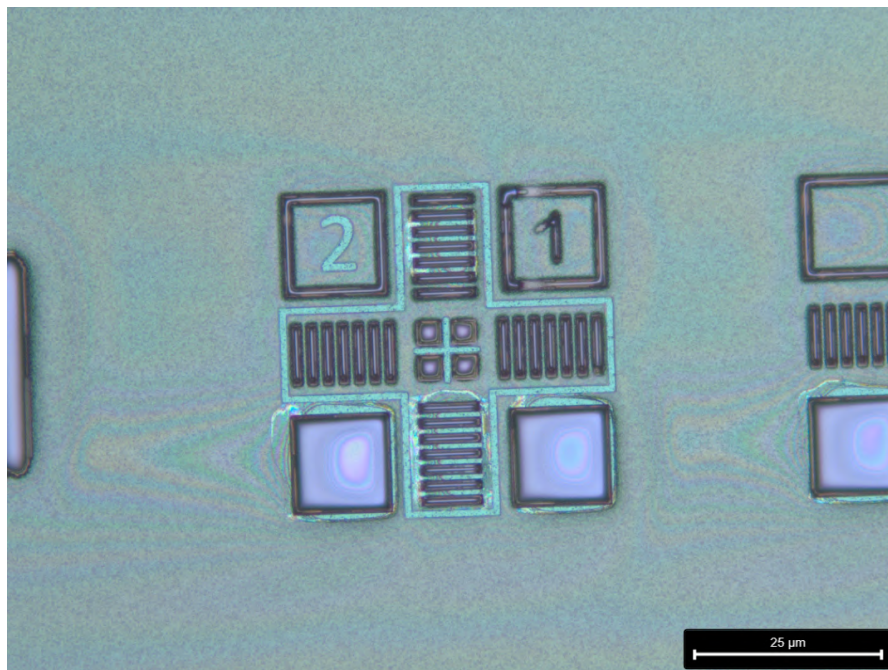


Figure 94: Correct alignment marks exposure

I also checked with SEM (scanning electron microscope) a third wafer that I exposed with

the e-beam, etched the Poly-Si away from the patterns and stripped the resist, I wanted to check the project from the electron microscope because the features are very small and the optical microscope can not reach a sufficient resolution if I need to verify in details how the etching was carried out. The overall lithography step and etching is good, however, I noticed I have some defects originated from the end of the trenches and the walls, I can see some tails which were not designed to be there, the reason on why I have these defects is due to the high thickness of the CSAR62 13 resist that I used for my project, I used a different and thinner resist for the second batch of my fabrication and the defects were practically solved, they did not manifest in the second batch of fabrication of the project. It is possible to appreciate the defects in figure 95.

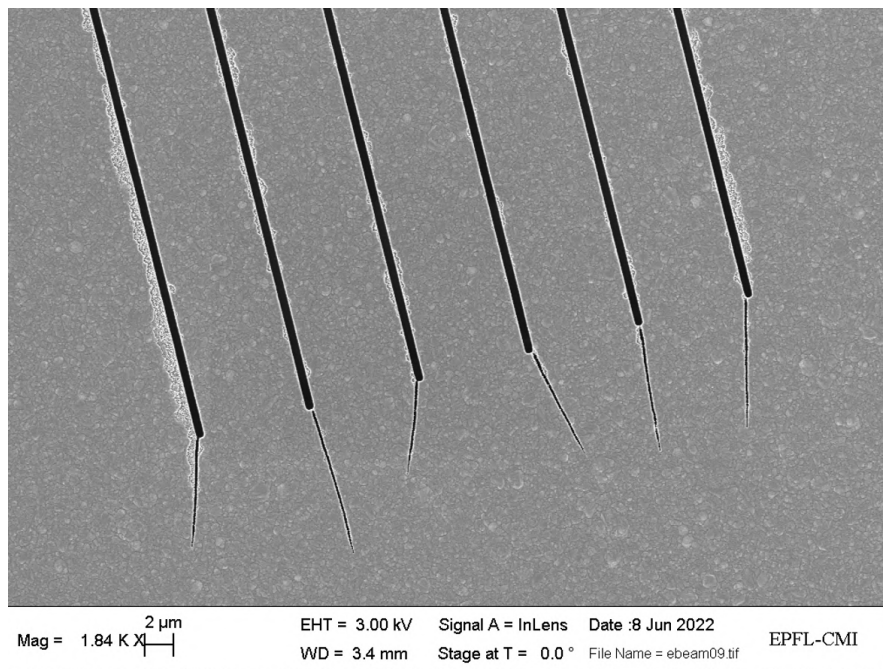


Figure 95: Detail wafers after second lithography

Before the deposition of the gold layer I need to remove the residues of the photoresist. In order to do so, I use the Tepla GiGAbatch at low power for 10 seconds, so that the surface is now clean from residues and I can deposit the gold quite uniformly.

The gold is deposited by evaporation. I deposit 50 nm of gold on the top surface, I need to attach copper disks at the bottom side of each wafer, in order to reduce the thermal shock of the wafers, because later I will do lift-off. I decide to use the maximum distance between the dome containing the wafers and the crucible location, in this way I will have a slightly slower deposition rate but I will have a more uniform deposition too, this is useful in my project because I do not want deposition of gold on the walls of the apertures. After deposition I checked the status of the wafer and I could observe that the gold layer had been deposited well. In figure 96 and figure 97 I show the result after the gold evaporation step for a chip with gold on each L1'/2 and for one with gold on all L1, respectively.

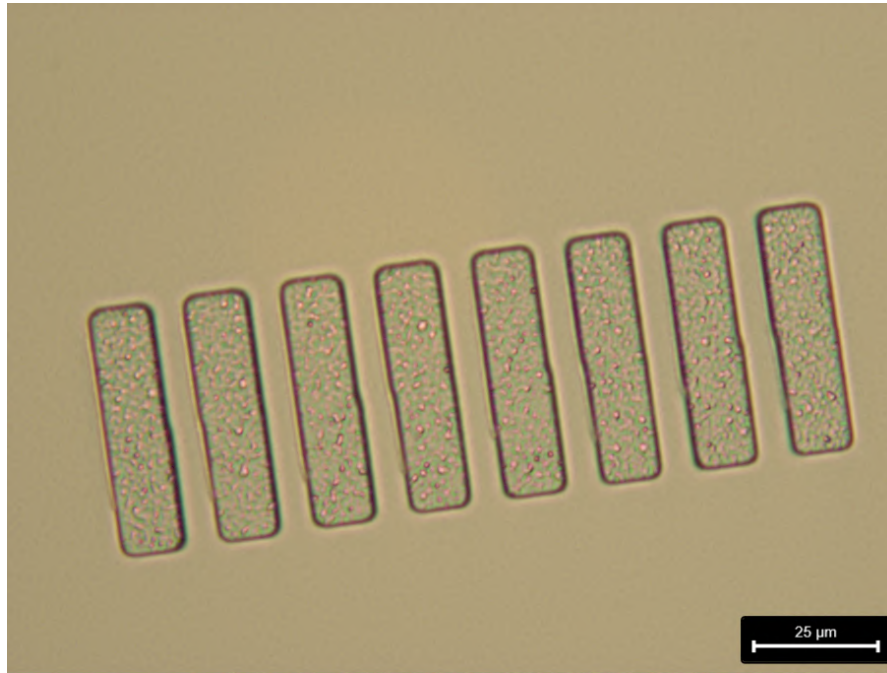


Figure 96: Detail of the wafer after 50 nm gold evaporation

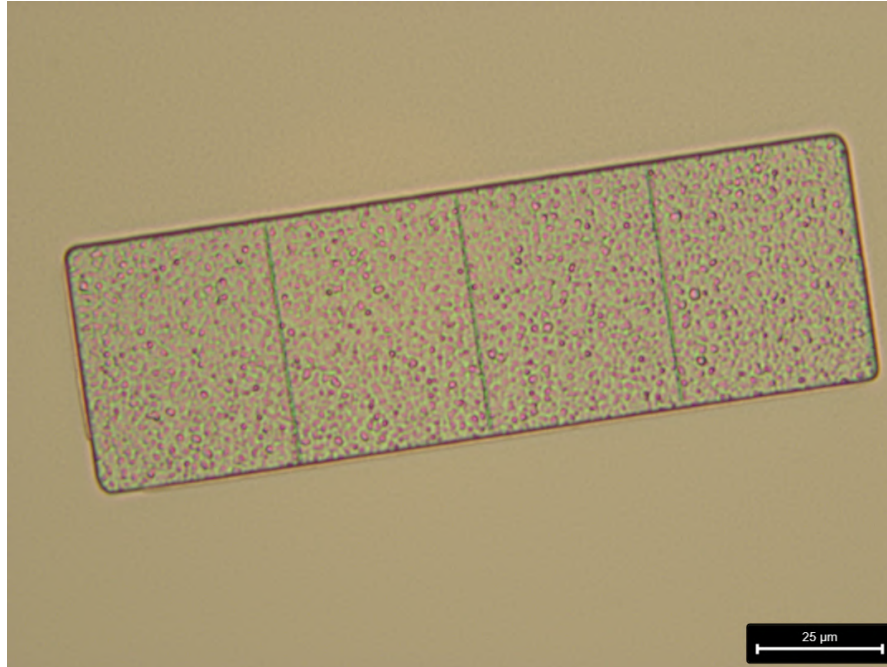


Figure 97: Another detail of the wafer after 50 nm gold evaporation

I then left the 2 wafers all the week-end in the remover 1165 for lift-off, I used ultrasound too

in order to speed up and clean the process, I could use ultrasound because the device is not too fragile for this, the result for this wafers after lift-off of the 2 layers of resist is very good, the gold remained exactly in the places in which I exposed the wafer, instead in the other parts I do not have gold anymore because the resist was stripped away thanks to the remover 1165. The result is shown in figure 98.

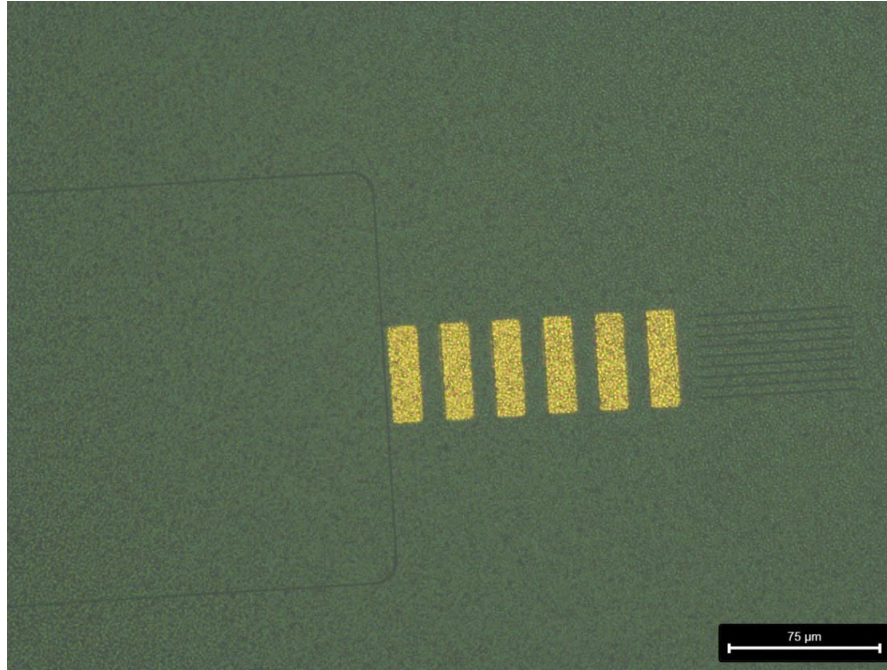


Figure 98: Wafer after gold lift-off

After lift-off of gold I need one more lithographic step on the front side of the wafers in order to define the cantilever shape. I coated the wafers with ACS200 GEN3 which is a modular automatic cluster tool used for coating and development. I want to deposit $3\text{ }\mu\text{m}$ thick resist AZ ECI, I want good adhesion of this layer therefore I need to select a recipe in which I have treatment of the wafer with HMDS, which enables better adhesion of the photoresist layer to the wafer. I then expose the wafer with the mask-less aligner and develop with the same machine I used for the coating.

The result of the wafers after this third lithographic step is shown in picture 99 and 100, we can observe that the alignment was done in the correct way, the cantilever shape has now been defined.

I now need to etch through the parts of the wafers not covered in photoresist, I will etch 500 nm SiN_x , $6\text{ }\mu\text{m Poly-Si}$, 300 nm SiN_x . I can use the end point detection system to check when I completely etch one layer. Moreover, when I am etching I have also a camera that looks into the details of the wafer in real time, so I know when to stop the process and start. The SiN_x will be etched with a different recipe from Poly-Si, the recipe for the etching of SiN_x is etching with the same speed the photoresist too, however, I do not need to worry about this because the resist is thick enough for these processes so it will not be eliminated from the etching of SiN_x . It is good practice to clean the chamber of the plasma etcher between a process that etched Poly-Si and one that etches SiN_x so that I will not have contamination. I clean the chamber with O_2 and I

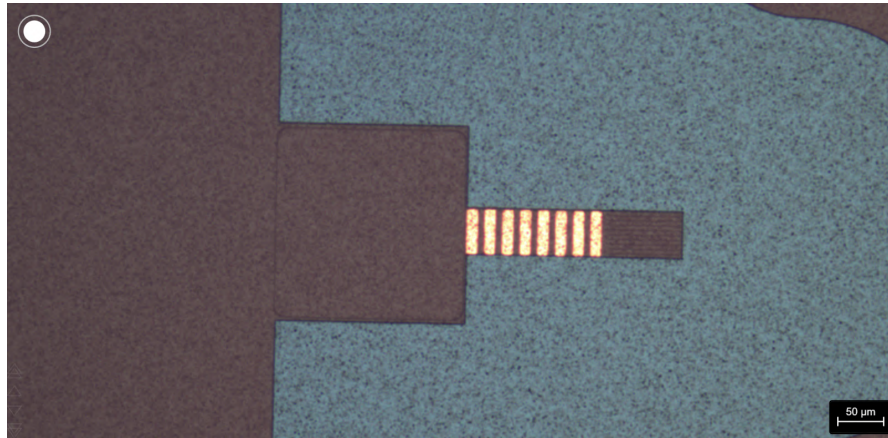


Figure 99: Third lithographic step, for chip with gold on each L1'/2

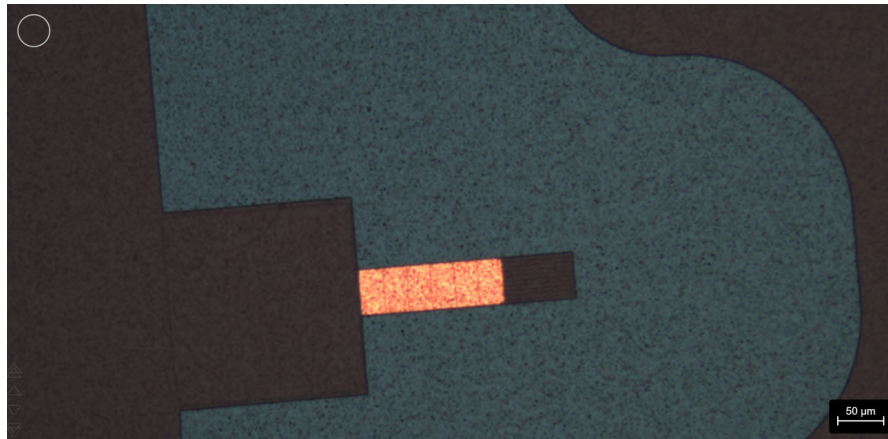


Figure 100: Third lithographic step, for chip with gold on L1

use a dummy wafer for this reason, because I have gold on my wafer therefore I do not want to damage it with O_2 .

Then I did the resist strip of the resist, I used only the remover 1165 at 70 °C, I did not use the Tepla GiGAbatch (plasma etcher) because I have gold on top. The wafers after the definition of the cantilever shape and the resist strip are looking good, we can see the result in figure 101.

Now the cantilever is complete from the front side, but I still need to release it. In order to release the cantilever I need to etch the back side of the chip so that I will obtain a thickness of the cantilever equals to 6 μm .

I now need to deposit 1.5 μm of Al on the top side to protect the features of the cantilever when I work with the back side. The deposition went smoothly. Now that the front side is protected I can start to work with the back side. I start by etching 500 nm SiN_x and 6 μm Poly-Si with the plasma etcher AMS200. Then I do the treatment with HMDS for the wafers, so that the photoresist will be attach to the back side very well, this is important because I will need to etch all the way through the back, therefore I need a stable resist. Then I coat the back

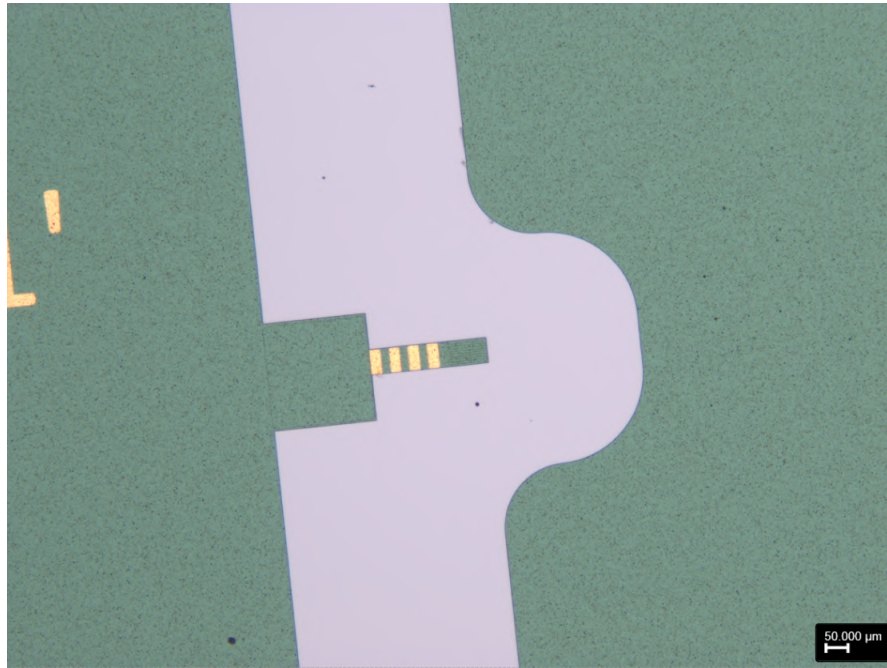
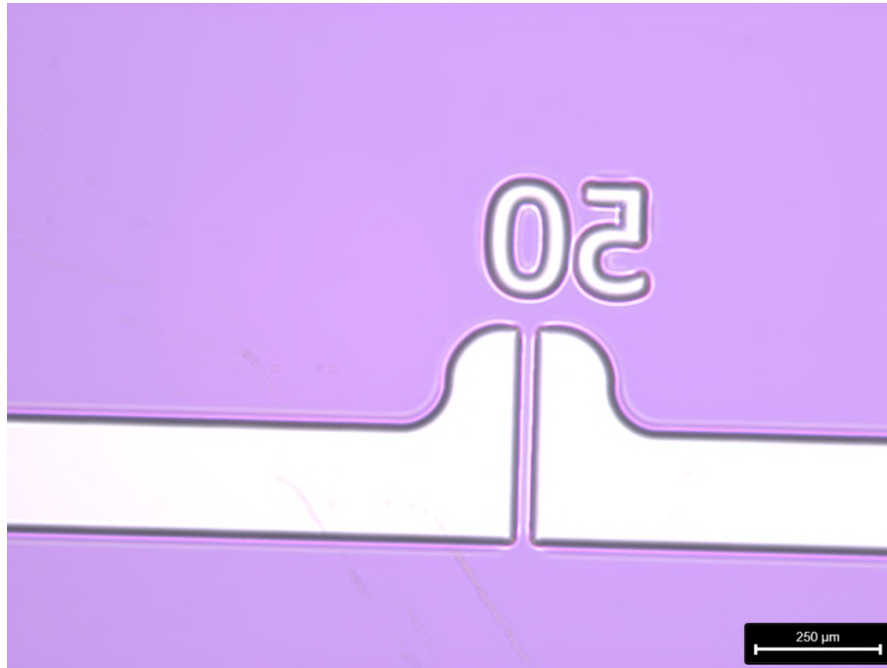


Figure 101: Wafer after cantilever shape definition and resist strip

side with $8\text{ }\mu\text{m}$ AZ 10XT, I expose the resist with the mask-less aligner and I develop with the same machine I used for the coating. I now need to place my wafers inside the oven at $85\text{ }^{\circ}\text{C}$, for at least 5 hours up to 2/3 days. I left the wafers overnight, this step is particularly important because it hardens the photoresist and this is particularly important in this case because I am going to etch the back side for more than an hour, this means I need a thick and hard photoresist. After the photoresist hardening I started plasma etching the backside, I start with 300 nm SiN_x , the result after the etching of this layer is shown in figure 102. I can see that the backside patterning went well.

Figure 102: Back side etching of SiN_x

I then etched the Si from the back side. I used plasma etching as usual for this type of etching, because I have good selectivity to the photoresist and moreover I use the Bosch process, which will enable to have a very vertical etching, in this way I can etch through small apertures with high aspect ratio. I etched for 1 hour and 12 minutes both my wafers, the results are very good, in fact now I can see the cantilever from the back side, because I released it, the figure 103, 104, 105 are taken from the back side of the wafer but I can see clearly the cantilever shape, this is because I eliminated all the Si below the cantilever so we can say that now the cantilever is floating. I can also observe that the alignment was done well, because I can see the back side apertures aligned with the cantilever that is on the top side.

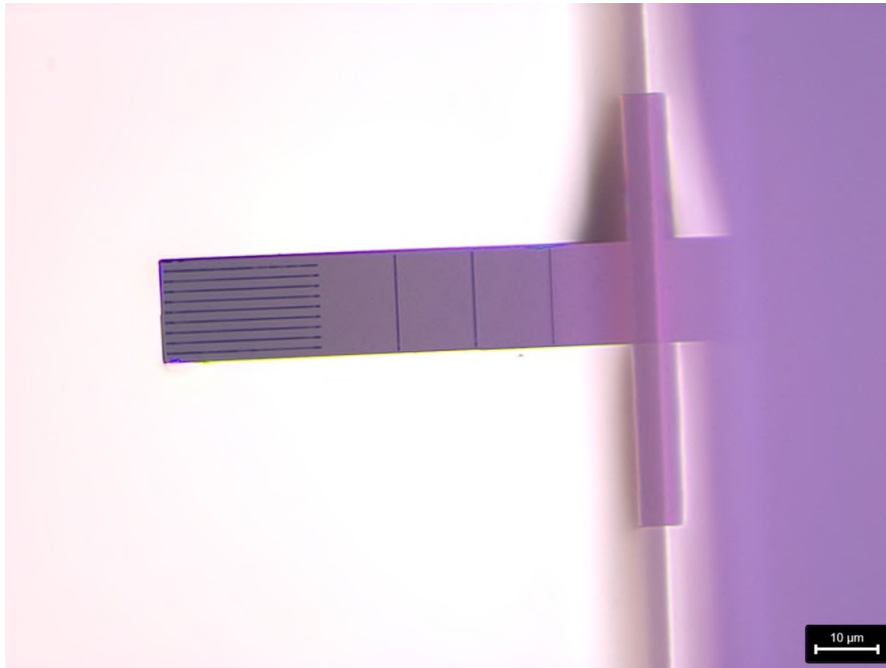


Figure 103: Cantilever released from the back side



Figure 104: Different cantilever released from the back side

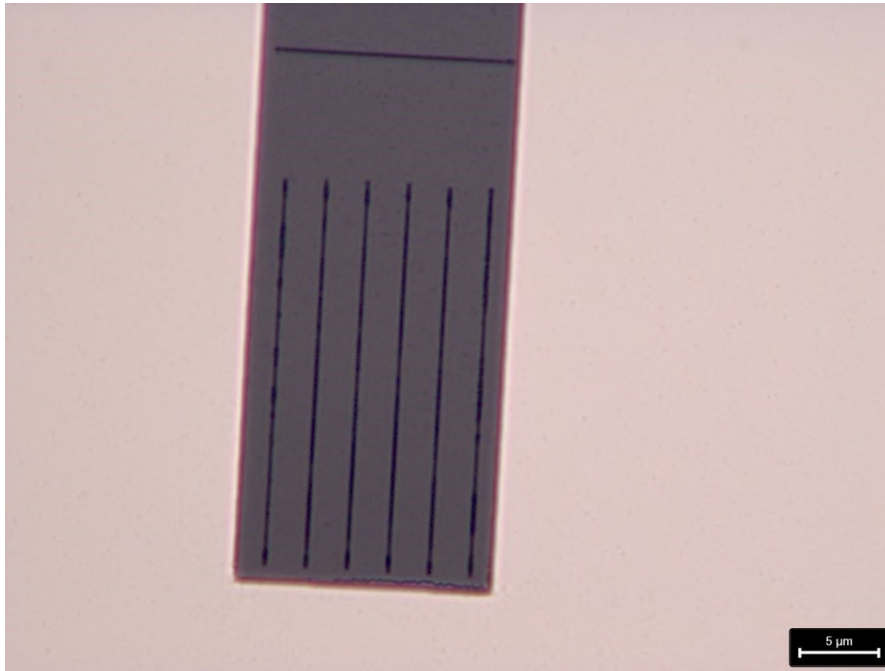


Figure 105: Detail of the walls after the releasing of the cantilever

Now that the etching of the back side was done successfully I will continue with the process flow. The next step is to strip the resist from the back side. It is useful to use both the Tepla GiGAbatch and the wet remover 1165, because the resist underwent 1 hour and 12 minutes of plasma etching and it was hardened in the oven for a day, so it is not easy to strip it just by the wet remover, I therefore need to use a plasma etcher too, in order to make it easier the removing process.

The last step is the KOH etching. I need to use a solution of 20% KOH and a temperature of 50 °C, in this way the etching will be fast, otherwise the etching will be too long. In the clean room I have 40% KOH so I need to mix it with deionized water, I want to use 20% KOH instead than 40% KOH because it has a faster etching rate. KOH etches silicon depending on the concentration of the KOH solution and temperature. [15]

I need to pour water before and then KOH for safety standards, I place the baker on the hotplate and immerse the sensor of the hot plate inside the solution, in this way I can monitor the temperature of the solution in real time, I need to set the set point to 50 °C so that the hot plate will heat the KOH solution until it reaches 50 °C, then it will stabilize at that temperature. I have to mix the solution because water and KOH have different densities so I need to use the magnetic stirrer, which is a magnetic bar that can be immersed in the solution, I will therefore switch on a magnetic field from the hot plate so that the magnetic stirrer will spin in the solution and I will get a mechanical mixing of the solution, I set the spinning speed to 50 rpm, which is the minimum I can have, this is because I do not want that the mixing of the solution impacts the stability of the cantilever. From literature the Si is etched with an angle and Poly-Si is etched faster than Si because I have multiple grain orientations, from literature I calculated that I will eliminate all the Poly-Si after 3 to 4 hours of KOH bath. I left the wafers for 2 hours but the Poly-Si was not yet etched, I therefore waited another hour (3 total hour of bath) and I

checked that there was a problem with the stability of the chips, in fact the majority of the chips were floating free in the solution because the bridge width was too small and it was completely etched. In many chips I did not have anymore the cantilever and gold was stripped too, however, I managed to save some chips, in figure 106 and 107 I show good chips which still have the cantilever attached. An example of a bad chip which had the cantilever stripped away is shown in figure 108.

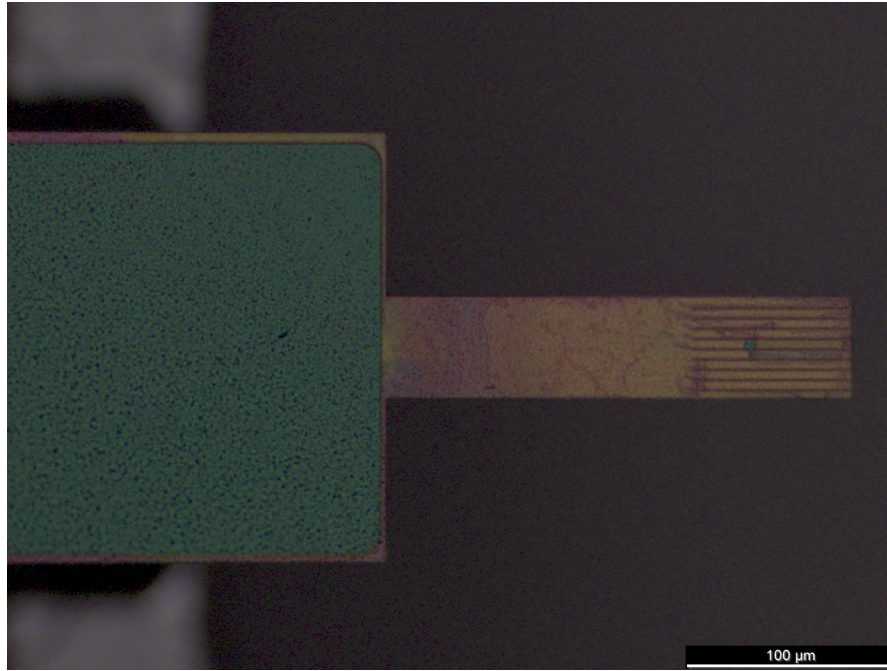


Figure 106: Cantilever survived to KOH

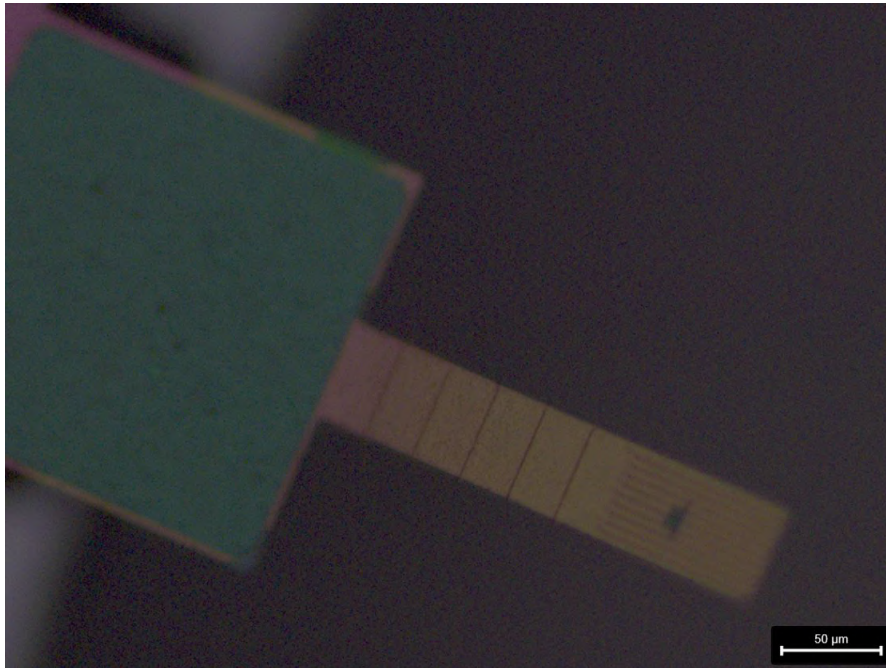


Figure 107: Another cantilever survived to KOH

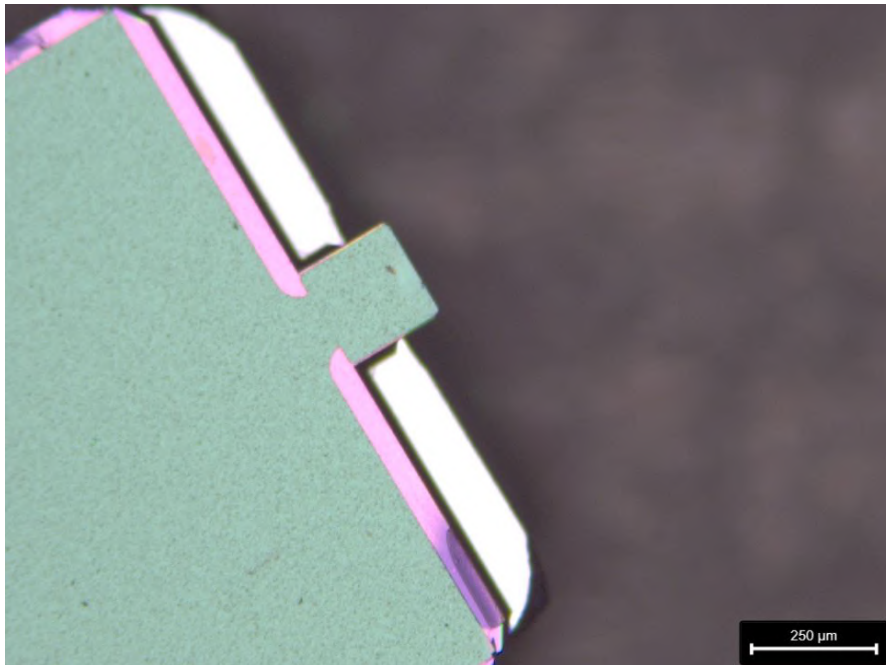


Figure 108: Detached cantilever from the chip after KOH

Now that I have some complete chips I want to check the cross section of the cantilever to

see if the various steps in the fabrication went well. I used the SEM for the imaging, setting the voltage up to 3kV. The picture that I took with the SEM are very useful because I managed to see that the cantilevers were fabricated really well, in fact I can see that the walls and the trenches are sufficiently robust for the device to not collapse, moreover I also checked the cantilevers with pillars and I can see that the stability of the cantilever is very good too. The figures 109 and 110 show the results.

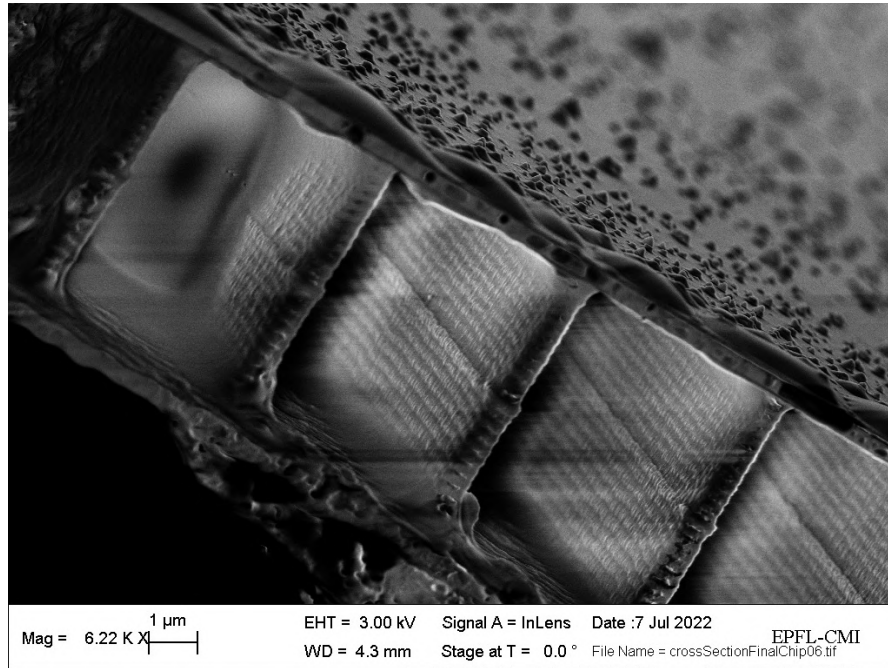


Figure 109: Cross section of the complete cantilever

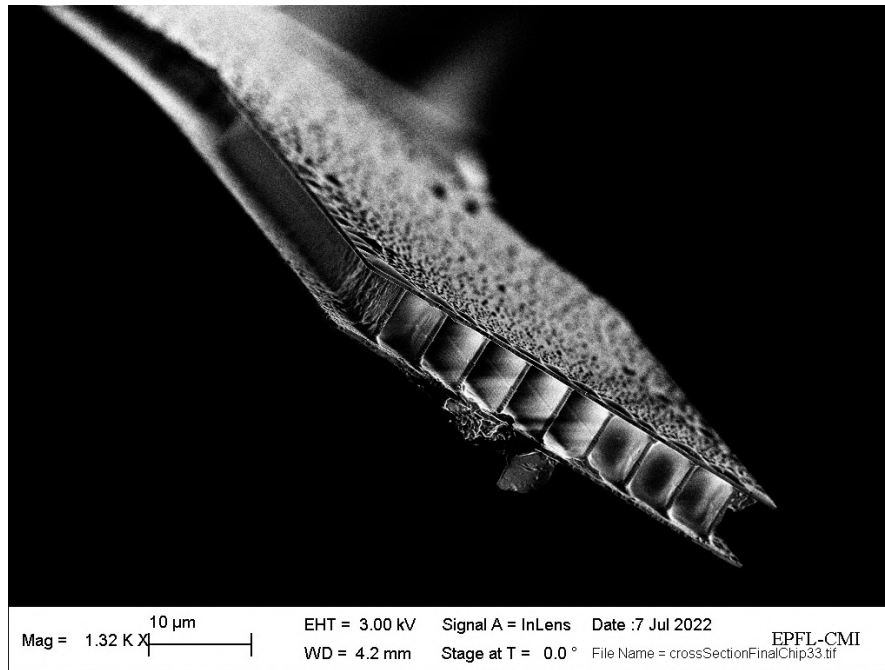


Figure 110: Cross section of the walls of the complete cantilever

5.2 Second batch

I will do again the whole fabrication process so that I can get better chips for the laser actuation. One aspect that I need to solve is the deposition of gold on the top surface of the cantilever, in the first batch I had the gold stripped away during the KOH bath, this time I need to deposit a layer of gold on top so that I will have a better actuation, I am interested in depositing a layer with good adhesion, so that it will not strip away during KOH.

I changed a bit the design for this second batch, in fact now I have designed a bridge 150 μm wide on the top side of the chip, in this way I have a better stability of the chip that will survive the KOH bath. In the first batch I did not have any bridge on the top side of the chip, the only connection between the chip and the rest of the wafer was the bridge from the back side which was just 50 μm wide. I can therefore build this bridge changing the third lithographic step design, as we can see in figure 111.

I also changed the width of the back side bridge, I consider now a 250 μm wide bridge from the back side (instead of the 50 μm bridge used in the first batch), in this way I will not have problems regarding the stability of the chip inside KOH, so if I use these improvements I will be sure that KOH will not etch through the Si bridges which are of fundamental importance for the attachment of the chip to the wafer.

This time I am fabricating in parallel 4 wafers. I started with the first lithography step using the e-beam machine, however, this time I am not using CSAR62 13 but another resist, I used ZEP 520A resist 620 nm thick (1500 rpm). The defects of the tails are smaller this time, if I reduce the thickness of the resist I get an advantage: during development it is more unlikely that this type of defect is generated. We can observe the absence of tail's defects in the figure 112.

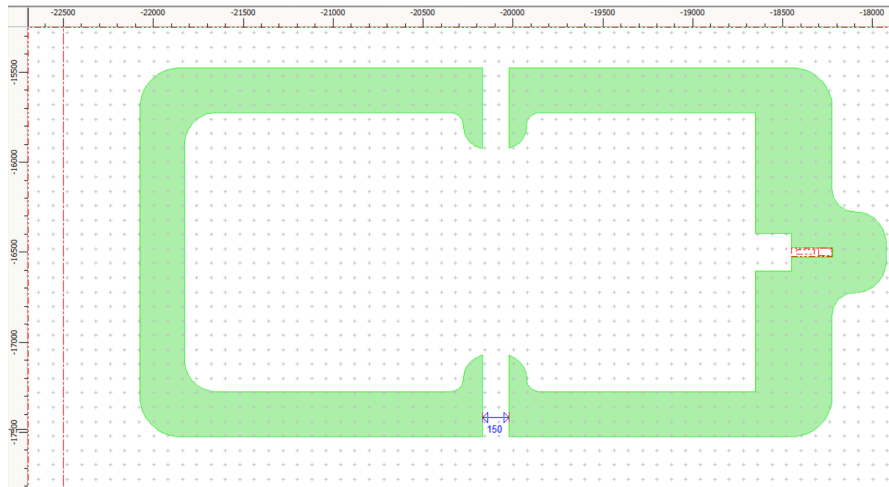


Figure 111: Top side bridge for the chip's stability

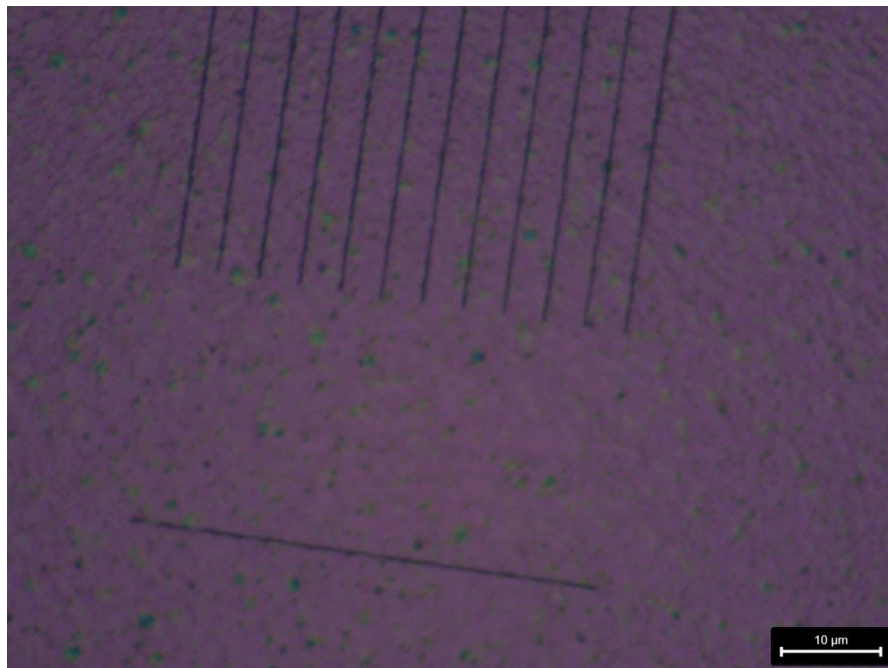


Figure 112: Walls and trenches without tail's defects

I then carried out the second lithography, which is the one for the gold pattern, the results were very good, the alignment was done well. In figure 113, I show the result of this second lithographic step.

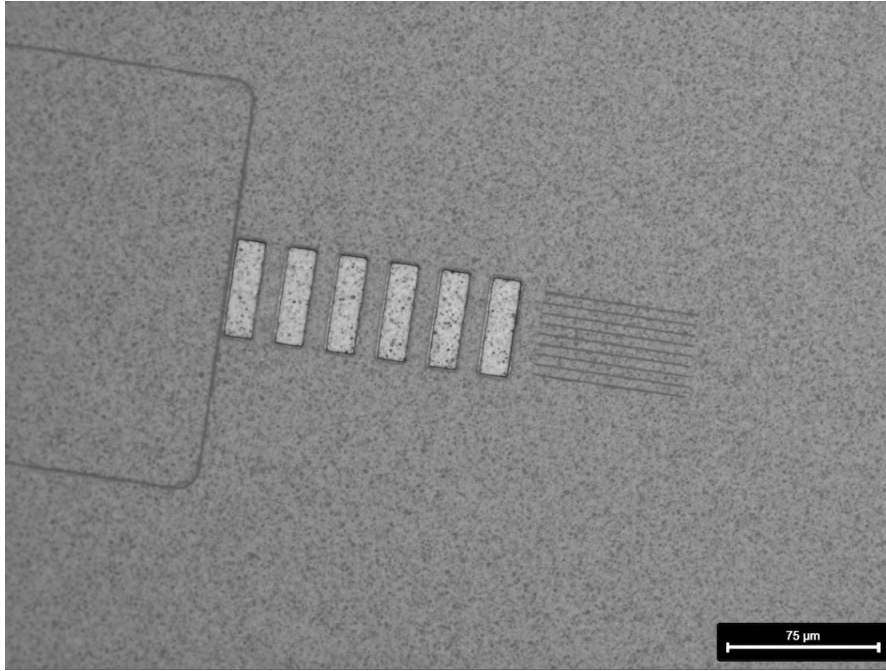


Figure 113: Cantilever after second lithographic step

I then continued with the process flow, I deposited 50 nm of Au and did lift-off, the pattern of gold is now well done, in fact I have gold on top of the cantilever in the places I wanted it from the design. The third lithographic step which defines the cantilever shape went well too. I then needed to etch the 3 layers SiN_x /Poly-Si/ SiN_x in the top side, to define the cantilever shape, the result of this etching is shown in figure 114.

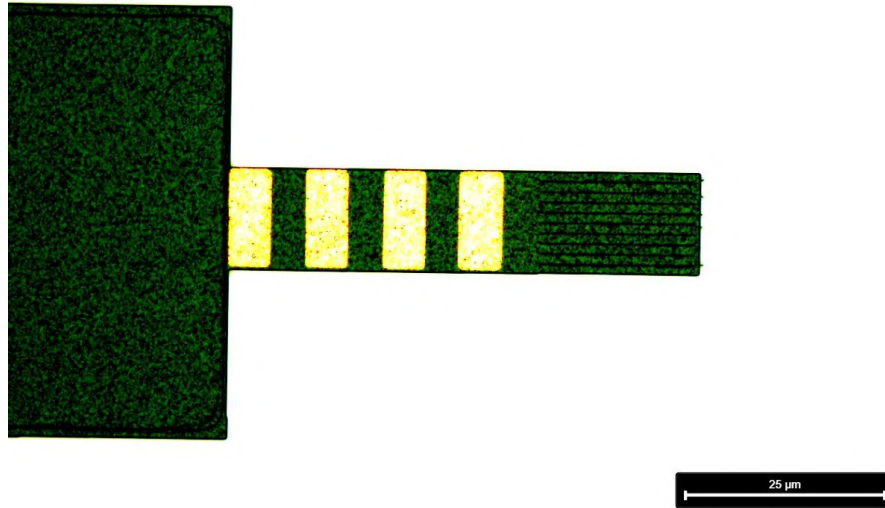


Figure 114: Cantilever defined

I then deposited Al on the top side as I did in the first batch and started the last lithographic step which is on the back side. The back side lithography was done well, the apertures of the bridges were $250\ \mu\text{m}$ wide as expected from design. The etching of the back side is the same as the one I did for the first batch: I need to etch $300\ \text{nm}\ \text{SiN}_x$, $200\ \text{nm}\ \text{SiO}_2$ and $380\ \mu\text{m}\ \text{Si}$. I needed 1 hour and 10 minutes for the complete etching of the Si from the back side and the releasing of the cantilever. The result of the complete etching is shown in figure 115, this picture was taken from the back side of the chip and I can see the back of the cantilever, in this way I know that the etching can be stopped. I can also observe that the length of the cantilever is the one I simulated and designed, equals to $225\ \mu\text{m}$. I then stripped the resist from the back.

Before immersing my wafers inside KOH I wanted to make a test with a wafer with the same materials as the one I am using. I want to immerse this test wafer inside KOH and check what is the etch rate of Poly-Si, I used the usual set up for KOH ($50\ ^\circ\text{C}$ and $20\ \%$ KOH) and I immersed the test wafer inside the solution for 1 hour. The result is shown in figure 116, I can see that I etched around $17\ \mu\text{m}$ of Poly-Si in all directions in 1 hour, I can see that I still need to etch more, at least another hour in order to etch all the Poly-Si from L2. I can also observe that SiN_x is a very good etch stop in KOH, it is not etched at all as expected. The pink part in picture 116 represents the etched Poly-Si underneath, whereas the green part shows that I still have Poly-Si underneath in those places.



Figure 115: Back side releasing of the cantilever

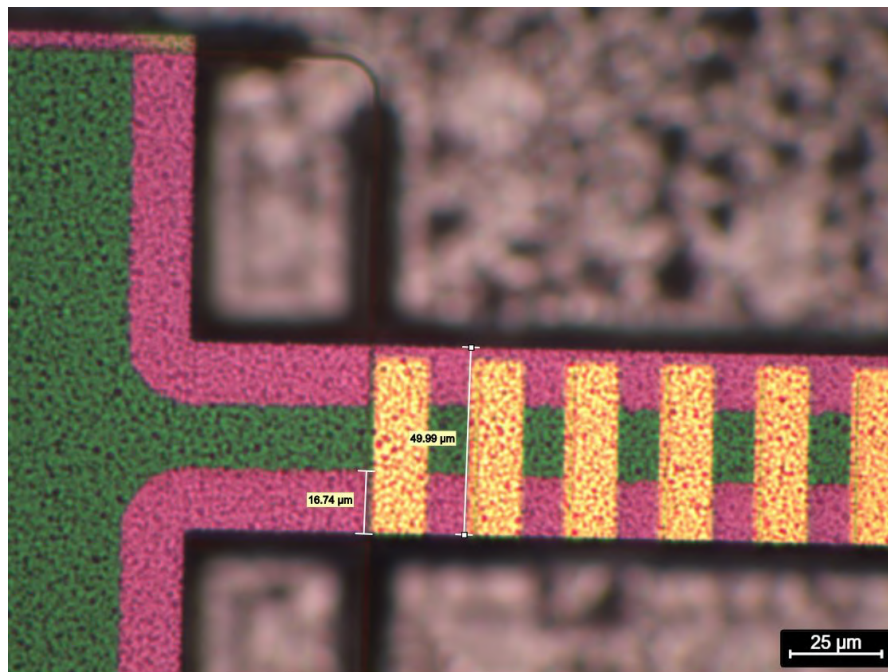


Figure 116: KOH test for Poly-Si etch rate

Considering now this etch rate I can start with the KOH etching of my wafers from the second

batch. Using the same set up at 50 °C and 20 % KOH I checked the wafers after 1 hour and 30 minutes and I saw that I etched all the Poly-Si from L1, however I still need to etch through L2. In conclusion I immerse the wafer for a total of 3 hours, in this way all the Poly-Si was etched away and so now I have an hollow part between the 2 plates of the cantilever. One side effect of this batch was that the gold was stripped away, the adhesion is not sufficient. In order to solve this problem I had the idea to evaporate 50 nm of Au on 10 nm of Cr, this layer of Cr helps the adhesion and actuation of Au. The results of this step are shown in figure 117 and 118.

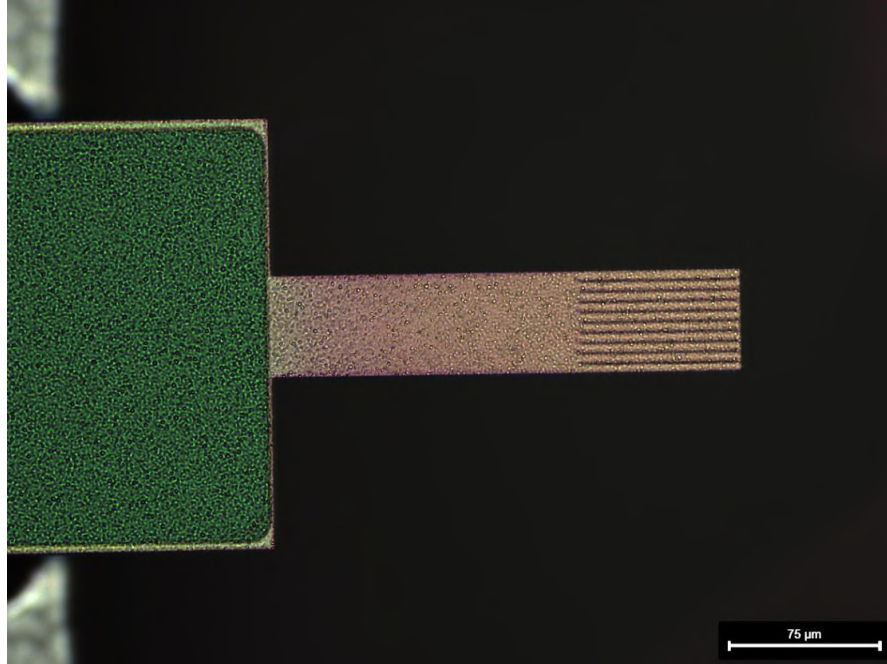


Figure 117: Complete Poly-Si etching

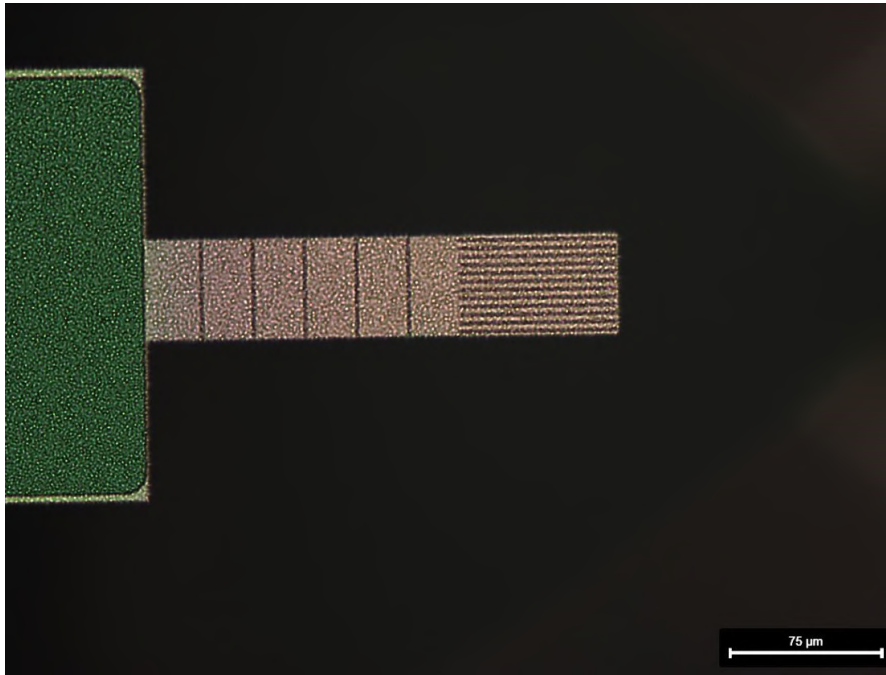


Figure 118: Complete Poly-Si etching for another chip

The last step is to deposit 50 nm of Au on 10 nm of Cr, in this way I can get good laser actuation of the cantilevers, the results is shown below in figure 119. The metal layer was deposited smoothly without problems over all the wafer.

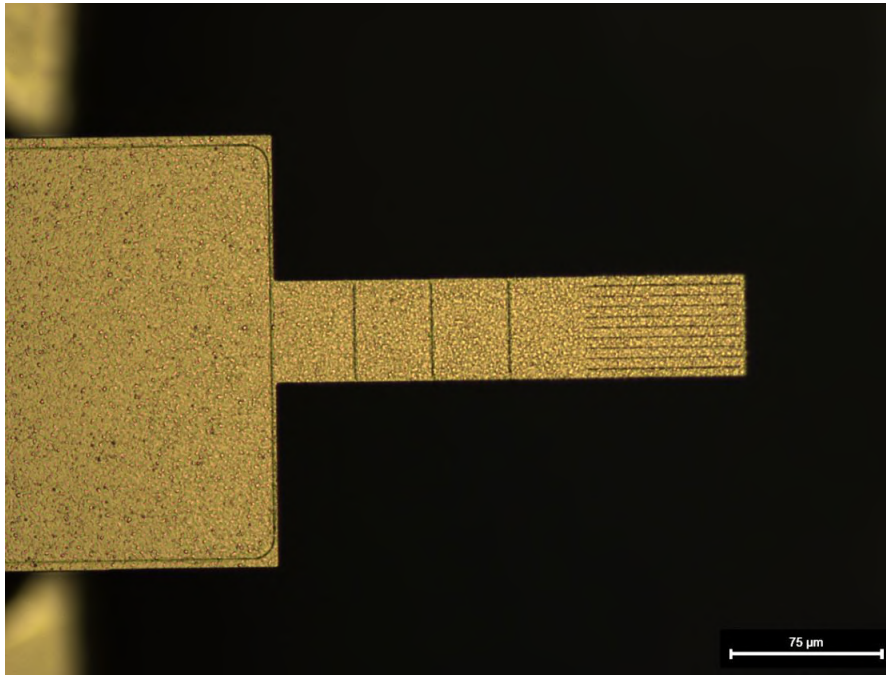


Figure 119: Complete cantilever with Au + Cr on top

6 Characterization

Now that the device is manufactured I need to characterize it. I am particularly interested in checking the resonance frequency of the cantilevers and the power actuation done with the laser focused on top of the gold.

6.1 LDV measurements

I used the LDV (Laser Doppler Velocimetry) for the measurement of the resonance frequency and the phase of the cantilevers. LDV is a crucial instrument for the study of turbulence due to its great spatial resolution and capacity to track swift velocity fluctuations. The instrument consists of a laser light source, optical setups for light transmission and collection, a photodetector, and signal processing hardware. A beam splitter divides the laser's light into two equal-intensity beams that intersect at the area of the cantilever where velocity measurements are needed, creating a fringe pattern. [16]. After post processing, I can calculate the oscillation frequency of the cantilever in function of the fringe pattern of the laser focus on top of the cantilever. I checked one cantilever with pillars and the resonance plot in amplitude and phase is shown in figure 120, I applied a voltage to the cantilever and I can observe that the amplitude is linearly dependant on the voltage applied. Moreover the resonance frequency is around 26kHz, which is very similar to the frequency of the cantilever with pillars that I simulated on Comsol. The calculated quality factor for this cantilever is 72.

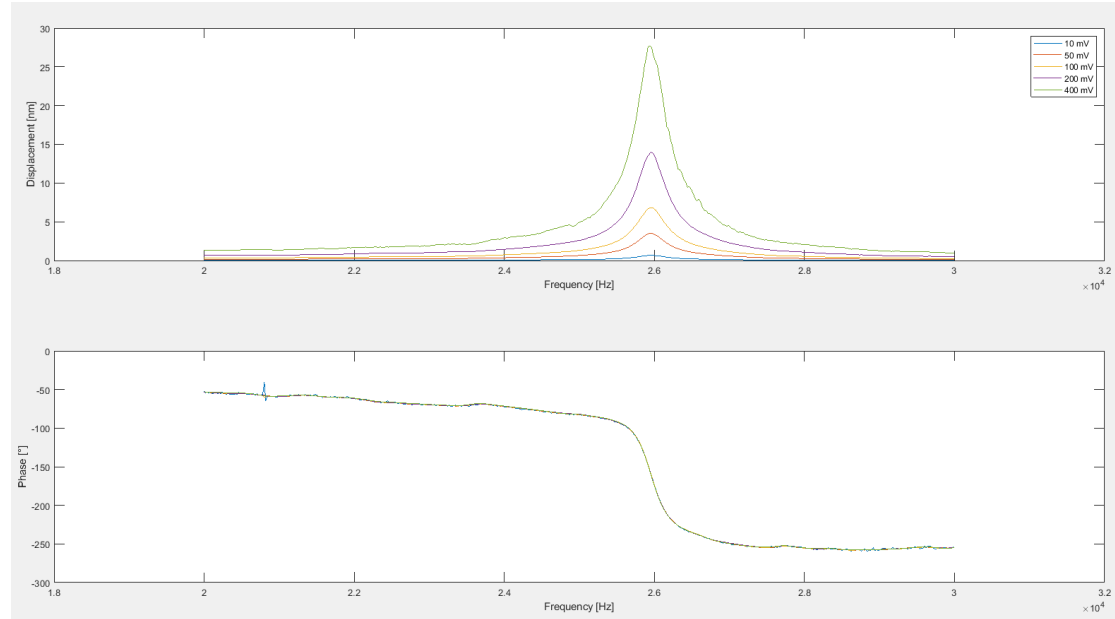


Figure 120: Oscillation amplitude and phase of the cantilevers

6.2 DHM measurements

DHM (Digital Holographic Microscopy) sets itself apart from previous microscopy techniques by not capturing the object's projected image. Instead, the item's light wave front information is digitally captured as a hologram, from which a computer can then use a numerical reconstruction

procedure to generate the image of the object. Thus, a computer algorithm takes the place of the classic microscopy's image generating lens.

To create the necessary interference pattern, i.e., the hologram, the illumination needs to be a coherent (monochromatic) light source, a laser for example. The sample is illuminated by the extended object beam, which also generates the object wave front. A beam splitter joins the object and reference wave fronts after a microscope objective collects the object wave front, interfering to produce the hologram. A numerical reconstruction algorithm is used by a computer acting as a digital lens to calculate a viewable image of the object wave front using the digitally recorded hologram.

With DHM I can measure the oscillation profile of the cantilevers and also check the oscillation behaviour of the 3D structure. I will observe now the oscillation profile, in this case I want to verify that the profile of the cantilever is horizontal at the free moving edge, I can see that this result is nicely observe in pictures 121, 122 and 123. The oscillation is linear even at higher voltages.

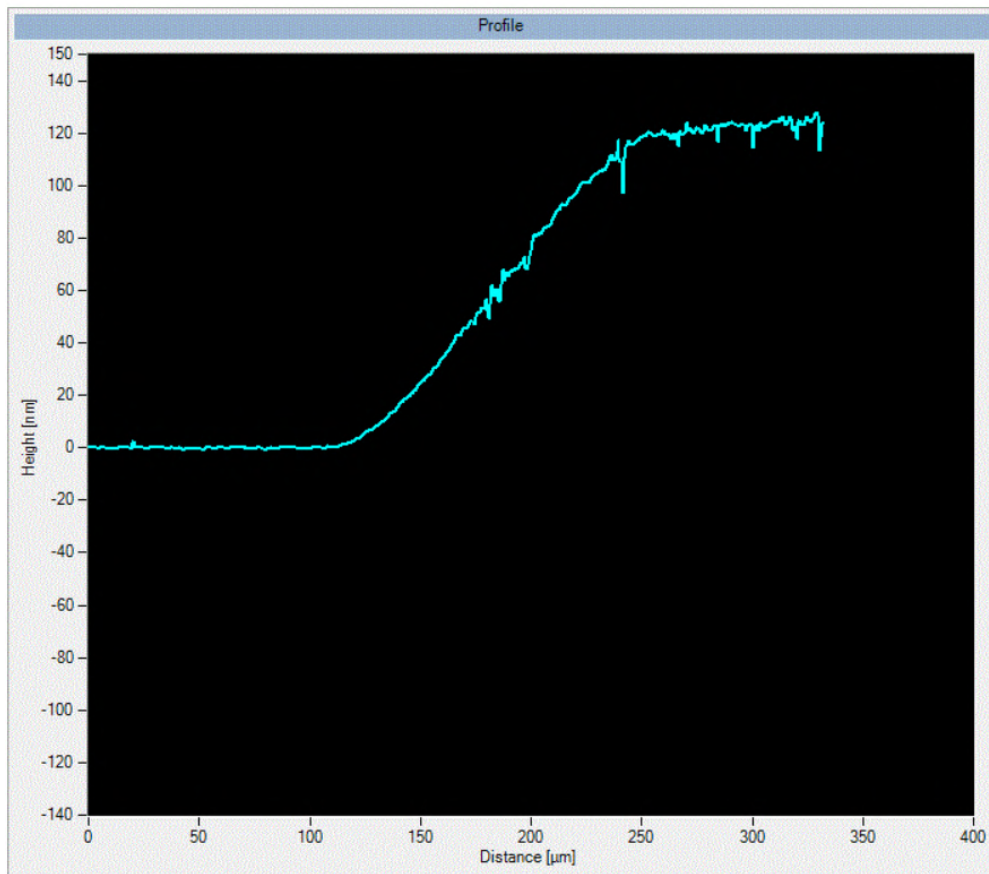


Figure 121: 2D profile of the oscillation at 1 V applied

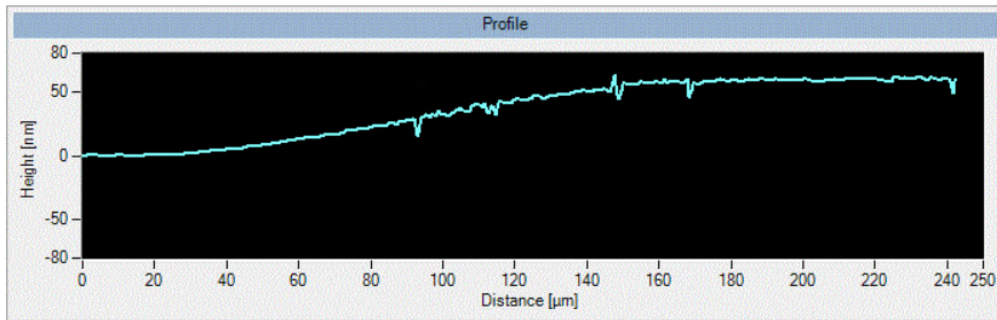


Figure 122: 2D profile of the oscillation at 500 mV applied

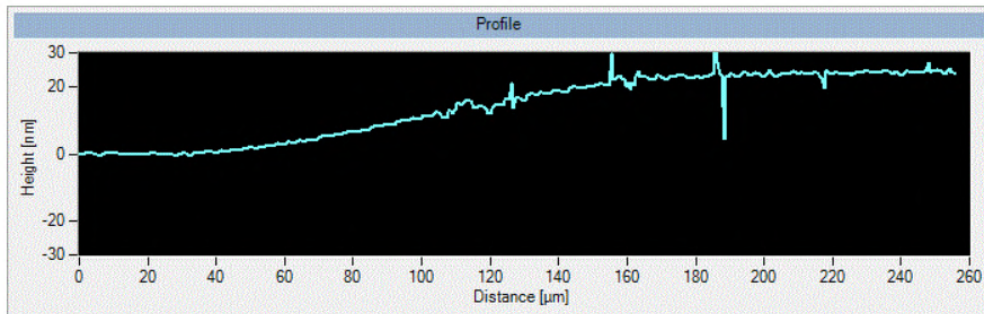


Figure 123: 2D profile of the oscillation at 200 mV applied

6.3 Power actuation with AFM laser

In the previous section I demonstrated that the cantilever behaves as expected, the last part of it is pretty flat during oscillation. Now I want to check how is the power actuation with the new gold layer that I deposited on top. I did these measurements with the AFM of Nanosurf, the company interested in this project. Therefore, I went to Liestal (Switzerland) in order to check this actuation. I checked different types of cantilevers, I will show in the following the cantilever with 3 pillars and 9 walls, I first attached my cantilever to the cantilever holder and then fixed the holder to the AFM. I did measurements in air and I found that the resonance frequency is very easily observable, I can see a clean Gauss curve without defects and the peak of this curve reflects the first resonance frequency of the cantilever. I focused 2 lasers on the cantilever, both laser are in the red spectrum. The first laser is focused at the base of the cantilever, in order to have a reference of the place in which I do not have oscillation, the other laser it is focused on the moving tip, to detect the movement of it.

The result for the cantilever in air is shown in figure 124, I can see that the vibration frequency is 28379 Hz, the amplitude due to laser actuation is 485.6 mV and the quality factor is 79, the curve of the amplitude is very neat, it is very easy to see the resonance frequency, the second graph in picture 124 represents the phase of the oscillation. On the right of the picture I can see the spots in which I focused the 2 lasers.

I immersed the cantilever in deionized water and checked again these results, I can now observe that being the cantilever in water the resonance frequency, the quality factor and the actuation have reduced by quite a bit, this decrease is quantitative coherent to what it is expected

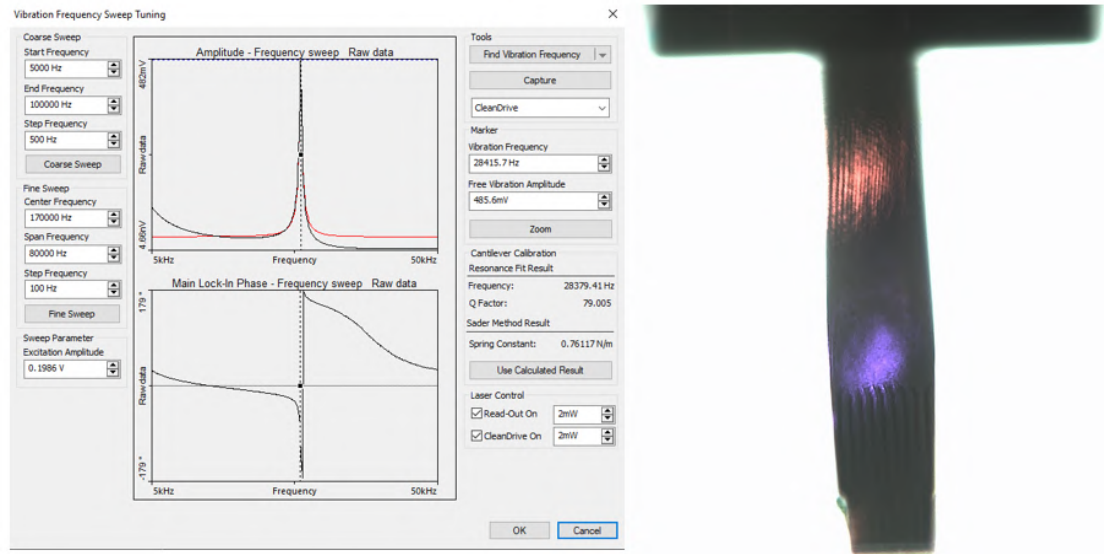


Figure 124: Power actuation of the cantilever in air

for standard resonant devices in water. In this case I get a resonance frequency of 7137 Hz, a power actuation of just 47.05 mV and a quality factor of 2. It is possible to see these results in figure 125.

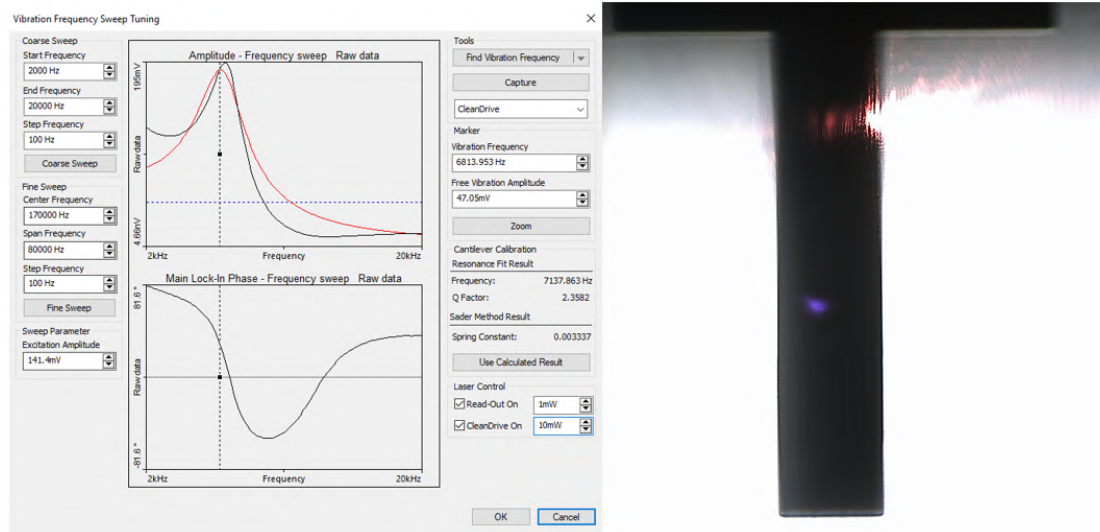


Figure 125: Power actuation of the cantilever in water

7 Conclusion

In this report I provided the simulation, design, fabrication and characterization of a modified cantilever that can be used for cell measurements. The power actuation and the horizontal oscillation of the free edge are very promising results for this device. The next step is to measure a cell placed on top of the cantilever. This device has been registered as a patent under EPFL, me and Prof. Guillermo Villanueva are the 2 inventors. It is of great interest to continue with this project and especially I am interested in developing it considering some improvements that I thought during the fabrication and design steps. It is also possible to change the position of the Au + Cr layer, I can deposit on each $L1'/2$ or on all $L1$ instead of depositing it all over the cantilever.

In conclusion, I am glad the project succeeded well and I am looking forward for the next challenges in my life.

References

- [1] G. Binnig, C. F. Quate, and C. Gerber, *Phys. Rev. Lett.* 56, 930, 1986
- [2] P. Maivald, H. J. Butt, S. A. Gould, C. B. Prater, B. Drake, J. A. Gurley, V. B. Elings, and P. Hansma, *Nanotechnology* 2, 103, 1991
- [3] V. B. Elings and J. Gurley, U.S. Patent No. 5,266,801, 1993
- [4] K. Yamanaka, H. Ogiso, and O. Kolosov, *Appl. Phys. Lett.* 64, 178, 1994
- [5] U. Rabe and W. Arnold, *Appl. Phys. Lett.* 64, 1493, 1994
- [6] B. Cretin and F. Sthal, *Appl. Phys. Lett.* 62, 829, 1993
- [7] Lang, K.M.; D. A. Hite; R. W. Simmonds; R. McDermott; D. P. Pappas; John M. Martinis. "Conducting atomic force microscopy for nanoscale tunnel barrier characterization", 2004
- [8] Binnig, G.; Quate, C. F.; Gerber, Ch. "Atomic Force Microscope". *Physical Review Letters*. 1986
- [9] Septiadi, Dedy; Crippa, Federica; Moore, Thomas Lee; Rothen-Rutishauser, Barbara; Petri-Fink, Alke, "Nanoparticle–Cell Interaction: A Cell Mechanics Perspective". *Advanced Materials*, 2018
- [10] Jong, Wim H De; Borm, Paul JA, "Drug Delivery and Nanoparticles: Applications and Hazards". *International Journal of Nanomedicine*, 2008
- [11] Pyrgiotakis, Georgios; Blattmann, Christoph O.; Demokritou, Philip, "Real-Time Nanoparticle-Cell Interactions in Physiological Media by Atomic Force Microscopy". *ACS Sustainable Chemistry and Engineering*, 2014
- [12] Evans, Evan A.; Calderwood, David A. "Forces and Bond Dynamics in Cell Adhesion". *Science*, 2007
- [13] Scheuring, Simon; Lévy, Daniel; Rigaud, Jean-Louis, "Watching the Components". *Biochimica et Biophysica Acta (BBA) - Biomembranes*, 2015
- [14] Alsteens, David; Verbelen, Claire; Dague, Etienne; Raze, Dominique; Baulard, Alain R.; Dufrêne, Yves F "Organization of the Mycobacterial Cell Wall: A Nanoscale View". *Pflügers Archiv: European Journal of Physiology*, 2008
- [15] <https://cleanroom.byu.edu/koh>
- [16] Pauline M. Doran, in *Bioprocess Engineering Principles (Second Edition)*, 2013
- [17] <https://www.epfl.ch/research/facilities/cmi/equipment/photolithography/acs200/>
- [18] <https://www.epfl.ch/research/facilities/cmi/equipment/photolithography/plade-solvent-wet-bench-for-lift-off-and-su-8-development/>
- [19] <https://www.epfl.ch/research/facilities/cmi/equipment/metrology/zeiss-leo-1550/>
- [20] <https://www.epfl.ch/research/facilities/cmi/equipment/etching/ams200/>
- [21] <https://www.epfl.ch/research/facilities/cmi/equipment/etching/tepla-gigabatch/>

- [22] <https://www.epfl.ch/research/facilities/cmi/equipment/etching/uft-resist/>
- [23] <https://www.epfl.ch/research/facilities/cmi/equipment/photolithography/evg-150-automatic-resist-processing-cluster/>
- [24] <https://www.epfl.ch/research/facilities/cmi/equipment/photolithography/sse-sb20/>
- [25] <https://www.epfl.ch/research/facilities/cmi/equipment/ebeam-lithography/raith-ebpg5000/>
- [26] <https://www.epfl.ch/research/facilities/cmi/equipment/thin-films/alliance-concept-eva-760/>
- [27] <https://www.epfl.ch/research/facilities/cmi/equipment/photolithography/mla-150/>

A Clean room machines

A.1 ACS200 - Coater and developer system for positive resist

The ACS200 is an automatic spin coater and developer used for both 100 mm wafer and 150 mm wafer. In all my fabrications I used wafers of 100 mm diameter. I used the ACS in step 9a and 9c of my process flow, in order to coat and develop the resist that it was used as a mask for the cantilever shape definition.

The ACS200 Gen3 is a modular cluster tool with two stacks of hotplates, two coater bowls, one developer bowl, one wafer centering station, and two loading/unloading cassettes. The device is offered for both DUV resist and positive UV photoresist (stepper). For HMDS priming, coating, development, softbake, PEB (post exposure bake), hardbake, and development, the sequence comprises of a specific chain of recipes in each individual module. Starting a sequence involves running a wafer process flow from a cassette for automatically detected or specified wafers. The software controls how many processes are operating at once, giving first-process critical latency and second-process maximum throughput the highest priority. [17].

A.2 Photolithography wet bench

I used the photolithography wet bench for lift-off of gold. It is formed of 4 baths with remover 1165 (one with Ultra Sound agitation), 1 IPA bath, a wet bench for SU-8 development, 2 DI H_2O baths and a Spin, rinse and dry (SRD) module. [18]

A.3 Zeiss LEO 1550 SEM

I used the LEO SEM for imaging the wafers after the first batch. I also managed to check the cross section of the cantilever fixing the chip to the holder number 2 in figure 126.

The CMi SEM LEO 1550 is composed of one GEMINI column, one process chamber with a motorized stage on 5 degree of freedoms (X, Y, Z, Tilt and Rotation) and one manual airlock.

There are four distinct holders: (1) for small samples fixed with conductive double-sided adhesive, (2) for split samples, (3) for 150 mm wafers, and (4) for 100 mm wafers. The SEM is managed through the graphical user interface program ZeissSmartSEM. Along with a main keyboard control panel providing easy access to 14 of the SEM's most used features, the instrument is also equipped with a twin joystick for navigating the stage and moving the specimens. The Schottky Field Emission type electron source used in the GEMINI column is constructed of tungsten and zirconium (ZrO_2).

The components that make up the instrument are: the Field Emission Gun, which acts as the electron beam's source, the Condenser Lens, which is only used in certain operating modes, the Beam Booster, which is made up of an anode, a vacuum tube, apertures, alignment coils, a stigmator, and an isolating valve, and the GEMINI Objective Lens, which focuses the electron beam onto the specimen and also houses the Deflecting System.

Coupled primary/turbomolecular pumps maintain the chamber vacuum (a few 10^{-7} mbar), while an ion pump maintains the secondary vacuum (a few 10^{-10} mbar).

The fundamental benefit of the GEMINI column is that the acceleration voltage can vary from 0.5 keV to several keV depending on the sample. This makes it possible to significantly lessen and perhaps even control the charging effects that arise when imaging insulating materials.

There are now two secondary electron detectors in place:

- InLens: installed inside the column (high resolution detector).



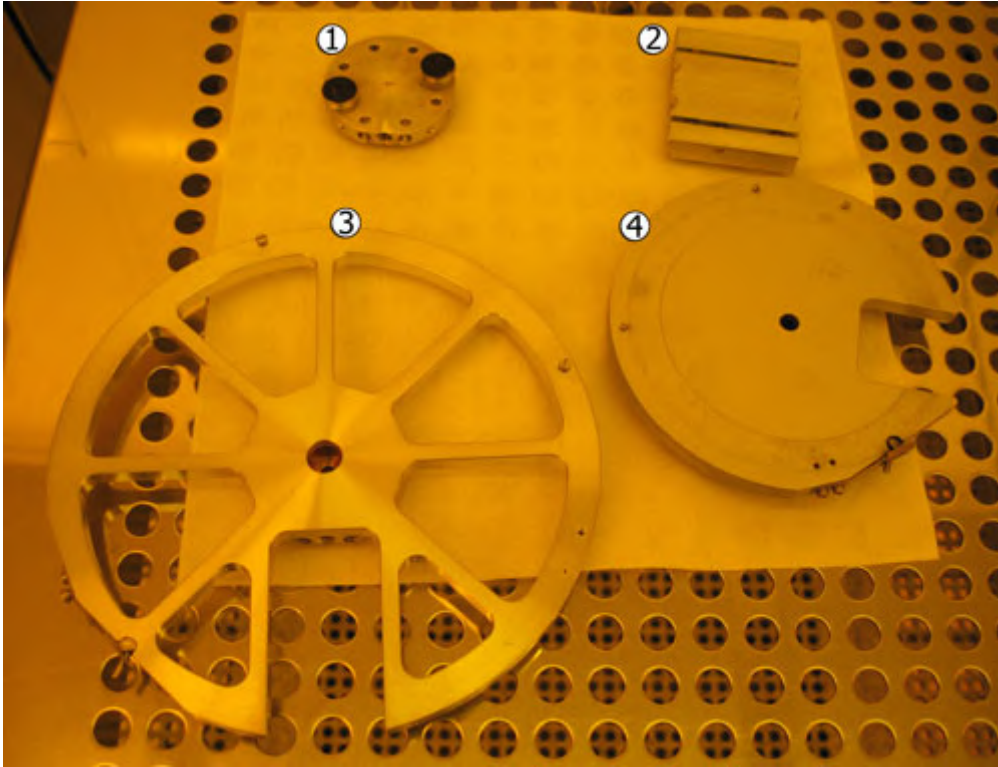


Figure 126: SEM holders [19]

- SE2: installed outside of the column axis (better topography visualization).

Due to the complementing nature of both detectors, switching between them is quite easy during imaging, choosing or even combining their signals to get the most illuminating results. [19]

A.4 Alcatel AMS 200 SE

Adixen AMS200 etcher is an optimized Deep Reactive Ion Etching (DRIE) system for Silicon (Si) and Silicon on Insulator (SOI) wafers. I used it multiple times for all the steps regarding the dry etching of Si and Si_3N_4 .

Major advantages on this system compare to older generation one are:

- Wafer voltage biasing choice (RF or pulsed LF).
- Heating the process chamber will reduce polymer contamination and improve process repeatability. In theory, mechanical cleaning is not required.

Main parts of the machine are: ICP source, diffusion chamber and ESC. End Point Detection (EPD) based on laser interferometry is performed through the viewport placed on the top of the chamber. [20].

A.5 Tepla GiGAbatch

The Tepla GiGAbatch uses high frequency plasma. Main applications are:



- Photo Resist (PR) stripping [21]
- Wafers surface cleaning before subsequent processes
- Descuming before wet etching

A.6 UFT remover

UFT Resist clears photoresist through two identical and successive baths of REM1165 (NMP) heated at 70 °C. It is not aimed at proceeding to metal lift-off. I immerse the wafers for 5 minutes in each tank of remover at 70 °C, then I need to rinse the wafers immersing them in DI wafer for 2/3 minutes in 2 subsequent tanks of DI water. [22]

A.7 EVG 150

The EVG machine was used a lot and it is very similar to the ACS 200 already shown above. The EVG 150 is a modular cluster equipment that includes a stack of three hotplates, a wafer centering station, a coater bowl, a developer bowl, and two loading/unloading cassettes. A central robot arm feeds to each processing station individually. The EPFL EVG 150 cluster can process transparent substrates or regular silicon wafers ranging in size from 100mm to 150mm. The apparatus can be used for development, PEB (post exposure bake), hardbake, and positive photoresist coating. One important thing that I need to remember is that in the EVG I need to perform appropriate surface preparation steps (dehydration, HMDS coating, . . .), whereas in ACS I did not need to perform HMDS before coating because the machine is doing it itself. [23]

A.8 ATMsse OPTIspin SB20

This coating station is used for e-beam coating. I used it for coating CSAR and then ZEP, having better results with the last one.

The ATMsse manual coater line includes a PTZ 28-2 ET Präzitherm hotplate, a Ceran500 high temperature ceramic hotplate, an ATMsse OPTIhot VB20 HMDS unit, an OPTIspin SB20 coater, and an ATMsse OPTIhot VB20 HMDS unit to perform all steps of a standard photoresist coating step: surface preparation, spin-coating, and softbake. [24]

A.9 Raith EBPG5000 – Ebeam tool

The ebeam lithography at CMi is performed with the EBPG5000ES system capable of writing smaller than 10 nm features and placing structures on a substrate with an accuracy of less than 20 nm.

System features:

- 100keV thermal field emission gun
- Gaussian beam
- 50MHz pattern generator
- Direct write mark detection alignment software
- Holders for 50 mm, 100 mm, 150 mm wafers, 5-inch masks and smaller piece parts.

The system is housed in a custom cleanroom which maintains a temperature of $21\text{ }^{\circ}\text{C} \pm 0.1\text{ }^{\circ}\text{C}$. Next to it is a dedicated resist processing lab.

A system that uses an electron focused beam to imprint a pattern onto an electron-sensitive resist is known as an electron beam lithography system. Through the use of an electromagnetic deflection mechanism, the beam is moved over the wafer. The equipment we utilize has a vector scan method, which means the beam is only ever deflected to the places where it is necessary to expose a portion of the pattern.

The resolution, location, and adaptability of the ebl are its benefits. You can use the machine to access length scales that are nearly impossible to use with any other lithography method. Additionally, it enables you to overlay various lithography levels with extreme accuracy ($20\text{ nm mean}+3\sigma$). Since the pattern is just described as a software mask, it is relatively simple to change designs without creating new masks.

The drawback is that it takes longer than photolithography using a stepper or a mask aligner. Additionally, it often takes longer than laser-based photolithography. This is due to the fact that ebl is fundamentally a serial process because the pattern must be exposed one pixel at a time, and because there are many more pixels in ebl than there are in laser writing. [25]

A.10 Alliance-Concept EVA 760

This machine is used for depositing metals on the wafers through evaporation. I used it for deposition of Cr+ Au and Al as the protective layer on the front side.

The EVA 760 is an equipment allowing the deposition of metallic layers on 100 mm or 150 mm wafers by evaporation.

The material is evaporated by heating up the crucible in which it is placed by electron beam. In the EVA 760, 3 working distances source-substrates can be chosen and manually adjusted by the user:

- 450 mm : Preferred distance for Lift-Off processes.
- 350 mm
- 250 mm : Preferred for fast deposition rates.

Depending on the working distance chosen, the substrate holds have varied curved dome shapes. 8 x 100 mm or 5 x 150 mm wafers can be placed inside each dome.

By tracking a quartz crystal's change in frequency, the thickness of the film is ascertained. The expanding quantity of material on top of its surface is what has caused this development. [26]

A.11 Heidelberg Instruments MLA150

The MLA has been very useful for exposing 3 of the 4 lithographic steps that I planned in my process flow. For every exposure I need to define quantitatively the focus and dose of the exposure.

Heidelberg Instruments GmbH in Germany created the MLA150, a next generation mask-less aligner (formerly known as the DLA). By exposing the photoresist with a UV laser (375 or 405 nm) focused and scanned over the wafer, researchers can instantly print a design without having to order or create a mask.

Within a few minutes, the MLA can convert CAD-generated layout in common file types (.gds,.cif,.dxf, etc.), align (top and backside), and expose it on a substrate.



The resolution can be as low as $1\ \mu m$ with thin photoresist (PR) thickness ($1\ \mu m$), and is dependent on the photoresist, wavelength, and resolving power of the optics (NA, depth of focus). [27]

The MLA150 system is equipped with:

- Exposure source: 405 nm or 375 nm laser diodes
- 3 cameras: overview for quick crosses localization, macro and micro for automatic detection of alignment crosses
- Optics for top-side and back-side alignment
- Real time autofocus
- Stage system, position control with interferometers, chuck with vacuum for various substrate sizes